Journal Pre-proofs

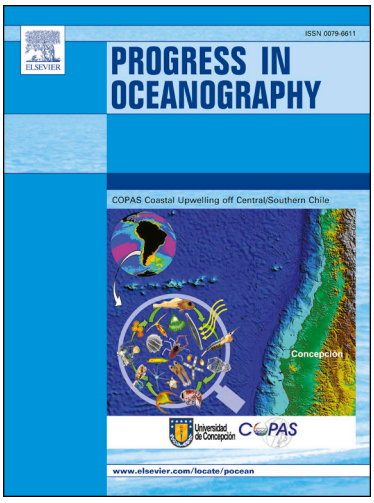

Variability and decadal trends in the Isfjorden (Svalbard) ocean climate and circulation - an indicator for climate change in the European Arctic

R. Skogseth, L.L.A. Olivier, F. Nilsen, E. Falck, N. Fraser, V. Tverberg, A.B. Ledang, A. Vader, M.O. Jonassen, J. Søreide, F. Cottier, J. Berge, B.V. Ivanov, S. Falk-Petersen

PII: S0079-6611(20)30133-6
DOI: https://doi.org/10.1016/j.pocean.2020.102394
Reference: PROOCE 102394

To appear in: *Progress in Oceanography*

Received Date: 4 April 2019
Revised Date: 9 January 2020
Accepted Date: 17 June 2020

Please cite this article as: Skogseth, R., Olivier, L.L.A., Nilsen, F., Falck, E., Fraser, N., Tverberg, V., Ledang, A.B., Vader, A., Jonassen, M.O., Søreide, J., Cottier, F., Berge, J., Ivanov, B.V., Falk-Petersen, S., Variability and decadal trends in the Isfjorden (Svalbard) ocean climate and circulation - an indicator for climate change in the European Arctic, *Progress in Oceanography* (2020), doi: https://doi.org/10.1016/j.pocean.2020.102394

Variability and decadal trends in the Isfjorden (Svalbard) ocean climate and circulation - an indicator for climate change in the European Arctic

Skogseth[1], R., L.L.A. Olivier[1,2], F. Nilsen[1,3], E. Falck[1,3], N. Fraser[4], V. Tverberg[6], A. B. Ledang[7], A. Vader[1], M.O. Jonassen[1,3], J. Søreide[1], F. Cottier[4,5], J. Berge[1,5], B.V. Ivanov[8,9], and S. Falk-Petersen[10,5].

[1] The University Centre in Svalbard, Postboks 156, 9171, Longyearbyen, Norway

[2] Geosciences department, Ecole Normale Supérieure, PSL Res. Univ., Paris, France.

[3] University of Bergen, Geophysical Institute, Postboks 7803, 5020, Bergen, Norway

[4] Scottish Association for Marine Science, Scottish Marine Institute, Oban, Argyll, PA37 1QA, Scotland

[5] Department of Arctic and Marine Biology, University of Tromsø - The Arctic University of Norway, 9037, Tromsø, Norway

[6] Nord University, Faculty of Biosciences and Aquaculture, Bodø, Norway

[7] Norwegian Institute for Water Research, Gaustadalléen 21, NO-0349, Oslo, Norway

[8] Arctic and Antarctic Research Institute, Atmosphere-Sea Ice-Ocean Interaction Department, Saint-Petersburg, Russian Federation

[9] Saint-Petersburg State University, Oceanography Department, Saint-Petersburg, Russian Federation

[10] Akvaplan-niva AS, The Fram Centre, Hjalmar Johansens Gate 14, 9007, Tromsø, Norway

Corresponding author: R. Skogseth. E-mail: Ragnheid.Skogseth@unis.no. Address: The University Centre in Svalbard, P.O. Box 156, 9171 Longyearbyen, Norway.

Abstract

Isfjorden, a broad Arctic fjord in western Spitsbergen, has shown significant changes in hydrography and inflow of Atlantic Water (AW) the last decades that only recently have been observed in the Arctic Ocean north of Svalbard. Variability and trends in this fjord's climate and circulation are therefore analysed from observational and reanalysis data during 1987 to 2017. Isfjorden experienced a shift in summer ocean structure in 2006, from AW generally in the bottom layer to AW (with increasing thickness) higher up in the water column. This shift, and a concomitant shift to less fast ice in Isfjorden are linked to positive trends in the mean sea surface temperature (SST) and volume weighted mean temperature (VT) in winter (SST_W/VT_W: 0.7 ± 0.1/0.9 ± 0.3 °C $10yr^{-1}$) and summer (SST_S/VT_S: 0.7 ± 0.1/0.6 ± 0.1°C $10yr^{-1}$). Hence, the local mean air temperature shows similar trends in winter (1.9 ± 0.4 °C $10yr^{-1}$) and summer (0.7 ± 0.1 °C $10yr^{-1}$). Positive trends in volume weighted mean salinity in winter (0.21 ± 0.06 $10yr^{-1}$) and summer (0.07 ± 0.05 $10yr^{-1}$) suggest increased AW advection as a main reason for Isfjorden's climate change. Local mean air temperature correlates significantly with sea ice cover, SST, and VT, revealing the fjord's impact on the local terrestrial climate.

In line with the shift in summer ocean structure, Isfjorden has changed from an Arctic type fjord dominated by Winter Deep and Winter Intermediate thermal and haline convection, to a fjord dominated by deep thermal convection of Atlantic type water (Winter Open). AW indexes for the mouth and Isfjorden proper show that AW influence has been common in winter over the last decade. Alternating occurrence of Arctic and Atlantic type water at the mouth mirrors the geostrophic control imposed by the Spitsbergen Polar Current (carrying Arctic Water) relative to the strength of the Spitsbergen Trough Current (carrying AW). During high AW impact events, Atlantic type water propagates into the fjord according to the cyclonic circulation along isobaths corresponding to the winter convection. Tides play a minor role in the variance in the

currents, but are important in the side fjords where exchange with the warmer Isfjorden proper occurs in winter. This study demonstrates that Isfjorden and its ocean climate can be used as an indicator for climate change in the Arctic Ocean. The used methods may constitute a set of helpful tools for future studies also outside the Svalbard Archipelago.

Keywords

Oceanography; TSD distribution, water masses and circulation; Ocean circulation and currents; Nearshore dynamics; Tides, surges and sea level; Atlantic Water intrusion; Arctic Ocean, Svalbard, West Spitsbergen Shelf, Isfjorden

Abbreviations

AW	Atlantic Water
ArW	Arctic Water
CTD	Conductivity, temperature and depth
DAC	Depth-averaged current
DFI	Days of fast ice
ESC	East Spitsbergen Current
IW	Intermediate Water
LW	Local Water
SPC	Spitsbergen Polar Current
SST	Sea surface temperature
STC	Spitsbergen Trough Current
SW	Surface Water
TAW	Transformed Atlantic Water
UNIS HD	UNIS hydrographic database
VM-ADCP	Vessel-mounted acoustic Doppler current profiler
VT	Volume weighted mean temperature
VS	Volume weighted mean salinity
WCW	Winter-Cooled Water
WSC	West Spitsbergen Current
WSS	West Spitsbergen Shelf

1 Introduction

The decline in Arctic sea ice is one of the most striking manifestations of climate change (Onarheim et al., 2018; Serreze and Barry, 2011; Stroeve and Notz, 2018), and in the recent

decades, Svalbard fjords have experienced a substantial reduction in winter sea ice extent (Muckenhuber et al., 2016). The reduced sea ice cover has been linked to an increased transport of warm Atlantic Water (AW) into the fjords (Cottier et al., 2007; Fraser et al., 2018b; Nilsen et al., 2016; Promińska et al., 2018; Tverberg et al., 2019). AW from the West Spitsbergen Current (WSC; Figure 1a) is able to reach the upper shelf along western Spitsbergen on Svalbard, and eventually flood into the fjords (Nilsen et al., 2016, 2008a). Wind forcing on the West Spitsbergen Shelf (WSS) on timescales from days to months is one of the mechanisms starting a circulation of AW towards the fjords (Cottier et al., 2007; Nilsen et al., 2016; Pavlov et al., 2013).

Fjords are commonly regarded as the link between the ocean and land through cross-shelf exchanges, and circulation and mixing in the fjords. Arctic fjords may additionally be regarded as extreme variants of standard fjord concepts as they are subject to intense seasonality through sea ice formation and glacial melt. The fjords on the west coast of Spitsbergen, which balance Atlantic, Arctic, brine- and freshwater inputs, are hence potentially sensitive indicators of environmental change. Increased understanding of important exchange processes between the oceanic heat source in the WSC and the WSS has recently been achieved. AW masses in the WSC, experiencing a warming trend (e.g. Onarheim et al., 2014; Tverberg et al., 2019; Walczowski et al., 2017), are transferred to the coastal shelf and fjord systems by wind generated cross-shelf exchange (Cottier et al., 2007; Goszczko et al., 2018; Inall et al., 2015; Nilsen et al., 2016; Tverberg et al., 2019). AW meets Arctic Water (ArW) on the shelf, transported northwards by the coastal Spitsbergen Polar Current (SPC; Figure 1a) first named by Helland-Hansen and Nansen (1909), and the density front between AW and ArW on the WSS defines the West Spitsbergen Polar Front (Nilsen et al., 2016). Ekman transport and pumping together with variable horizontal density gradients across the continental slope and shelf, caused by the surface heat flux, are likely to give rise to frontal instabilities (Saloranta and Svendsen, 2001; Teigen et

al., 2011, 2010) initiating a residual (eddy and Ekman) overturning circulation across the front (Tverberg and Nøst, 2009). Eddy activity along the shelf edge front is essential for residual overturning to take place (Tverberg et al., 2019; Tverberg and Nøst, 2009), and moreover, there must be some degree of topographic steering to bring AW from the shelf edge to the inner shelf (Nilsen et al., 2016).

The continental shelf adjoining the west coast of Spitsbergen is complex, with alternating shallow banks (50–100 m depths) and deep troughs (200–400 m depths) cutting across the shelf. Model results compared with observations have shown that the deep Isfjorden Trough (Isfjordrenna) is a significant pathway for AW in the Spitsbergen Trough Current, flowing along the troughs across the WSS (Nilsen et al., 2016), owing to the tendency to conserve potential vorticity. AW flooding events on the WSS have become more frequent during the recent decades because of changes in the atmospheric pressure field and the winter cyclone tracks around Svalbard (Barnes et al., 2014; Francis and Vavrus, 2012; Rogers et al., 2005). Moreover, trends from reanalysis studies show increasing numbers of deeper low-pressure systems passing over Svalbard in winter during the recent decades (Zahn et al., 2018). Hence, there is a potential link between the wind forced circulation on the WSS (Ekman transport and pumping), the observed wintertime intrusion of AW on the WSS and into the fjords, and the lack of sea ice around Svalbard (Muckenhuber et al., 2016; Nilsen et al., 2016; Tverberg et al., 2019).

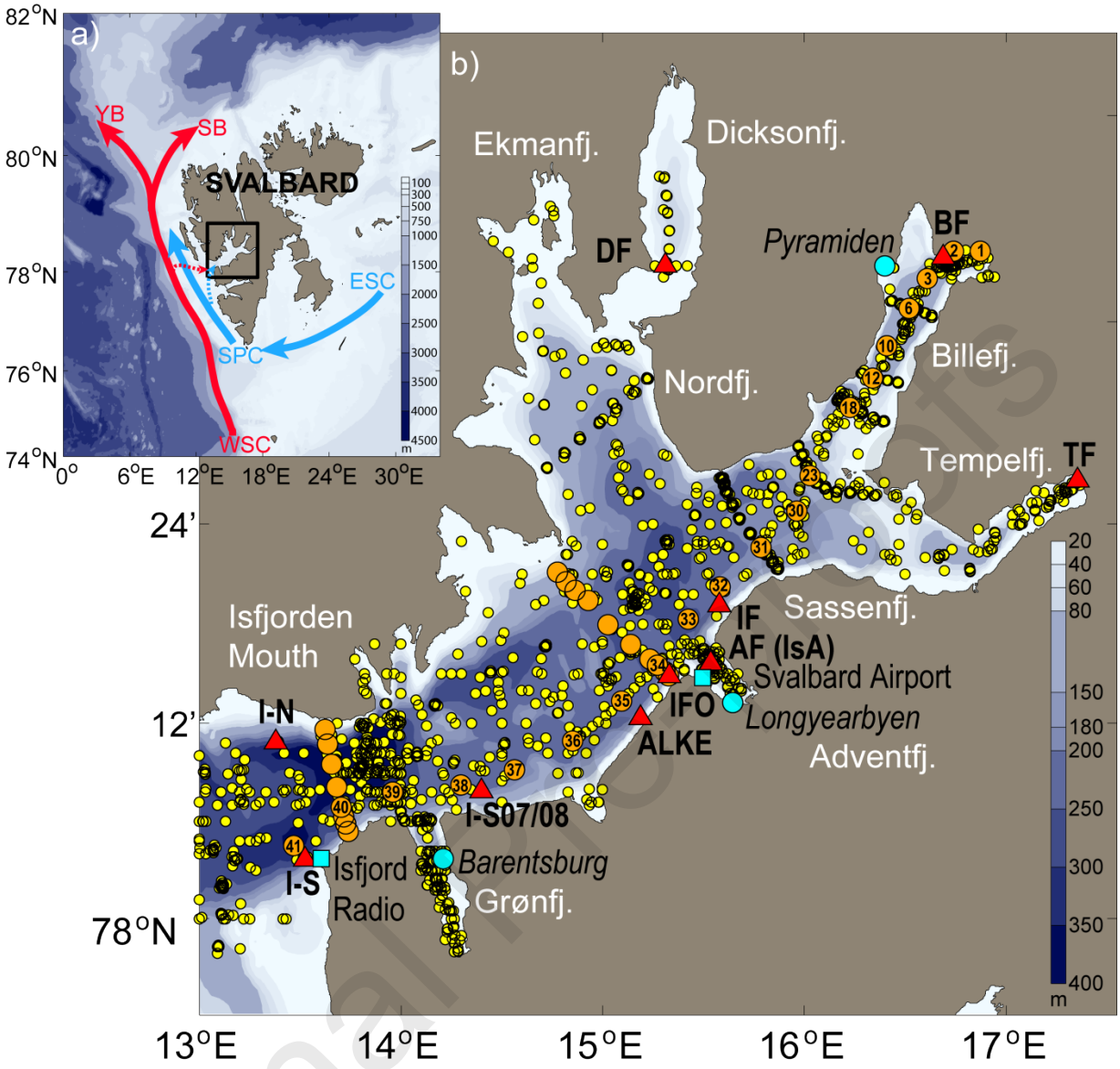

Figure 1: a) The ocean bathymetry around Svalbard Archipelago with the two main currents; West Spitsbergen Current (WSC) and East Spitsbergen Current (ESC) drawn with red and blue arrows, respectively. WSC separates into two branches; the Svalbard Branch (SB) and the Yermak Branch (YB). ESC continues as Spitsbergen Polar Current (SPC) west of Svalbard. The red and blue stippled arrows indicate inflow from WSC and SPC, respectively. The black box outlines the area covered in b), which shows the bathymetry of the Isfjorden system with its side fjords. The numbered orange dots indicate the Isfjorden Transect (see Table 2) from the head of Billefjorden (Station 1) to the Isfjorden Mouth (Station 41) as well as the cross sections (not numbered) at the mouth and in Isfjorden proper. The positions of CTD profiles obtained from

UNIS hydrographic database (UNIS HD) are shown with smaller yellow dots. The red triangles show the location of the moorings listed in Table 3, and the Isfjorden-Adventfjorden sampling station (IsA). The cyan squares show the location of the meteorological stations at Isfjord Radio and Svalbard Airport. The settlements: Barentsburg, Longyearbyen and Pyramiden are indicated with cyan dots. The bathymetry is from the International Bathymetric Chart of the Arctic Ocean (IBCAO) version 3.0 (Jakobsson et al., 2012).

Currently there is enormous interest and activity in investigating the role of increased ocean heat on the stability of ocean terminating glaciers (Fraser et al., 2018a; Fraser and Inall, 2018; Inall et al., 2014; Jackson et al., 2018; Luckman et al., 2015; Straneo et al., 2010). The propagation of warm oceanic waters into fjords has the potential to increase the melt rates of glaciers, which can result in the destabilisation of glacial flow. Moreover, the halted sea ice formation and the large areas of ice free waters have a great impact on the Arctic ecosystem (Hegseth and Tverberg, 2013). More frequent episodes of AW intrusion in Arctic regions support the appearance of boreal species like the blue mussel (Berge et al., 2005), Atlantic cod, haddock and mackerel (Berge et al., 2015; Renaud et al., 2012), and the helmet jellyfish (Geoffroy et al., 2018). Some of these species, such as the blue mussel, are now able to establish viable populations inside western Svalbard fjords (Leopold et al., 2019), whereas for other groups such as the decapods, the community appear to be more resilient towards changes in the hydrography (Berge et al., 2009). On the other hand, significant changes in the community structure of algae (Kubiszyn et al., 2014; Paulsen et al., 2016), zooplankton (Dalpadado et al., 2016; Darnis et al., 2017; Gluchowska et al., 2016; Hop et al., 2019) and krill (Hünerlage, 2015) have been documented to occur in relation to increased influx of AW, and to regime shifts in shallow benthic communities (Kortsch et al., 2012). For demersal fish communities in Svalbard fjords changes are less prominent (Bergstad et al., 2018). Changes in community structures at the base of the food web

have impact on higher trophic levels such as sea birds (Vihtakari et al., 2018; Vogedes et al., 2014) and seals (Lowther et al., 2017), whereas the diet to polar bears are more sensitive to decline in sea ice and restricted access to marine prey (Tartu et al., 2017). In order to understand the leading mechanisms linking the physical oceanographic environment to the Arctic coastal ecosystem, it is necessary to improve our knowledge of exchange and circulation on Arctic shelves and in fjords in response to regional atmospheric and oceanic variability. In essence, the observed changes in the physical system are leading to changes at multiple trophic levels. Isfjorden in western Spitsbergen is exceptionally well suited for studying AW intrusion and ecosystem effects due to guiding of AW along the Isfjorden Trough from WSC towards the sill free mouth of Isfjorden.

Based on an ongoing long term mooring program and construction of longer hydrographic time series, we will show that fjord systems along western Spitsbergen, and in particular the Isfjorden system, went from an ArW state to a more AW state after winter 2006 (Cottier et al., 2007). This is reflected in a distinct shift to less sea ice in Isfjorden from 2006 (Muckenhuber et al., 2016). Moreover, observations of the ice cover north of Svalbard further demonstrate the intimate link between the heat of AW and distribution of sea ice. Onarheim et al. (2014) have shown that the sea ice area north of Svalbard has been decreasing for all months since 1979 with the largest ice reduction occurring during the winter months at a rate of 10% per decade. This is related to inflow of warmer AW higher up in the water column when entering the Arctic Ocean north of Svalbard (Onarheim et al., 2018; Polyakov et al., 2017; Walczowski et al., 2017), and cannot be linked to any increase in AW volume flux in the WSC (Beszczynska-Moller et al., 2012). The northern Barents Sea has also experienced a rapid climate shift, as demonstrated by Lind et al. (2018), and the region is described as the Arctic's warming hotspot where the surface warming and loss of winter sea ice are the largest in the entire Arctic (Onarheim et al., 2018; Stroeve and

Notz, 2018). It is clear that the warming signal and the reduced sea ice cover have been visible in the western Svalbard fjords in the last decade, and are now starting to become significant in the Eurasian part of the Arctic Ocean. Svalbard is dominated by its marine setting and many of the processes occurring in the region are strong indicators of changes that will take place in the Eurasian Basin in the Arctic Ocean in the years to come, both the AW warming signal and the changes in marine life at multiple trophic levels. Major issues are the loss of a surface freshwater layer (Lind et al., 2018) and the shoaling of the AW layer (Carmack et al., 2015; Polyakov et al., 2017), leading to increased upward mixing with the Atlantic layer. More heat will then be brought up from the usually deeper Atlantic layer, resulting in a warmer Arctic layer above. Falk-Petersen et al. (2015) suggested that the reduced winter ice cover north of Svalbard facilitated upwelling of nutrient rich AW, fuelling higher primary and secondary production and the return of the Bowhead whales to these waters. In this study, we will show that the shoaling of the AW layer on the west coast of Spitsbergen has dominated the variability and decadal trends in the Svalbard climate and that the Isfjorden system can be used as an indicator for climate change in the Arctic Ocean.

In the following, Isfjorden and water masses defined for the Isfjorden system are presented in Section 2, before a thorough description of data and analysis methods in Sections 3 and 4, respectively. The results are presented and discussed in parallel in Section 5, ending with a conceptual summary and conclusions in Section 6. More detailed information about the data and analysis in this study is provided in Supplementary data, where also interpolated winter and summer distributions of hydrography and water masses along the Isfjorden Transect are displayed for every year with enough data to produce interpolated sections.

2 Isfjorden

Isfjorden is the largest fjord in western Spitsbergen with its mean width of 24 km and a length of about 100 km from the mouth to the head of the side fjord, Billefjorden (Figure 1b), and has a total area of 3084 km^2 and a volume of 390 km^3 (Nilsen et al., 2008a). The orientation of the 70 km long and 200-300 m deep main basin (Isfjorden proper) is SW-NE (78.12°N; 13.8°E - 78.45°N; 16.1°E), making a 60° clockwise angle with the north direction (Nilsen et al., 2008a). Isfjorden proper divides into Sassenfjorden in the east, Nordfjorden in the north, and the side fjords Grønfjorden and Adventfjorden on the southern side; all with no sill (Figure 1b). Sassenfjorden further leads to the sill fjords Tempelfjorden and Billefjorden, whereas Nordfjorden leads to the sill fjords Dicksonfjorden and Ekmanfjorden. Isfjorden is connected to the WSS slope through the 300-400 m deep Isfjorden Trough, leading AW from WSC to the fjord mouth (Figure 1a), which consists of a 412 m deep waterway instead of a shallower protecting sill. These topographic features have profound effect on the AW circulation on the shelf in front of Isfjorden, leading to the topographically guided Spitsbergen Trough Current following the troughs across the WSS while carrying Transformed Atlantic Water (TAW) and AW (Nilsen et al., 2016). Additionally, Arctic Water (ArW) originating from the Barents Sea and Storfjorden with the East Spitsbergen Current (ESC) enters Isfjorden in the south with the Spitsbergen Polar Current (SPC), the continuation of ESC (Figure 1a). The water masses defined for the Isfjorden system are given in Table 1.

Table 1: Water masses and their temperature (T) and salinity (S) characteristics for the Isfjorden system adapted from (Loeng, 1991; Nilsen et al., 2008a; Svendsen et al., 2002). Salinity characteristic is given in both practical salinity unit (psu) and in absolute salinity (g/kg).

Water mass	T (°C)	S (psu)	S (g/kg)
External:			
Atlantic Water (AW)	≥ 3	≥ 34.9	≥ 35.07
Arctic Water (ArW)*			

	≤ 0	34.3 - 34.8	34.46 - 34.97
Local:			
Surface Water (SW)	≥ 1	< 34	< 34.16
Local Water (LW)	< 1	≥ 32	≥ 32.15
Winter-Cooled Water (WCW)	< -0.5	≥ 34.4	≥ 34.56
Mixed:			
Intermediate Water (IW)	> 1	34 - 34.7	34.16 - 34.87
Transformed Atlantic Water (TAW)	1 - 3	34.7 - 34.9	34.87 - 35.07

*ArW as defined for the Barents Sea. Outside Isfjorden, ArW might be heavily modified with a wider range of salinity as it is further freshened while moving northward with SPC.

Internal processes in Isfjorden produce local water masses as listed in Table 1. Heat loss to the atmosphere and corresponding sea ice formation and brine release to the water below, have normally been driving processes of the winter convection in the fjord, and the following production of Local Water (LW) and Winter-Cooled Water (WCW). In cold winters with water close to the freezing point in the upper layer, Isfjorden can be regarded as a latent heat polynya where effective formation of frazil ice takes place in open water during favourable wind, transporting continuously formed sea ice out the fjord (Nilsen et al., 2008a). Winters with strong polynya events, and hence more sea ice and brine formation, produce the coldest, most saline, and densest WCW. Cold winters with less polynya favouring wind and hence more fast ice cover, resulting in less total sea ice and brine formation, produce cold, but less saline and dense WCW. The density of the winter water sets the premise for inflow of AW in summer; whether it flows in at deep or intermediate depths, or not at all (Nilsen et al., 2008a). In recent years with no sea ice formation in Isfjorden proper and the southern side fjords, and also reduced sea ice cover on the sill fjords, the latent heat polynya approximation with winter water at the freezing point is no longer valid to explain the interannual variability in the characteristics of the winter water, and hence in the following inflow pattern of AW. Recently, three types of winters have been identified in order to classify winters in Arctic fjords facing potential inflow of water of Atlantic origin (Tverberg et al., 2019). Winters with deep thermal and haline convection are identified as Winter Deep; winters with thermal and haline convection to intermediate depths are identified

as Winter Intermediate; whereas recent winters with no sea ice formation (open water above freezing) and only thermal convection of water of Atlantic origin are identified as Winter Open. This winter type classification will also be used for Isfjorden in the following study.

Surface Water (SW) forms in summer as a result of wind mixing of a surface layer exposed to increased radiation from the sun, heat transfer from a warmer atmosphere, and added freshwater. Sources of freshwater to Isfjorden are either local (precipitation, runoff from land, input of glacial ice (calving), and sea ice melt) or advected into the fjord (freshwater carried by SPC). Precipitation is generally low on Svalbard, but varies locally. For the Isfjorden area, the mean annual precipitation varied from 196 mm at Svalbard Airport to 581 mm in Barentsburg (see Figure 1b for location) for the period 1971-2000 (Hanssen-Bauer et al., 2019). River runoff mostly occurs during a few months from June to September, with maximum normally in July. In June and July, the runoff is mainly dominated by snowmelt, while in August and September the runoff mainly comes from rainfall and glacial melt (Killingtveit et al., 2003). In the autumn, the rivers generally freeze up completely. Regular and continuous runoff measurements are sparse on Spitsbergen. For the Isfjorden area, there are established regular runoff measurements in two catchments near Longyearbyen with an average annual runoff of around 0.03 km^3 or a water equivalent of 540 mm (Killingtveit et al., 2003). Iceberg calving appears in Svalbard to be about 16 % of the runoff from surface melting, and an annual value for Svalbard was estimated to be about 110 mm (Hagen et al., 2003). Isfjorden has about ten tidewater glaciers, most of which are located on the northern side of the fjord. On the southern side there are none before reaching the inner part of Tempelfjorden in the east where there are two, and the inner part of Billefjorden which has one. No detailed studies have been performed to determine the relative contributions of the different sources of freshwater to the various fjords of Svalbard, but precipitation and

glacial melt have generally been determined as the two largest sources of freshwater in these regions (Killingtveit et al., 2003; Svendsen et al., 2002).

Intermediate Water (IW) and TAW are formed both locally and externally on the shelf. IW is a mixture between SW and the water below, which can be AW, TAW, or LW inside Isfjorden, and AW, TAW, or ArW on the shelf (Nilsen et al., 2008a; Svendsen et al., 2002; Tverberg et al., 2019). IW in Isfjorden can therefore come from the shelf in addition to being formed locally, and being warm or cold depending on the water masses present below the surface layer (Tverberg et al., 2019). TAW is a mixture between AW and ArW on the shelf (Svendsen et al., 2002), and is formed along the path of STC, which is aligned with the front between AW in WSC and ArW in SPC (Nilsen et al., 2016). In Isfjorden, TAW is therefore either from the shelf or a mixture between inflowing AW and LW produced in winter.

Reconstruction of inflow of AW to Isfjorden reveals changing seasonal summer inflow during the Holocene, and a close interaction between the flow of AW and the development of the terrestrial climate, the amount of ArW (polar meltwater) and sea ice (Rasmussen et al., 2013). More recently in the last decade, the calving rate of the tidewater glacier Tunabreen at the head of Tempelfjorden varied with the heat content in Isfjorden (Luckman et al., 2015). Satellite data from 2000 to 2014 reveal a diminishing sea ice cover in Isfjorden, with an abrupt decline since 2006 (Muckenhuber et al., 2016), indicating increased inflow of AW also in winter. Concurrently, a change from an Arctic to a more Atlantic dominated plankton community has been observed in Isfjorden during the last decade (Dalpadado et al., 2016; Gluchowska et al., 2016). Based on all these observed changes related to the ocean climate in Isfjorden, it is essential to increase our understanding of variability and trends in the governing physical processes and

in that way increase our knowledge of the driving mechanisms behind the changes in the Arctic Ocean climate.

3 Data

In order to make a robust analysis of interannual variability and trends in the hydrography and circulation in the Isfjorden system, all non-published hydrographic profiles obtained by UNIS and collaborating partners were collected and combined with hydrographic profiles available in public databases. The time period with sufficient amount of profiles span from 1987 to 2017. Variability on shorter time scales is analysed from time series of hydrography and current from moorings that have been deployed in different locations in the Isfjorden system during the time period 2005 to 2017. Combined with additional current data from glider campaigns and vessel-mounted acoustic Doppler current profiler (VM-ADCP) sections, the general circulation in Isfjorden is described.

3.1 Hydrographic profile data

3.1.1 UNIS hydrographic database

The UNIS hydrographic database (UNIS HD; Skogseth et al., 2019) is a collection of temperature and salinity profiles from UNIS student and research cruises around Svalbard (since 1994) compiled with hydrographic data from the same area (1-30°E and 75-81.5°N) in the Norwegian Marine Data Centre (NMDC, https://www.nmdc.no/), the International Council for the Exploration of the Sea (ICES) dataset on ocean hydrography (https://ocean.ices.dk/HydChem/), the PANGAEA data publisher (https://www.pangaea.de/), and the database from the project Norwegian Iceland Seas Experiment (NISE; Nilsen et al., 2008b), in addition to available data in Isfjorden and the shelf outside from the Arctic and Antarctic Research Institute (AARI) and Murmansk Marine Biological Institute (MMBI). Duplicate data and outliers have been removed before the analysis. The locations of the conductivity, temperature, and depth (CTD) profiles

extracted from UNIS HD, are shown in Figure 1b. Also shown is the Isfjorden Transect (Table 2) from the head of Billefjorden (Station 1) to the Isfjorden Mouth (Station 41) which has been taken repeatedly since 1996 during UNIS student cruises in typically September and April (less often). Additionally, one cross-section at the mouth and one in Isfjorden proper are shown.

Table 2: The stations that make up the Isfjorden Transect, from the head of Billefjorden (Station 1) to the mouth of Isfjorden (Station 41). See Figure 1b for locations.

Station	Latitude	Longitude	Bot. depth (m)
1	78° 40.13’ N	16° 52.47’ E	191
2	78° 40.13’ N	16° 44.47’ E	191
3	78° 38.54’ N	16° 36.57’ E	181
6	78° 36.80’ N	16° 31.17’ E	147
10	78° 34.61’ N	16° 24.60’ E	94
12	78° 32.69’ N	16° 20.40’ E	110
18	78° 30.97’ N	16° 13.63’ E	132
23	78° 26.90’ N	16° 01.74’ E	114
30	78° 24.79’ N	15° 57.83’ E	192
31	78° 22.61’ N	15° 47.17’ E	175
32	78° 20.26’ N	15° 35.05’ E	188
33	78° 18.31’ N	15° 25.58’ E	265
34	78° 15.54’ N	15° 16.36’ E	237
35	78° 13.35’ N	15° 05.64’ E	241
36	78° 10.93’ N	14° 51.09’ E	222
37	78° 09.18’ N	14° 33.74’ E	213
38	78° 08.23’ N	14° 17.89’ E	209
39	78° 07.80’ N	13° 57.61’ E	300
40	78° 06.88’ N	13° 42.33’ E	305
41	78° 04.53’ N	13° 28.18’ E	361

The CTD data were collected with different types of instruments; mostly with a Sea-Bird Scientific SBE911+ CTD system or a Sea-Bird Scientific SBE 19plus V2 CTD, and some with a Neil Brown CTD, a SAIV SD204 CTD, and a SAIV SD208 CTD. The initial accuracies of the temperature, conductivity, and pressure sensors are listed in Table S1 in Supplementary data. Only the Sea-Bird instruments have reported a typical inaccuracy in salinity of 0.001, following standard procedures for calibration.

3.1.2 Isfjorden-Adventfjorden time series sampling station (IsA)

The high-resolution time series sampling station IsA (Isfjorden-Adventfjorden, Figure 1b) has been sampled on a weekly to monthly basis since December 2011, to study seasonal and interannual variation in microbial (Kubiszyn et al., 2017; Marquardt et al., 2016; Marquardt et al., 2019) and zooplankton (Stübner et al., 2016) communities, carbon cycle (Ericson et al., 2018), sedimentation (Wiedmann et al., 2016), and the potential effects of increased inflow of AW. During each sampling event a CTD profile was obtained. The profiles at IsA have been taken with the CTD instruments SAIV SD204/208, SBE911+, SBE 19plus V2, and SBE 37. Details of the sampling routines from 2015 to 2017 and calibration of the SAIV CTDs are provided by Ericson et al. (2018).

3.2 Hydrographic and current time series from moorings

Available hydrographic and current time series from moorings deployed by UNIS and collaborating partners in the Isfjorden system during the time period 2005 to 2017 (Table 3), have been collected, quality checked, and de-spiked for further analysis in this study. The locations of the moorings are shown in Figure 1b, and the full deployment details of each mooring are given in Section S.1.3 in Supplementary data. The hydrographic data from the moored instruments have, when possible, been calibrated against available CTD profiles taken nearby. Initial accuracy and resolution of each instrument type are given in Table S1 in Supplementary data.

Table 3: Overview of the oceanographic moorings that have been deployed in the Isfjorden system during the time period 2005 to 2017, with the name, location, position(s), and deployment period(s) given for each mooring. The locations are shown in Figure 1b.

Name	Location	Position	Deployment period
I-S	Southern Isfjorden mouth	78°03.650’ N; 013°31.369’ E 78°03.674’ N; 013°31.464’ E	Sep 2005 - Sep 2006 Sep 2006 - Sep 2007

		78°03.502’ N; 013°35.609’ E	Sep 2010 - Sep 2011
		78°03.637’ N; 013°31.271’ E	Sep 2011 - Sep 2012
		78°03.643’ N; 013°31.327’ E	Sep 2012 - Sep 2013
		78°03.625’ N; 013°31.267’ E	Sep 2013 - Sep 2014
		78°03.764’ N; 013°31.701’ E	Sep 2014 - Sep 2015
		78°03.667’ N; 013°31.492’ E	Sep 2015 - Aug 2016
		78°03.644’ N; 013°31.442’ E	Aug 2016 - Oct 2017
$I\text{-}S_{0708}$	Southern outer Isfjorden	78°08.300’ N; 014°25.030’ E	Sep 2007 - Feb 2008
I-N	Northern Isfjorden mouth	78°10.829’ N; 013°22.737’ E	Sep 2015 - Aug 2016
		78°10.927’ N; 013°23.000’ E	Aug 2016 - Oct 2017
ALKE	Southern Isfjorden proper	78°12.300’ N; 015°11.202’ E	Aug 2010 - Sep 2011
IFO	Southern Isfjorden proper	78°14.845’ N; 015°19.870’ E	Sep 2016 - Mar 2017
AF	Isfjorden-Adventfjorden	78°15.636’ N; 015°10.698’ E	Sep 2011 - Sep 2012
IF	Isfjorden-Sassenfjorden	78°19.129’ N; 015°34.643’ E	Oct 2013 - Jan 2014
TF	Inner Tempelfjorden	78°26.606’ N; 017°21.269’ E	Jan 2016 - Jun 2017
BF	Inner Billefjorden	78°39.760’ N; 016°41.247’ E	Sep 2008 - Aug 2009
		78°39.800’ N; 016°41.500’ E	Oct 2010 - Aug 2011
		78°39.799’ N; 016°41.283’ E	Sep 2011 - Sep 2012
		78°39.340’ N; 016°41.329’ E	Oct 2012 - Sep 2013
DF	Outer Dicksonfjorden	78°39.294’ N; 015°18.606’ E	Oct 2016 - Sep 2017

3.2.1 Combined time series at I-S

The yearly temperature and salinity time series from mooring I-S (Table 3 and Table S3 in Supplementary data) since 2010 were combined to obtain a depth-resolved daily time series at I-S spanning from September 2010 to October 2017. The data were first interpolated to every hour in time and to every meter in depth between the upper and lower instruments, and then extrapolated to surface and bottom at 205 m depth. Missing data points were replaced by linear interpolation of the nearest known data points. The hourly and 1 m depth-resolved time series were then combined to form the full time series. Time series of presence and vertical distribution of water masses at I-S were obtained from the combined depth-resolved time series of temperature and salinity by following the characteristics in Table 1. Daily averages of the constructed time series were obtained for plotting.

3.2.2 Combined times series at IsA

To obtain a one year longer depth-resolved time series at IsA spanning from September 2010 to October 2017, temperature and salinity time series from mooring ALKE (Table 4 and Table S4 in Supplementary data) were combined with the hydrographic profiles taken at IsA (Section

3.1.2). The ALKE data were first interpolated to a daily time resolution and to every meter in depth, and the 1 m depth-resolved IsA profiles were also interpolated to a daily time resolution. Then these interpolated time series were combined to form the full time series at IsA. Time series of presence and vertical distribution of water masses at IsA were obtained as for I-S.

3.2.3 Mean currents

For every mooring position (Table 3 and Figure 1b) the mean current over each deployment period was obtained. For moorings I-S, I-N and BF several yearly mean currents were then obtained. Before the estimation of the mean current at moorings with current meter profilers or several current meters over the mooring depth (all except TF and DF; see Tables S3 and S4 in Supplementary data), the current time series were interpolated to the same time interval (hereafter described as synchronised) over depth and then depth-averaged.

3.2.4 Concurrent time series from several locations in winter

Temperature and salinity time series from December to May from moorings with concurrent deployment periods were extracted for investigation of signal propagation in temperature and salinity in Isfjorden. Each deployment period since 2010/2011 have had several moorings in the Isfjorden system at the same time except for the period 2014/2015 (see Table 3). The time series from each of the relevant moorings were first synchronised over depth and then depth-averaged. For mooring BF, only the time series above sill depth were considered. Sub-tidal variability and variability on timescales less than 3 days were smoothed out with a 72-hrs low-pass filter.

3.3 Depth-averaged current (DAC)

3.3.1 Glider data

Glider-based surveys of the Isfjorden system were carried out in both November 2014 and November 2016 as part of UNIS student courses in collaboration with the Norwegian National Facility for Ocean Gliders (NorGliders). The instruments provided temperature, salinity, and

depth-averaged current (DAC) data along the conducted glider tracks. In November 2014, a 200m rated Slocum glider made in total five sections in the Isfjorden system, and a second 1000m rated Slocum glider took a section along the approximate centreline of Isfjorden. Fraser et al. (2018b) give a detailed account of the 2014 glider mission. The 200m rated Slocum glider deployed in November 2016 made in total 13 sections in Isfjorden proper and in Nordfjorden. Details of both deployments are listed in Table S5 in Supplementary data.

As gliders have no GPS information while submerged, they navigate underwater using a "dead reckoning" method and a magnetic compass. After each dive, the discrepancy between the predicted and actual surfacing location is attributed to advection and used to infer the depth-averaged current in the water column over the course of the dive. Barotropic tidal velocities were calculated at the mid-point (and mid-time) of each dive using the 5 km Arctic Ocean Tidal Inverse Model (AOTIM-5; Padman and Erofeeva, 2004) and subtracted from the DACs in order to eliminate tidal signal. Analysis by Fraser et al. (2018b) indicates that the approach will act to reduce the tidal signal in the DAC data, particularly away from coastal boundaries, though it may not be fully eliminated (roughly 50% of the full amplitudes). According to Merckelbach et al. (2008), the error in DACs from gliders may be up to 2-3 cm s^{-1}.

3.3.2 Vessel-mounted ADCP data

DAC data were retrieved from a 75 kHz RDI vessel-mounted acoustic Doppler current profiler (VM-ADCP) mounted on R/V Jan Mayen during a campaign in Kongsfjorden and Isfjorden from 25 to 29 July 2007. Six sections were obtained on 29 July from the Isfjorden mouth area towards Isfjorden proper (see Table S6 in Supplementary data). By using the log data from the on-board gyro, the velocity components were found from the acoustic signals reflected by plankton (krill and alike about 1 cm in length) floating in the water column. The water column was divided into 4 m bin cells; hence a smoothing was applied on the data in order to highlight the current features.

Only measurements below 32 m depth were used due to erroneous data above. The DACs were averaged over; 1) 30 to 100 m depth; 2) 100 m depth to bottom. Barotropic tidal velocities from AOTIM-5 (Padman and Erofeeva, 2004) were then removed from the DACs.

3.4 Sea surface temperature

To relate sea surface temperature (SST) with heat content in Isfjorden, daily SST data from the area 13-16.05°E and 78.02-78.50°N with a resolution of 1/20° (~6 km), and the time period 1987 to 2017 were downloaded from the Operational Sea Surface Temperature and Sea Ice Analysis (OSTIA; Donlon et al., 2012). The SST data showed that the data point closest to Station 34 (SST_{St34}) in the Isfjorden Transect was representative for the other points in Isfjorden proper, whereas the data point closest to Station 41 (SST_{St41}) by the Isfjorden Mouth showed similar values to the inner shelf points. The positions of SST_{St34} and SST_{St41} were 78º 16.5' N; 015º 16.5' E and 78º 04.5' N; 013º 31.5' E, respectively. Unrealistically low values were set to -1.9°C as they occurred during near freezing temperatures. On average, the analysis error in the SST data is from ±1.2ºC in July to ±1.7ºC in March at SST_{St41} and from ±1.5ºC in September to ±2.0ºC in March at SST_{St34}. The summer values at SST_{St34} before 2007 seemed unrealistic and were not used, but from 2007, the data quality improved especially inside Isfjorden. The daily SST_{St34}, representing Isfjorden proper, and the daily SST_{St41}, representing the Isfjorden Mouth, were averaged over the winter (January-May) and summer (July-September) months for each year.

3.5 Meteorological data

Wind speed and direction (10 m above sea level) every six hours for sea surface points over Isfjorden proper were obtained from the Norwegian Reanalysis Archive (NORA10; Reistad et al., 2011) to compare with interannual variability in local mean air temperature. NORA10 is a high resolution (10-11 km) downscaling of ERA-40 (Uppala et al., 2005) and ECMWF IFS (European Center for Medium-Range Weather Forecasts Integrated Forecasting System)

operational analyses (after 2002), covering the northern North Atlantic. The six hourly data were averaged over the extracted data points, and further averaged over the winter (January-May) and summer (July-September) months for each year in the time period 1987 to 2017.

To demonstrate the interannual variability and trends in local mean air temperature, near surface (2 m above sea level) air temperature data every six hours from the meteorological stations at Isfjord Radio and Svalbard Airport (Figure 1b) were extracted from the eKlima database at the Norwegian Meteorological Institute. As for the NORA10 data, the six hourly data were averaged over the winter and summer months for each year in the time period 1987 to 2017.

3.6 Sea ice index

To relate interannual variability and trends in local atmospheric forcing and hydrography with sea ice cover in Isfjorden, the sea ice index for Isfjorden by Muckenhuber et al. (2016) was used. The sea ice index indicates the days of fast ice (DFI) cover, i.e. sea ice attached to the coastline, in Isfjorden from 1 March to the end of the freezing period each year from 2000 to 2014. The index is based on manual interpretations of sea ice conditions (fast ice, drift ice and open water) from satellite images and ice charts displaying the area of Isfjorden.

4 Analysis methods

4.1 Annual mean hydrographic profiles

To obtain one mean temperature and salinity profile for each winter (January-May) and summer (July-September), hydrographic profiles reaching deeper than 100 m were extracted from UNIS HD inside the area 14.1-16.1°E and 78.1-78.6°N (inside Isfjorden proper) and in the time period 1987 to 2017. For some summers, data from early October were included to get enough data. The averaged profiles were then extrapolated to surface and to 250 m to obtain equal length profiles. Further, the extrapolated profiles were smoothed with a low-pass filter to reduce any

noise. One annual mean profile was obtained for all summers except for 1989, 1997, and 2001, and only for winters since 1999 with the exceptions 2000, 2002, and 2009. The mean profiles were regarded as representative for the Isfjorden proper and were estimated from at least one profile in the central basin, but mostly from more than 10 profiles (more in summer than winter) distributed as seen in the inserted maps in Figures S.7 to S.12 in Supplementary data.

As a measure of interannual variability in heat and freshwater content in Isfjorden, the volume weighted mean temperature and salinity for Isfjorden were obtained from the winter and summer mean temperature and salinity profiles by weighting the mean profiles with the volume of Isfjorden proper every meter. The hypsometry and volume of Isfjorden proper were obtained from Nilsen et al. (2008a).

To study the effect of winter convection and the inflow of AW on interannual variability and trends in the mean summer ocean structure in Isfjorden, the annual mean summer presence and vertical distribution of water masses were found, based on the water mass characteristics in Table 1. From this, the annual mean summer fraction of AW and TAW occupying the water column in Isfjorden proper was estimated.

To identify any inflow pattern of AW to Isfjorden both in winter and summer, temperature and salinity profiles reaching deeper than 100 m within the area 14.1-14.7°E and 78.1-78.16°N (around Stations 38 and 39) at the southern side of the entrance, and the area 15-15.4°E and 78.2-78.3°N (around Stations 34 and 35) on the southern side in Isfjorden proper, were extracted from UNIS HD. These areas were chosen as they represent the outer and inner part of the potential inflow path of AW to Isfjorden proper. Each profile was further interpolated to every meter and smoothed with a low-pass filter to reduce any noise. Finally, these profiles were used to obtain

annually averaged profiles for the entrance and Isfjorden proper over the end of winter (April-May) and the summer (July-early October) during the time period 1987 to 2017. Winters with profiles in the entrance area were fewer than in the Isfjorden proper area.

To get annual characteristics of WCW, temperature and salinity profiles, taken in the deepest part of Billefjorden (around Station 3) in summer (July-September), were also extracted from UNIS HD during the time period 1987 to 2017. Typically, at least one profile was obtained each year in August-September since 1999, but for summers with several existing profiles, the earliest of these was chosen as the representative profile. Based on years with several profiles during summer, changes in WCW characteristics below the sill due to mixing and outflow during August and September seem to be insignificant.

4.2 Section averaging and interpolation

To reveal interannual variability and trends in the depth reach of the winter convection and inflow pattern of AW to Isfjorden, all available hydrographical profiles within a distance of ±0.05° latitude from the Isfjorden Transect (Table 2 and Figure 1b) were used to obtain annual mean winter (January-May) and summer (July-early October) hydrographic sections from 1987 to 2017. The number of profiles available for the winters and summers with good enough data coverage to create interpolated sections along the Isfjorden Transect, is given in Table S2 in Supplementary data. In total, 23 annual mean summer sections and 16 annual mean winter sections (since 1999) could be obtained. The profiles were first bin-averaged with the bin centres at the positions of the Isfjorden Transect, and the bin size in the longitudinal direction was the half distance between two neighbouring bin centres. At the end points of the Isfjorden Transect, profiles within 0.3° west (east) of the western (eastern) bin centre were included in the bin average. Each profile was weighted with its distance to the bin centre in order to produce weighted bin-averaged sections of temperature, salinity, and potential density anomaly with 1m

vertical resolution. The weighted bin-averaged sections were then interpolated onto a 500m horizontal times 1m vertical grid resolution using the kriging interpolation method from Golden Software Surfer 12 through the matlab function surfergriddata.m using Matlab version R2013b. Finally, the interpolated sections were smoothed vertically with a low-pass filter to reduce any remaining noise.

For mean sections over the time period 1987 to 2017, only bins with more than 7 years represented (to avoid any biases) were used in the kriging interpolation. For sections averaged over years with specific winter types (Winter Deep, Intermediate, and Open), only bins with more than 4 years represented were taken into account. For the open winter type, the limit was set to 2 years to get sufficient amount of data to create kriging interpolated sections. Winters and summers with good enough data coverage to create interpolated sections along the Isfjorden Transect, their number of included profiles, and their winter types are listed in Table S2 in Supplementary data.

Water mass sections were obtained from the interpolated sections of temperature and salinity by following the characteristics in Table 1. Similar hydrographic and water mass cross sections at the mouth and in Isfjorden proper (Figure 1b) were also obtained from available hydrographic profiles within a distance of ±0.5° longitude from the sections.

4.3 Fresh water content

The horizontal distribution of mean freshwater content in Isfjorden was estimated from salinity profiles over summers (July to early October) in the time period 1987 to 2017, and over summers following the three winter types (see Table S2 in Supplementary data). The freshwater content (FWC) in each salinity profile were estimated from

$$\mathrm{FWC} = \int_{z_1}^{z_2} \frac{(\mathrm{S_r} - \mathrm{S(z)})}{\mathrm{S_r}} \mathrm{dz} \ ,$$

where S(z) is the salinity profile with 1m resolution from bottom z_1 to surface z_2, and the reference salinity S_r is set to 34.9, which is the salinity limit for pure inflowing Atlantic Water to Isfjorden (Table 1). To avoid negative contributions, salinity values above 34.9 were set to 34.9. A weighted bin-averaged horizontal distribution of the freshwater content was then estimated on a 0.1° longitude times 0.02° latitude grid resolution, where each profile was weighted with its distance from the bin centre it belonged to. Further, the weighted bin-averaged freshwater content with only bins with more than 7 years represented (to avoid any biases), was interpolated onto a 4 times finer grid using the kriging interpolation method described in Section 4.2. In both grids the land points were excluded. Similarly as for the mean vertical sections, 4 and 2 years were required for producing the horizontal kriging interpolated distribution of freshwater content averaged over summers after specific winter types (see Table S2 in Supplementary data).

4.4 Monthly climatological time series

Monthly climatological time series of temperature, salinity, and the velocity components at I-S were obtained by taking the monthly average over all the yearly depth-averaged time series from 2005 to 2017 (see Table 3). The deviation from this monthly climatology was then found for the monthly averaged time series of temperature, salinity, and the velocity components for each year-long time series.

4.5 Atlantic Water index

Atlantic Water (AW) indexes, one for the Isfjorden Mouth (I-S) and one for Isfjorden proper (IsA), were obtained from the combined depth-resolved temperature and salinity time series at I-S (Section 3.2) and IsA (Section 3.1.2), respectively, based on the method provided by Tverberg et al. (2019) for another western Spitsbergen fjord. In our study, the AW index was defined as the fraction of the 205m deep water column occupied with AW (T > 3°C and S >

34.9) times the mean temperature of this AW. Since AW normally gets modified from I-S to IsA, the index at IsA was based on the fraction of both TAW and AW (i.e. T > 1°C and S > 34.7) occupying the 90m deep water column there. The product of the depth fraction and the mean AW temperature was then estimated for each time step at I-S (hourly) and IsA (daily). By taking the monthly mean of this product, the monthly AW indexes for I-S and IsA were obtained.

4.6 Tidal analysis

Harmonic analysis for tidal components were performed using the Matlab t_tide function of Pawlowicz et al. (2002) on pressure and depth-averaged current time series over the measured periods of each deployment. The deepest pressure time series were used from each mooring. The tidal predictions were based on the most significant tidal components that appeared with a signal to noise ratio above 2, ignoring the seasonal components. The tidal ellipse of the semi-diurnal component M2 was obtained for each mooring deployment, based on output from the harmonic analysis on the depth-averaged current time series.

5 Results and discussion

Here, interannual variability and trends in winter and summer hydrography are presented in relation to atmospheric forcing and sea ice cover. The variability in hydrography and water mass distribution is further related to the winter convection types and corresponding inflow pattern of AW to Isfjorden. Moreover, the general circulation in Isfjorden is described from hydrography and supported by current data from moorings, gliders and VM-ADCP. The tidal contribution to the fjord circulation is also found and presented. Finally, propagation of AW signals in winter, following the general circulation pattern in Isfjorden, are traced from concomitant hydrographic time series from several locations during winter. All presented salinity data are in practical salinity unit.

5.1 Variability and trends in hydrography

5.1.1 Annual mean summer temperature and salinity profiles

Annual time series of the mean summer temperature and salinity profiles during 1987 to 2017 reveal large interannual variability over depth (Figure 2). The mean water column in Isfjorden had temperatures generally above 0°C in summer, but with exceptions (i.e. 1988, 1992, 1993, 1995, 1998, 2003, 2004, 2008, and 2010) when parts of the mean water column were colder. Isfjorden was coldest and least saline in summer 1993, and warmest and most saline in summer 2014. Other warm and relatively saline summers were 1991, 2002, 2006, and 2017.

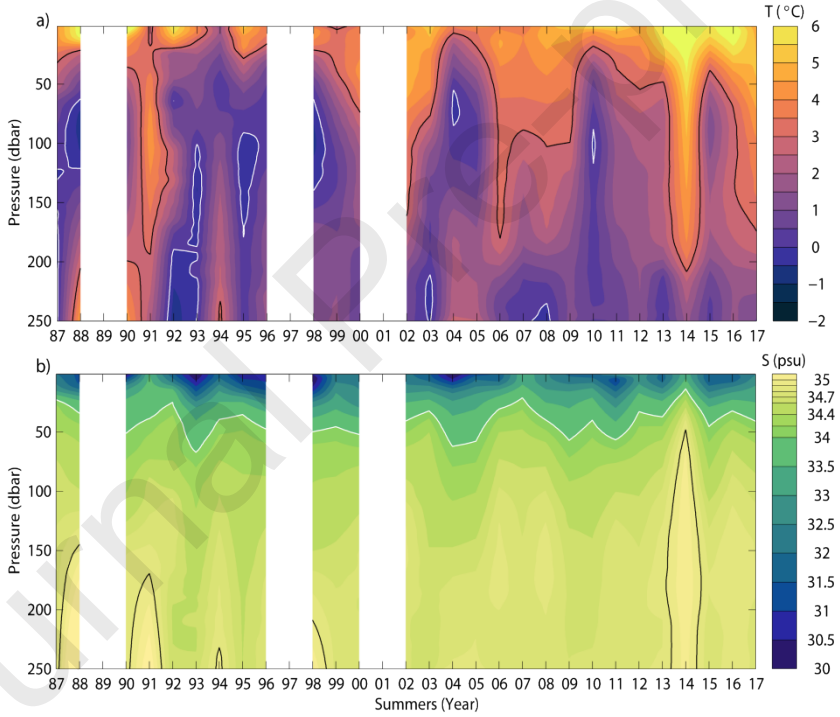

Figure 2: Time series of mean summer (July-September) profiles of a) temperature and b) salinity based on profiles deeper than 100 m from Isfjorden proper during the time period 1987 to 2017. The black (white) lines indicate the 3°C (0°C) isothermal and the 34.9 (34) isohaline.

The warm and low salinity surface layer (T > 1°C, S < 34) varied in thickness between 20 and 70 m (white line in Figure 2b), with the thinnest, warmest (T ≈ 6°C), and most saline (33 < S <

34) layer in 2014, and the thickest, quite cold (T < 4°C), and least saline (30 < S < 34) layer in 1993. In general, the surface layer became warmer and more saline from summer 2006 and onwards. The intermediate layer (down to ~150-200 m depth) varied between cold and relatively less saline water (T < 0°C and 34 < S < 34.7), and relatively warm and more saline water (T > 4.5°C and S > 34.9). Also here, it became generally warmer and more saline from 2006, but with some exceptions (2010 and 2015 with colder and less saline water; 1991 and 2002 with warmer and more saline water than in the pre 2006 period). The mean temperature and salinity over 100-200 m depth increased from respectively 1.1°C and 34.66 over the pre 2006 period to 2.3°C and 34.77 over the period after 2006. At the same time, the bottom layer (below ~200 m depth) changed oppositely to the intermediate layer and became colder and less saline from 2006, but with the exceptions 1992, 1993, and 2003 with the coldest and least saline water at the bottom in the whole studied period. The mean temperature and salinity below 200 m depth decreased from respectively 1.3°C and 34.80 over the pre 2006 period to 1.0°C and 34.78 over the period after 2006. The bottom layer was generally warmer and more saline than the intermediate layer in the summers before 2006, whereas in the post 2006 period the intermediate layer was warmer and more saline than the bottom layer.

These observations suggest the following two summer modes in Isfjorden; 1) Pre 2006, a warm and low salinity surface layer on top of a cold and more saline intermediate layer, which again overlies a warmer and the most saline bottom layer; 2) Post 2006, a warmer and slightly saltier surface layer over a warm and the most saline intermediate layer, which overlies a colder and less saline bottom layer. Later we will demonstrate that the first mode is related to the winter convection type Winter Intermediate, whereas the second mode is related to Winter Deep or Winter Open.

5.1.2 Connectivity to local atmospheric forcing and sea ice cover

As demonstrated in Figure 3, the variability in hydrography can to some extent be linked to local atmospheric forcing and the sea ice cover in Isfjorden. The mean wind speed over Isfjorden varied between 4.5 m s^{-1} (2003) and 5.8 m s^{-1} (1995) in winter, and between 2.8 m s^{-1} (2006) and 4.2 m s^{-1} (1994) in summer, and was on average 1.7 m s^{-1} stronger in winter than in summer (Figure 3a). This implies that Isfjorden was more influenced by wind mixing in winter than in summer. The mean wind direction in winter varied from mostly northeasterly to southeasterly (blue arrows in Figure 3a). This is in accordance with the dominating wind direction over Svalbard, which is northeasterly in winter (Skeie and Grønås, 2000). In summer, the mean wind direction over Isfjorden was more variable (red arrows in Figure 3a).

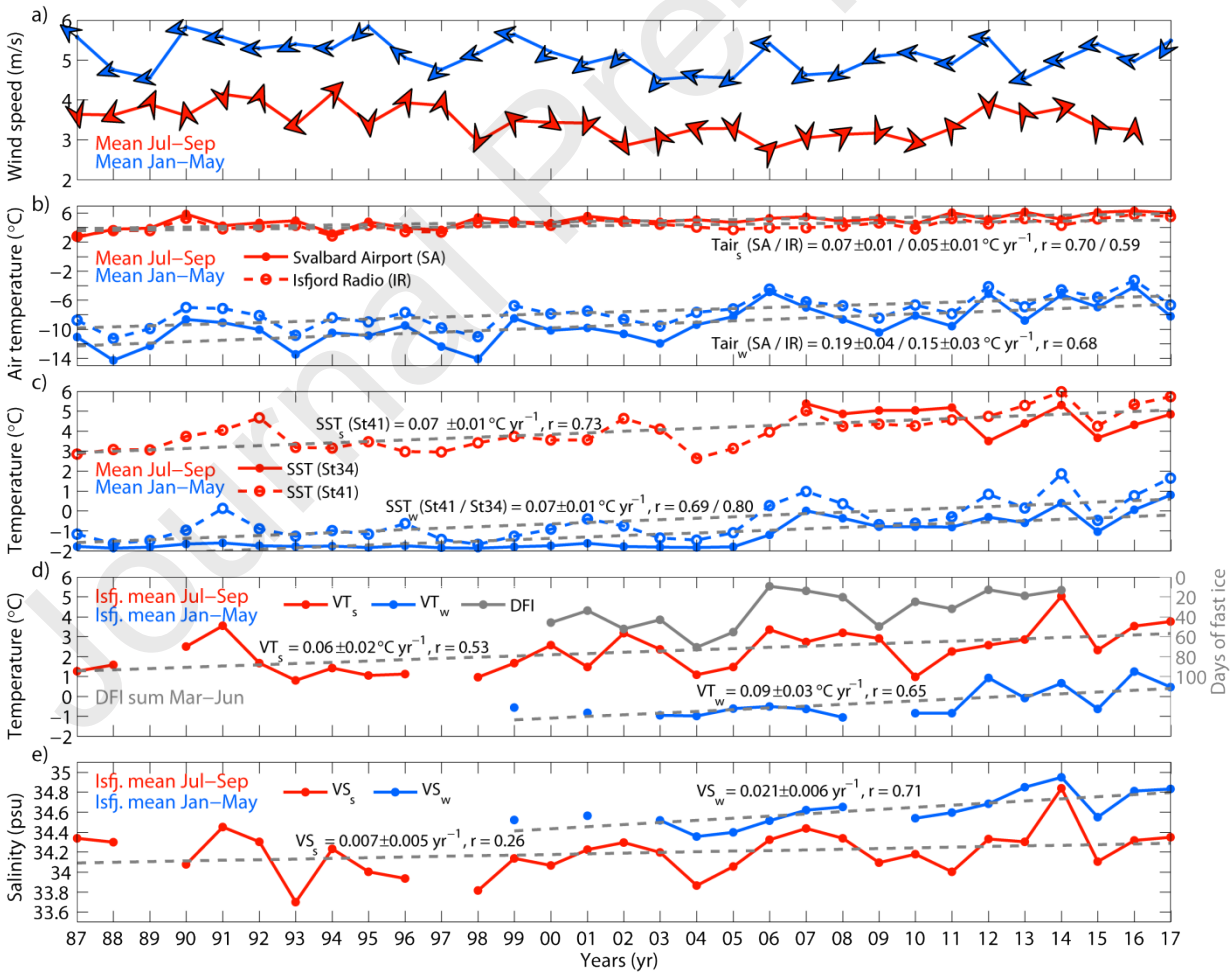

Figure 3: Annual mean winter (blue) and summer (red) time series of a) 10m wind speed and direction (arrows) from averaged NORA10 data points over Isfjorden proper, b) 2m air temperature at Svalbard Airport (solid line) and Isfjord Radio (stippled line), and c) OSTIA sea surface temperature in Isfjorden (SST_{St34}) and at the mouth (SST_{St41}) during 1987 to 2017. Annual volume weighted mean d) temperature (VT) and e) salinity (VS) from summer (red) and winter (blue) CTD profiles deeper than 100 m from Isfjorden proper for the same period as in a) to c). Also shown in d) are days of fast ice (DFI) in Isfjorden from March to June each year from 2000 to 2014 (grey line, reversed axis). Winter (w) and summer (s) trends (per year) are indicated by the grey stippled lines, with the slope values (± errors) and correlation coefficients (r) given in the corresponding panels.

Over the studied time period, the mean air temperature at both Svalbard Airport and Isfjord Radio increased by respectively 1.9 ± 0.4°C and 1.5 ± 0.3°C per decade in winter, and 0.7 ± 0.1°C and 0.5± 0.1°C per decade in summer (Figure 3b). This is in accordance with the published long-term trend in the extended Svalbard Airport air temperature data series (Nordli et al., 2014). Since Isfjord Radio is more influenced by the shelf and open ocean and Svalbard Airport by land, the mean air temperature was higher (0.4-3.1°C warmer) at Isfjord Radio than at Svalbard Airport in winter, and opposite (0-1.5°C colder) in summer. The warmest winters were 2006, 2012, 2014, and 2016 with the smallest differences between Isfjord Radio and Svalbard Airport, whereas the coldest winters were 1988, 1993, and 1998 with the largest differences between the two stations. The smaller (larger) differences in the warmest (coldest) winters most likely reflect winters with less (more) sea ice cover in Isfjorden which increased (decreased) the heat exchange from the fjord to the atmosphere. Due to the more rapid warming at Svalbard Airport than at Isfjord Radio, the difference in mean winter air temperature between Isfjord Radio and Svalbard Airport decreased over the studied time period, whereas in summer the difference slightly increased.

This implies that the mean air temperature over Isfjorden proper became more equal to the mean air temperature on the shelf in winter and even warmer than on the shelf in summer.

The mean winter air temperature seemed to follow the wind direction with higher air temperatures in winters dominated by strong southeasterly and easterly winds, and lower air temperatures in winters dominated with northeasterly winds (Figure 3a and b), but was not significantly correlated ($r = 0.26$; $p = 0.15$). This may be linked to the winter cyclone activity around Svalbard. Rogers et al. (2005) found that warmer winters typically have relatively more cyclone activity in the Fram Strait than in the Barents Sea and vice versa for colder winters. No similar connection between air temperature and wind direction existed in summer (Figure 3a and b). Over the studied period, no trend was seen in the mean wind speed and direction in winter or summer even though an increasing number of deeper low-pressure systems passing Svalbard in winter is found (Zahn et al., 2018). Hence, other factors explaining the positive trend in mean local air temperature need to be found.

A likely candidate to explain the increase in mean local air temperature is the mean sea surface temperature (SST; Figure 3c), which displays positive trends (0.7 ± 0.1°C per decade) both in Isfjorden (SST_{St34}) and at the mouth (SST_{St41}) in winter and summer (SST_{St41} only). In winter, the SST followed the mean local air temperature very closely both in Isfjorden ($r = 0.67$, $p = 4\times10^{-5}$) and at the mouth ($r = 0.77$, $p = 4\times10^{-7}$). A positive correlation was also found in summer at the mouth ($r = 0.61$, $p = 3\times10^{-4}$), opposed to no significant correlation in Isfjorden based on the data from 2007 to 2017.

The volume weighted mean temperature (VT; Figure 3d) also revealed a positive trend in winter (0.9 ± 0.3°C per decade from 1999), and seemed to follow the mean air temperature at Svalbard

Airport closely (r = 0.71, p = 0.002), especially during the last winters with little sea ice cover. SST well above the freezing point (-1.87°C for seawater with practical salinity of 34) in winter, indicates no or little sea ice formation, which is confirmed by a high correlation with the sea ice index (SST_{St41}: r = -0.85, p = 6×10^{-5}; SST_{St34}: r = -0.77, p = 8×10^{-4}), showing fewer days of fast ice (DFI) at the mouth and in Isfjorden in winters with warmer SST, and opposite in winters with colder SST. The mean SST and VT seemed to follow each other in winters with available data (SST_{St41}: r = 0.70, p = 0.003; SST_{St34}: r = 0.66, p = 0.005), indicating that increased VT (or heat content) and hence SST in Isfjorden, will reduce sea ice formation, and most likely increase the air temperature locally. The latter is supported by a significant negative correlation between the mean winter air temperature at Svalbard Airport and DFI (r = -0.71, p = 0.003). With less DFI from 2006 (Muckenhuber et al., 2016), the mean air temperature followed the mean SST more closely in these winters compared to the pre 2006 period.

In summer, the SST and VT in Isfjorden also show positive trends (SST_{St41}: 0.7 ± 0.1°C per decade; VT: 0.6 ± 0.2°C per decade; Figure 3c and d), but did not vary as coherently with the mean local air temperature (SST_{St41}: r = 0.61, p = 3×10^{-4}; VT: r = 0.59, p = 7×10^{-4}) as in winter. A twice as large positive trend in VT over the same period as in winter (1.2 ± 0.4°C per decade since 1999), indicates a stronger increase in heat content over the last two decades, but also shows that the trends over the whole studied period are influenced by the warm early 1990s. The mean SST_{St41} was between 0.3°C (2014) and 4.1°C (2010) warmer than the VT, but they seemed to follow each other's variation between most summers (r = 0.79, p = 4×10^{-7}). This reveals a warmer surface layer separated from a colder water column below. Notably in summer, the VT and the mean SST_{St41} seemed to partly follow the sea ice cover the preceding winter (VT: r = -0.49, p = 0.06; SST_{St41}: r = -0.69, p = 0.004), indicating a warmer water column and surface layer in Isfjorden in summers following winters with smaller DFI and vice versa.

The volume weighted mean salinity (VS; Figure 3e) showed positive trends in both winter (0.21 ± 0.06 per decade since 1999) and summer (0.06 ± 0.05 per decade; 0.15 ± 0.10 per decade since 1999), hence suggesting a tendency of higher salinity and warmer water in Isfjorden, especially in winter over the last two decades. As for the trend in VT, the trend in VS over the whole studied period seemed to be influenced by the saline early 1990s. The impact of warm and saline water on the sea ice cover in Isfjorden is supported by negative correlations between VS and DFI (winter: $r = -0.71$, $p = 0.01$; summer: $r = -0.72$, $p = 0.002$). The VS in winter was always higher than in summer for the years with available data, and the difference varied between 0.11 in 2014 when the salinity was highest, and 0.60 in 2011. Higher values in winter were expected due to the ceased freshwater supply and increased wind mixing in winter.

To summarize, the positive trend in local mean air temperature was possibly directly linked to the increased heat content in Isfjorden proper and the reduced sea ice cover. This was most likely due to advection of warmer and more saline water from the shelf originating from the WSC (Nilsen et al., 2016), as indicated by the increased VS. The interannual variability in local mean air temperature in winter was directly and indirectly linked to the mean wind direction, which is related to the path of passing low-pressure systems emanating from the North Atlantic, resulting in either cold or warm air masses advected over Svalbard. Warm southerly winds also accelerate the WSC and force warm and saline water to enter Isfjorden (Nilsen et al., 2016). This in turn reduces the sea ice cover, which again increases the local air temperature.

5.1.3 Mean presence and vertical distribution of water masses in summer

Local atmospheric forcing, sea ice production, and advection of water into Isfjorden are clearly connected. Nilsen et al. (2008a) have shown that cold winters with favourable wind conditions for strong sea ice production (like in a polynya situation) creates dense Local Water (LW) and

Winter-Cooled Water (WCW) that leads to inflow of Atlantic Water (AW) in intermediate layers the following summer, while warmer winters, or winters with less favourable wind conditions for effective sea ice production, both resulting in less sea ice production, creates lighter LW and WCW that leads to inflow of AW along the bottom. The mean presence of Transformed Atlantic Water (TAW) and AW in Isfjorden in summer (Figure 4a) varied between 0% (1987, 1993, 1995, 2003, and 2010) and 80% (2014), and could to some extent be linked to the DFI in Isfjorden ($r = -0.47$, $p = 0.07$). More AW was probably present in summers following winters with fewer DFI and vice versa, which is in line with the strong correlation of VT and especially VS with DFI.

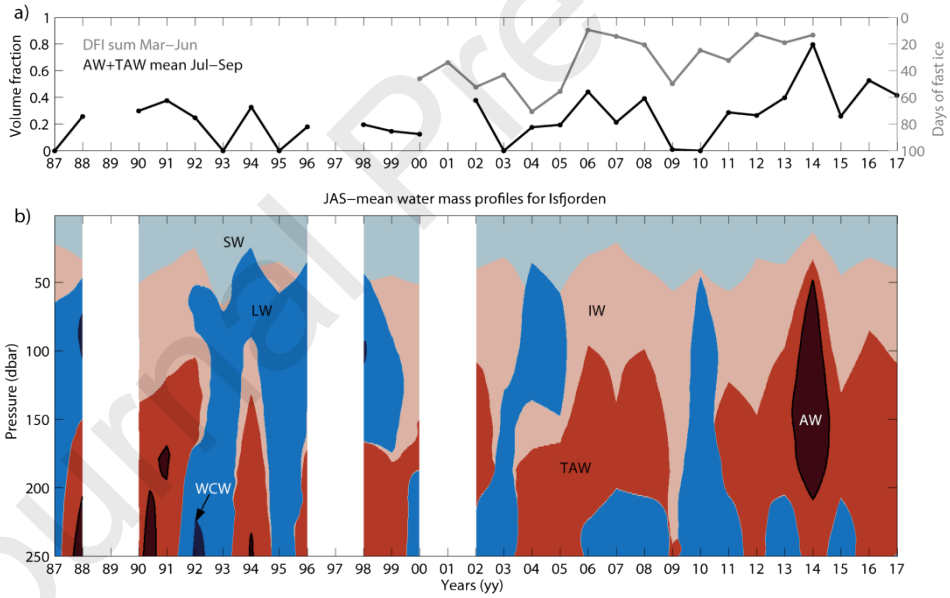

Figure 4: Time series of annual a) Atlantic Water (AW) and Transformed Atlantic Water (TAW) volume fraction (black line) and days of fast ice in Isfjorden (DFI, grey line), and b) water mass distribution from the mean summer temperature and salinity profiles reaching deeper than 100 m inside Isfjorden proper (see Figure 1) during the time period 1987 to 2017. The water masses indicated are listed in Table 1. Notice the reversed axis of DFI in a).

Three structures appear from the mean vertical distribution of water masses in summer (Figure 4b); 1) Surface Water (SW) over Intermediate Water (IW) with LW or WCW at the bottom, i.e. no TAW/AW; 2) TAW/AW at the bottom; 3) TAW/AW above LW, WCW or cold TAW at the bottom. Summers before 2006 seemed more dominated by the first and second structures, whereas summers from 2006 were more dominated by the third structure. Hence after 2006, AW was present higher up in the summer water column in Isfjorden, indicating inflow of AW at intermediate depths due to denser LW being produced in winter. This also happened, to a varying degree, in the pre 2006 period (1991, 1992, 2000, and 2002), but the general structure was TAW and AW in the deepest part of Isfjorden when they were present.

5.1.4 Annual mean winter profiles at the entrance and in Isfjorden proper

The three water mass structures in summer seem to be the result of domination of one of three winter processes during winter giving different densities of the LW and WCW. Mean temperature and salinity profiles at the entrance and in Isfjorden proper in winter (Figure 5) indicate three different winter inflow pattern of warm water of Atlantic origin; 1) no inflow of warmer water, where profiles at the entrance and in Isfjorden proper showed a cold water column and increasing salinity with depth resulting in dense LW (2001, 2003, 2006, and 2015), or alternatively, cold and very saline water through the whole depth suggesting that cooled TAW or AW (from inflow during previous fall) had been transformed to the densest LW (2013, 2014, and 2016); 2) inflow of warmer water along the bottom, where profiles showed cold and low salinity water in the surface and increasing values with depth, reaching towards the characteristics of TAW and AW at the bottom, but through those of less dense LW at intermediate depths (2004, 2005, 2010, 2011, and 2012); and 3) inflow of warmer water at intermediate depths, where profiles had cold and low salinity water in the surface with increasing values with depth down to intermediate depths, here reaching the characteristics of TAW and AW, and then decreasing temperature with depth resulting in dense LW at the bottom (2007,

2008, and 2017). In winter 2003 and 2015, warm TAW was present at the entrance, but did not reach Isfjorden proper.

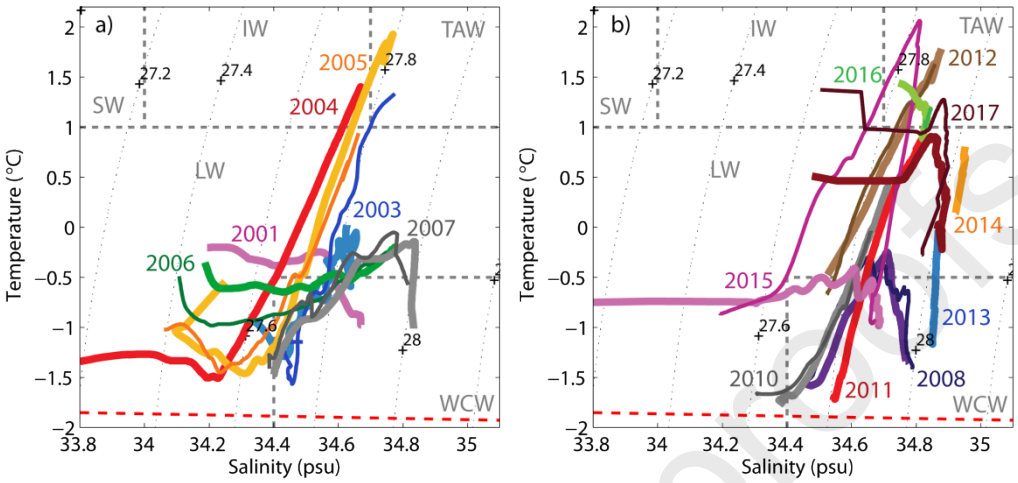

Figure 5: Temperature and salinity diagrams with the mean winter profiles from an area around Stations 38 and 39 at the entrance (thin solid line with darker colour tone) and Stations 34 and 35 in Isfjorden proper (thick solid line with lighter colour tone) for a) winter 2001 to 2007 and b) winter 2008 to 2017. No profiles were available at the entrance in 2001, 2004, 2011, 2013, and 2014. Water masses are indicated by the grey dotted lines, and the freezing point temperature is given by the red dotted line.

Three winter types with different winter water production mechanisms were introduced by (Tverberg et al., 2019) to explain similar inflow regimes in Kongsfjorden. *Winter Deep* describes winters with strong heat flux to a cold atmosphere, accompanied with effective sea ice formation and salt input, producing dense LW and WCW reaching the bottom of Isfjorden. *Winter Intermediate* describes winters with weaker heat flux due to more fast ice cover or a less cold atmosphere, and hence less effective sea ice formation. The resulting lighter LW or WCW will not be able to displace the existing water at the bottom where inflow of TAW with higher density will take place. *Winter Open* describes winters with only thermal convection of cooled TAW

that has entered Isfjorden before the cooling starts, and no sea ice is formed. These winters produce the densest winter water displacing the water at the bottom, and only winters with very strong heat flux and large sea ice formation can produce equally dense WCW.

Winter Deep and Winter Open will hinder inflow of Atlantic type water to Isfjorden due to denser water in the fjord, and when it happens, it will be in intermediate (Winter Deep) or shallower (Winter Open) depths, where the density matches the fjord water density. Hence in some deep winters, warm water can be present high up in the water column delaying or hindering any further sea ice formation. Winter Intermediate will allow inflow of denser TAW or AW along the bottom, and hence being separated from the surface layer and the sea ice. Based on the above, Figure 5 indicates that winters 2001, 2003, 2006-2008, and 2015 were Winter Deep, winters 2004, 2005, and 2010-2012 were Winter Intermediate, and winters 2013, 2014, 2016, and 2017 were Winter Open. Isfjorden has changed in the last decades in winter from being an Arctic type fjord with sea ice and limited or deep inflow of TAW (dominated by Winter Intermediate and Deep) to a more Atlantic type fjord with no sea ice and occasional inflow of TAW higher up in the water column (dominated by Winter Open).

5.1.5 Isfjorden Transect: temperature, salinity, and density

5.1.5.1 Winter and summer mean (1987-2017)

In view of the mean winter sections over the 1987-2017 time period (Figure 6a-c), the mean winter hydrography of Isfjorden was dominated by Winter Deep and Intermediate. Winter water with temperatures below 0.5°C and salinities below 34.8 was on average present in the whole fjord. The warmest and most saline water (T > 0°C and S> 34.7) was on average at the bottom of Isfjorden, reflecting the importance of Winter Intermediate over the years with available data in winter (Table S2 in Supplementary data). Notably, warm and saline water (T > 1°C and S> 34.8) was present at the mouth (Station 41). On average, the potential density anomaly (density

hereafter) was 27.7-28 kg m^{-3} in the intermediate and bottom layer in Isfjorden, and above 28 kg m^{-3} below sill depth in Billefjorden. The density at the mouth of Isfjorden was on average below 27.9 kg m^{-3} in winter, and was equally dense as the mean bottom water in outer Isfjorden, but less dense than the bottom water in inner Isfjorden.

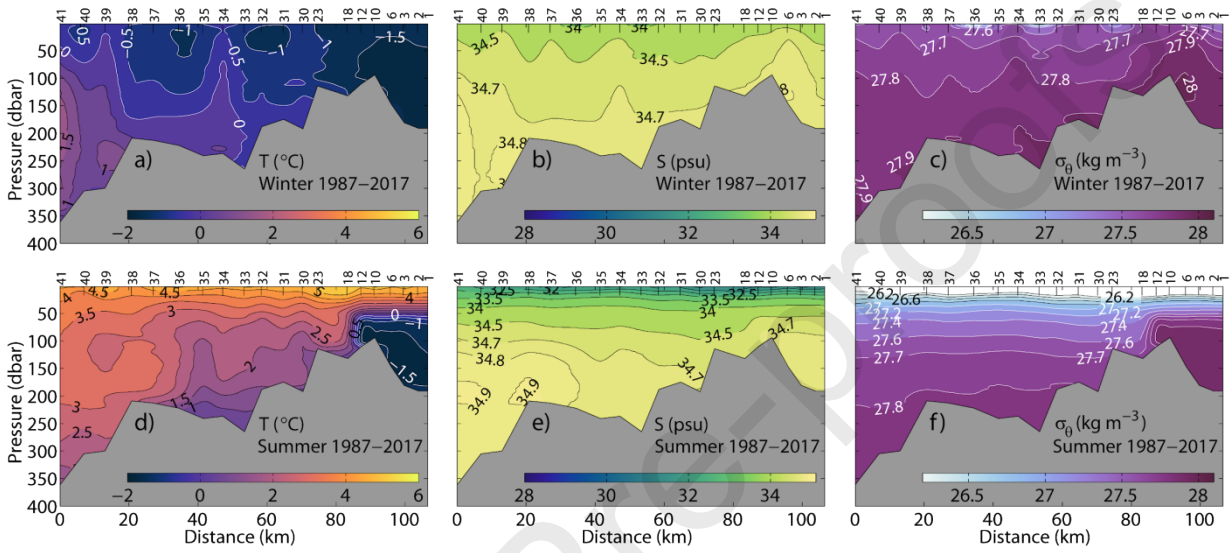

Figure 6: Distribution of mean a) and d) temperature, b) and e) salinity, and c) and f) density along the Isfjorden Transect from the mouth area (Station 41) to the head of Billefjorden (Station 1) over all available years in the time period 1987-2017 for a) to c) the winter months (Jan-May) and d) to f) the summer months (Jul-Sep).

The mean situation in summer (Figure 6d-f) reveals a strong stratification in temperature, salinity, and density with warm and less saline water visible in the upper 40-50 m of the section, while colder and more saline water occupied the bottom layer. Cold (T < -1.5°C) and dense water was on average still present behind the sill in Billefjorden (Stations 1 to 18) in summer, and warm and saline water (T > 3°C; S > 34.8) was present at the mouth and the entrance of Isfjorden. TAW and AW are expected to flow into Isfjorden at intermediate depths in summers after Winter

Deep and along the bottom after Winter Intermediate. The mean picture over all summers evened out these two distinct patterns.

5.1.5.2 Winter and summer mean over winter types

To classify the effect of each winter type on the hydrography of Isfjorden the following summer, the winter sections along the Isfjorden Transect were classified as Winter Deep, Winter Intermediate, or Winter Open, and the following summer sections were classified accordingly. Some years only had summer sections, and they were classified according to their observed patterns (Table S2 in Supplementary data).

A clear pattern for each winter type is revealed from the averaged sections (Figure 7). Every winter and summer section are shown in Figures S1 to S6 in Supplementary data. Deep winters (Figure 7a-c) show cold water ($T < -0.5°C$) over the whole fjord-depth with increasing salinity ($34 < S < 34.8$) with depth. The coldest and most saline water was inside Billefjorden, and some patches of relatively warmer water ($T > -0.5°C$) is seen in intermediate depths inside Isfjorden. Warm and saline water ($T > 1°C$; $S > 34.8$) occupied the mouth area. A horizontal density gradient is observable especially in the lower layer with increasing density towards Isfjorden proper and less dense water at the mouth at similar depths. The densest water ($28 < \sigma_\theta < 28.05$ kg m^{-3}) occupied Billefjorden below sill depth. Intermediate winters (Figure 7d-f) reveal the coldest and least saline water ($T < 0°C$; $S \sim 34.5$) in a well-mixed water column down to ~100 m depth, and then gradually warmer and more saline water appears with depth. At the mouth, warm and saline water was mostly present at the bottom, and no clear horizontal density gradients are observable. Unfortunately, no profiles were taken inside Billefjorden in intermediate winters, and hence the horizontal lines appear from Stations 18 to 1. Open winters (Figure 7g-i) showed the most homogenized, warmest, most saline, and densest ($0.5 < T < 1°C$; $S > 34.8$; $\sigma_\theta > 27.90$ kg m^{-3}) water column. The whole water column was occupied with even warmer and more saline

water (T > 1.5°C; S > 34.9) than in deep winters at the mouth, and some patches of similar water are seen close to surface in inner Isfjorden proper. The coldest and most saline (T < 0.5°C; S > 34.9) water is seen in the bottom layer, and despite a warmer Isfjorden proper, the water behind the sill in Billefjorden was still cold with high salinity and density (σ_θ > 28.05 kg m^{-3}). Billefjorden was clearly protected by the sill, and the convection was in addition more effective due to the shallower depths.

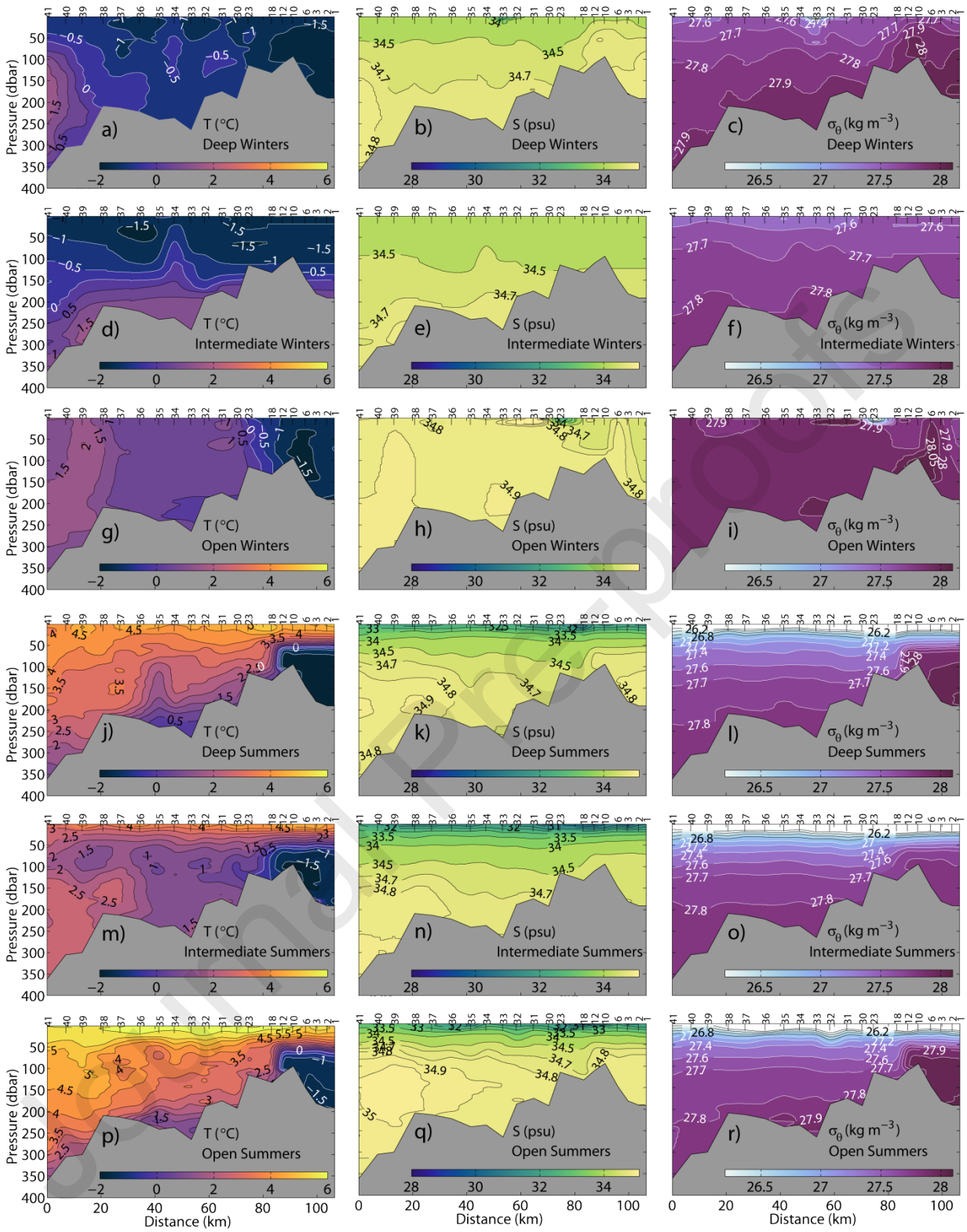

Figure 7: Distribution of mean a)-p) temperature, b)-q) salinity, and c)-r) density along the Isfjorden Transect from the mouth area (Station 41) to the head of Billefjorden (Station 1) over Winter a)-c) Deep, d)-f) Intermediate, and g)-i) Open, and over j)-r) corresponding following summers.

Summers following deep winters (Figure 7j-l) revealed strong stratification in temperature, salinity, and density with a warm (T > 4°C) surface layer reaching down to 30-40 m depth. The intermediate layer was also warm and with increasing salinity with depth until ~200 m depth. At this depth, patches of warm and high salinity water (S > 34.9) were seen at the mouth and entrance of Isfjorden. Below this depth, salinity decreased, and temperatures were less than 1°C inside Isfjorden. No horizontal density gradients are seen except in the bottom layer with denser water inside Isfjorden than at the mouth at equal depths. Cold, saline, and dense water was still present behind the sill in Billefjorden, which was also the case for the summers following the other winter types. The surface layer was colder and thicker reaching down to 40-50 m depth in summers following Winter Intermediate (Figure 7m-o). Also the intermediate layer was colder with the lowest temperatures at 100-150 m depth, whereas the bottom layer was warmer and more saline. Notably, the cold water behind the sill in Billefjorden was the least saline and dense of the different summers. This was most likely due to the heavy fast ice cover in Billefjorden during Winter Intermediate resulting in less effective sea ice formation and corresponding salt release. Indications of horizontal density gradients from the mouth towards Isfjorden are seen both in intermediate depths and in the bottom layer with increasing density towards Isfjorden in intermediate depths and vice versa in the bottom layer. This suggests outflow of the less dense winter water from Billefjorden in intermediate depths (like an intermediate plume). Summers following open winters (Figure 7p-r) revealed the warmest (T > 6°C) and shallowest (20-30 m thick) surface layer, and a very warm and saline water column below with the highest salinities (S > 34.9) in intermediate depths around 150 m. At the mouth and entrance of Isfjorden, very warm and saline (T > 4°C; S > 35) water occupied the water column below 100 m depth. As for summers following Winter Deep, the coldest water was the densest and present in the deepest parts of Isfjorden.

The vertical structures resulting from the different types of winter convection clearly appears from the mean water mass distribution in winter and summer along the Isfjorden Transect (Figure 8; see Figures S7 to S12 in Supplementary data for individual winter and summer sections). Over the time period 1987 to 2017 (Figure 8a and b), the mean distributions signalise the dominance of Winter Intermediate and particularly Winter Deep over the studied time period. The mean distributions over the different winter types (Figures 8c to h) clearly visualize how the strength of the water transformation in winter influenced the inflow pattern in winter and following summer. In addition, they also indicate how the presence of TAW at the mouth affected the inflow and hence the properties of the winter water inside Isfjorden, transforming WCW to LW in winter, and LW to TAW in summer.

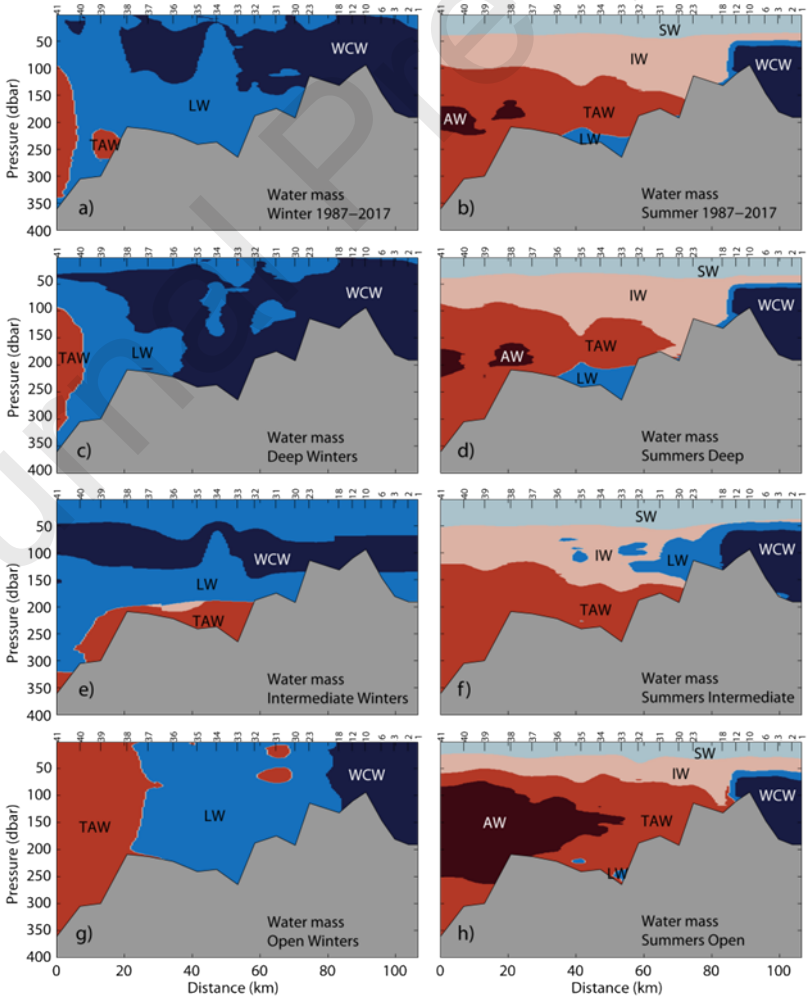

Figure 8: Distribution of mean water masses over a)-g) winters and b)-h) summers during a)-b) the time period 1987 to 2017, and of Winter c)-d) Deep, e)-f) Intermediate, and g)-h) Open along the Isfjorden Transect from the mouth area (Station 41) to the head of Billefjorden (Station 1). The water masses indicated are listed in Table 1.

5.1.5.3 Mean summer profiles in Isfjorden proper and Billefjorden over winter types

The averaged sections reveal that the hydrographic properties in Isfjorden in winter and summer depend largely on the winter types. The winter water produced in Isfjorden set the premise for inflow both in winter and especially the following summer. The lack of sill at the entrance makes it difficult to determine the final winter water in Isfjorden. Instead, the water trapped behind the sill in Billefjorden in summer is used as an archive for final winter water. The grouped (into winter types) temperature and salinity diagrams with mean summer profiles in Isfjorden proper (Figure 9a-c) are shown alongside the corresponding profiles from the deepest part of Billefjorden (Figure 9d-f). Winter Intermediate resulted in the coldest surface and intermediate waters in summer, whereas Winter Open resulted in the warmest, both resulting from their respective inflow pattern of warm and saline water in summer. In Isfjorden, the water towards the bottom was cold and least saline in Winter Deep compared to the warmer and more saline water in Winter Intermediate, but their densities were undistinguishable. Interestingly, the profiles in Billefjorden reveal more saline and denser bottom water in Winter Deep than in Winter Intermediate. The winter convection reached the bottom in Winter Deep and to intermediate depths in Winter Intermediate, as expected. The exceptions in Winter Deep seafloor conventions were 2003, 2009, and 2015, which all occurred after winters when very dense bottom water was produced, hence making it harder to replace the bottom water from the previous winter. Winter Open produced warmer and the most saline and densest bottom water of all winters, and in winter 2014 it seems to be solely produced from cooling in both Isfjorden and Billefjorden.

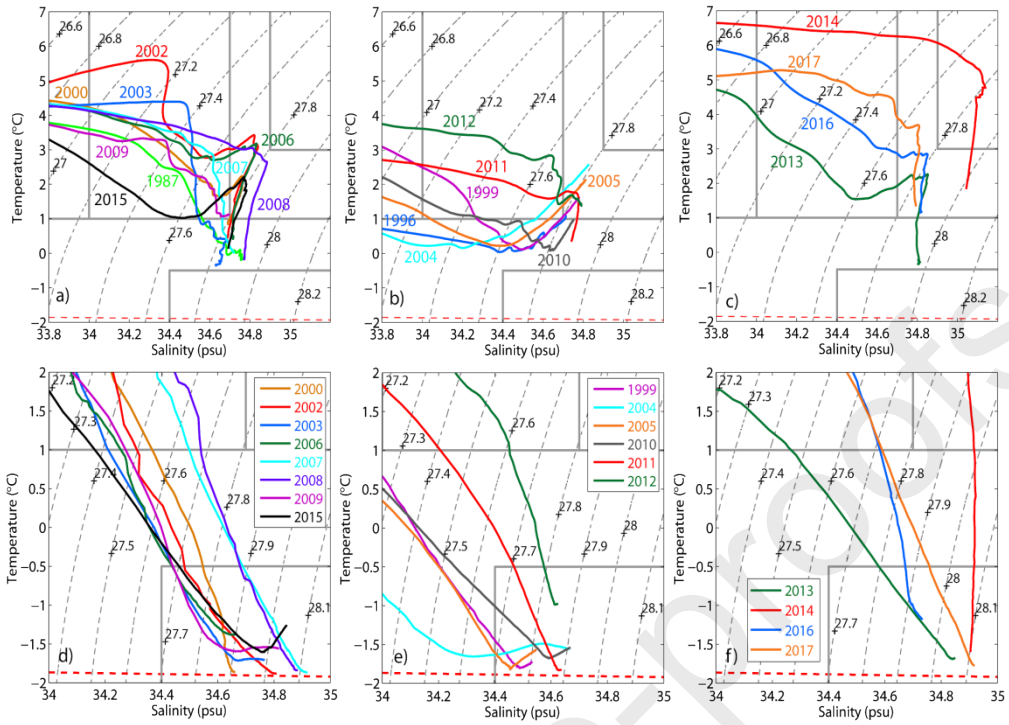

Figure 9: Temperature and salinity diagrams with a)-c) the mean summer profiles reaching deeper than 100 m inside Isfjorden proper (around Stations 34 and 35) and d)-f) the summer profiles in the deepest part of Billefjorden (around Station 3) grouped into summers after winter of type a) and d) deep, b) and e) intermediate, and c) and f) open. Notice the different axis range in a)-c) and d)-f).

5.1.6 Mean summer distribution of fresh water content

The mean water mass distributions in summer reveal different thicknesses of the summer surface layer following the different winter types (Figure 8), and the amount of TAW and AW present in Isfjorden varied considerably. This had a significant impact on the summer freshwater content (FWC) in Isfjorden (Figure 10) with largest FWC following Winter Intermediate (Figure 10c) and smallest FWC following Winter Open (Figure 10d). The mean over 1987 to 2017 (Figure 10a) showed almost similar amount and distribution of FWC as after Winter Deep (Figure 10b), again indicating the dominance of Winter Deep over the studied time period.

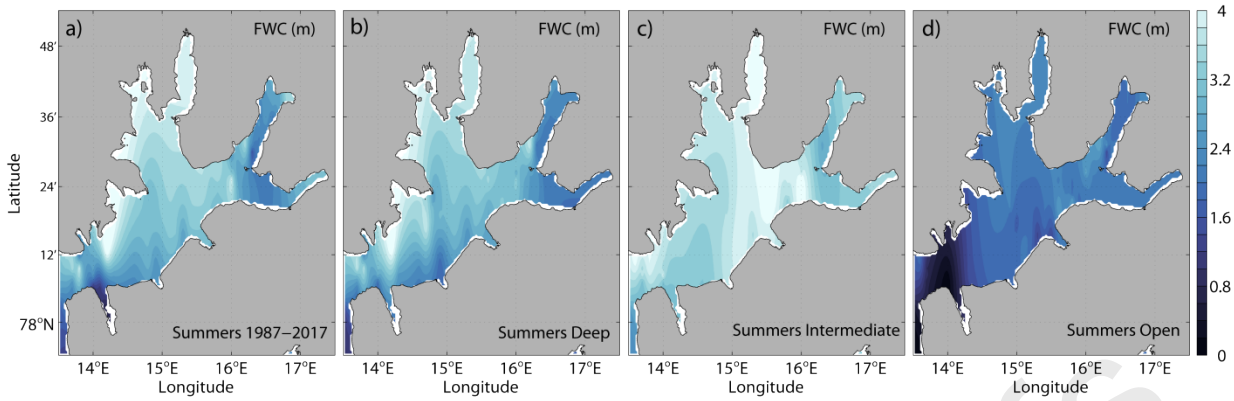

Figure 10: Horizontal distribution of mean full-depth freshwater content (FWC) in meters from salinity profiles over summers a) in the time period 1987 to 2017, and after Winter b) Deep, c) Intermediate, and d) Open.

The general distribution shows more FWC (up to 4 m) on the northern side of Isfjorden, which can be expected due to the large glaciers situated there, and less (down to 1.2 m) on the southern side. The latter was especially the case at the entrance and in Grønfjorden, and also Sassenfjorden and Billefjorden. An accumulation of freshwater is observed in inner Isfjorden proper for all winter types. It should be kept in mind when interpreting these data; the fresh surface layer responds quickly to wind forcing, which can change the FWC distribution (out- or in-fjord wind). The effect of wind on the surface layer in another western Spitsbergen fjord is demonstrated by Skarðhamar and Svendsen (2010). Accompanying wind-induced circulation can either speed up or slow down the estuarine circulation that transports freshwater out of the Isfjorden system. Nevertheless, the distribution of FWC indicates a general cyclonic circulation with inflow of water with less FWC in the south and outflow of transformed water with higher FWC in the north due to added freshwater along the flow path.

5.2 General fjord circulation from hydrography

The mean distribution of FWC shows that Isfjorden is a broad fjord where baroclinic geostrophic flow will occur when stratification allows it. Nilsen et al. (2008a) found an internal Rossby radius

of about 5 km in summer, which is much smaller than the mean width of the fjord (24 km), indicating that rotational effects are important for the fjord circulation. When stratification is weak like in winter, the flow becomes more barotropic and topographically steered (small Burger number; Pedlosky, 1987). Further, the STC (Nilsen et al., 2016) is topographically steered along the Isfjorden Trough transporting TAW and AW towards Isfjorden. The general circulation in Isfjorden is therefore expected to be geostrophically controlled in a cyclonic direction with inflow on the southern side and outflow on the northern side, following the isobaths with shallower depths to the right of the flow direction. Additionally with rotational dynamics included, Ekman transport to the right of the wind direction will push the surface layer towards the southern or northern side during in- or out-fjord wind events, respectively. This will result in changing surface tilt, and down- and upwelling with sometimes outcropping of the intermediate layer below. Barotropic- and baroclinic geostrophic flow adjustments will take place due to the changed surface tilt and horizontal density gradients in the layers below.

5.2.1 Mean winter and summer cross-sections: temperature, salinity, and density

At the mouth of Isfjorden (Figure 11a-f) patterns with inflow of warm and saline water in intermediate depths on the southern side were typical both in winter ($T > 1°C$; $S > 34.8$) and summer ($T > 3°C$; $S > 34.9$). Patterns with outflow of colder and less saline water were typical on the northern side. A deep cyclonic circulation of dense, relatively warm, and saline water is on average seen below 300 m depth in winter, whereas relatively cold and dense water occupied this part in summer. The mean density stratification at the mouth resulted in a mean internal Rossby radius of about 2 km in winter and 5 km in summer, which confirms the importance of rotational dynamics at the mouth both in winter and summer. In winter, the upper 100m layer shows typical inflow of cold and less saline water on the southern side and a broader outflow of similar water on the northern side. On average in summer, a 40 m thick surface layer was more detached (stronger stratification) from the water column below, and shows the warmest and least

saline water on the northern side due to added freshwater along the cyclonic flow path inside Isfjorden.

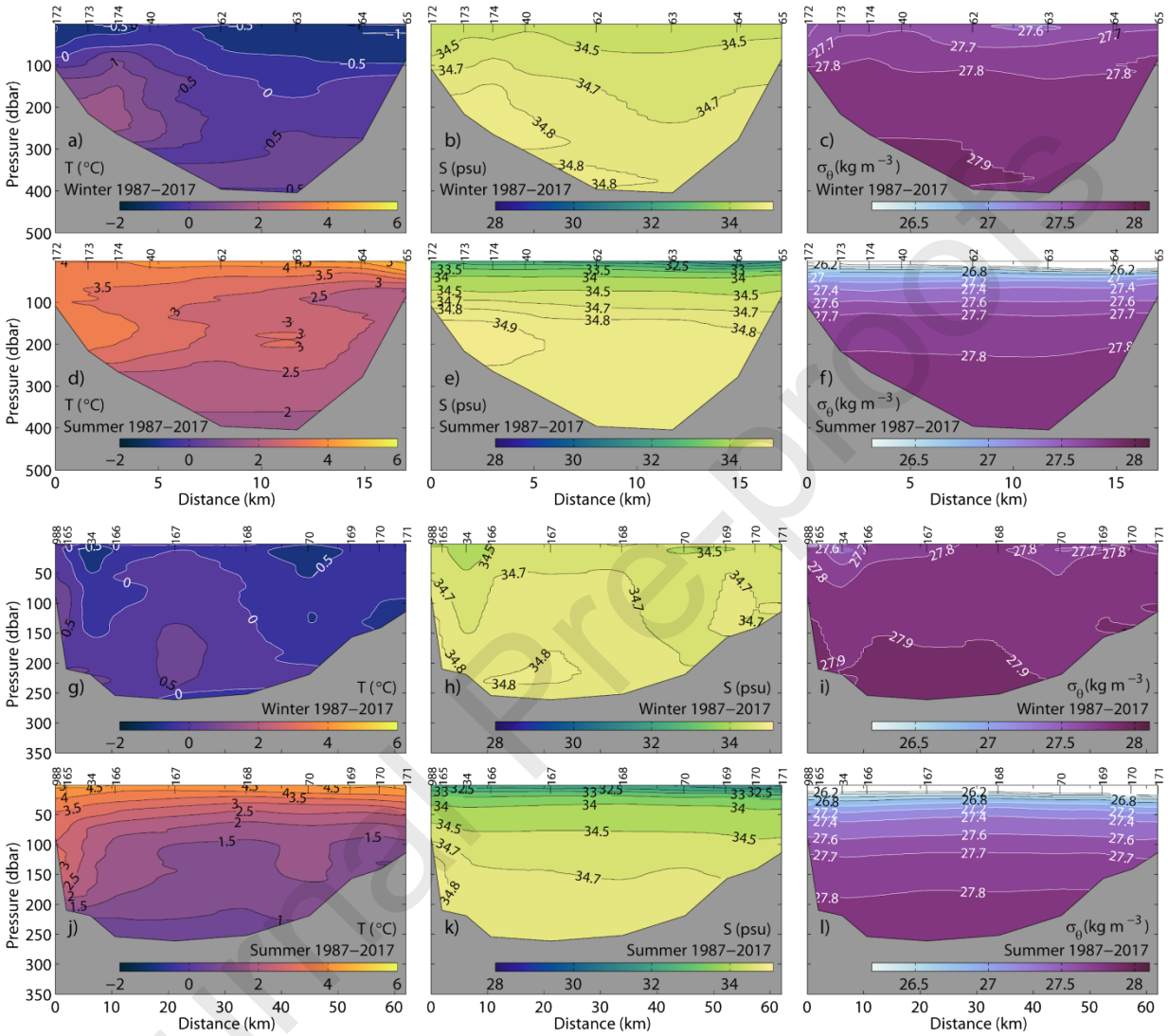

Figure 11: Distribution of mean a)-j) temperature, b)-k) salinity and c)-l) density across a)-f) the mouth from south (Station 172) to north (Station 65) and g)-l) Isfjorden proper from south (Station 988) to north (Station 171) over a)-c) and g)-i) winters and d)-f) and j)-l) summers during the time period 1987 to 2017. For section locations see Figure 1b.

In Isfjorden proper (Figure 11g-l), similar patterns were typical both in winter and summer, but with colder and slightly less saline water in intermediate depths. Inflow of warmer and more

saline water is seen on the southern side in intermediate depths in winter (T > 0.5°C; S> 34.8) and summer (T > 3°C; S> 34.8), whereas outflow of colder and less saline water was seen in similar depths on the northern side. Further, a separate cyclonic circulation seems to be present in the deepest part of Isfjorden proper with warm and saline water relative to the mean winter values in winter, and cold and slightly less saline water relative to mean summer values in summer. The mean density stratification in Isfjorden proper resulted in a mean internal Rossby radius of about 1.5 km in winter and 4 km in summer, which confirms the importance of rotational dynamics also in Isfjorden proper. In winter, the upper circulation happened in a 50m layer with inflow on the southern side and outflow on the northern side with equally cold and saline water, and again with a broader outflow area than inflow area when looking at the density. The 40m summer surface layer indicates a general cyclonic circulation pattern with thicker layer of warmer water on the southern and northern side than in the middle, but still with the least saline water on the northern side indicating added freshwater along the path.

5.2.2 Mean winter and summer cross-sections: water mass distribution

The cross-fjord distributions of mean water masses over the winters and summers classified as Deep, Intermediate, or Open (see Table 2 in Supplementary data) clearly visualise the winter type signature in the flow pattern and the rotational effects on the water mass distribution (Figure 12). In Winter Deep at the mouth (Figure 12a) water with similar characteristics as LW flowed in on the southern side in the upper 100 m. This was most likely water from the Spitsbergen Polar Current (SPC; Figure 1a). Outflow of LW and colder WCW from Isfjorden are seen in the same depths on the northern side. Below, inflow of TAW by the Spitsbergen Trough Current (STC) is seen on the southern side typically down to nearly 300 m depth. Across Isfjorden proper (Figure 12g), this inflow has resulted in LW on the southern side, indicating a closed cyclonic circulation inside Isfjorden proper with limited inflow of TAW.

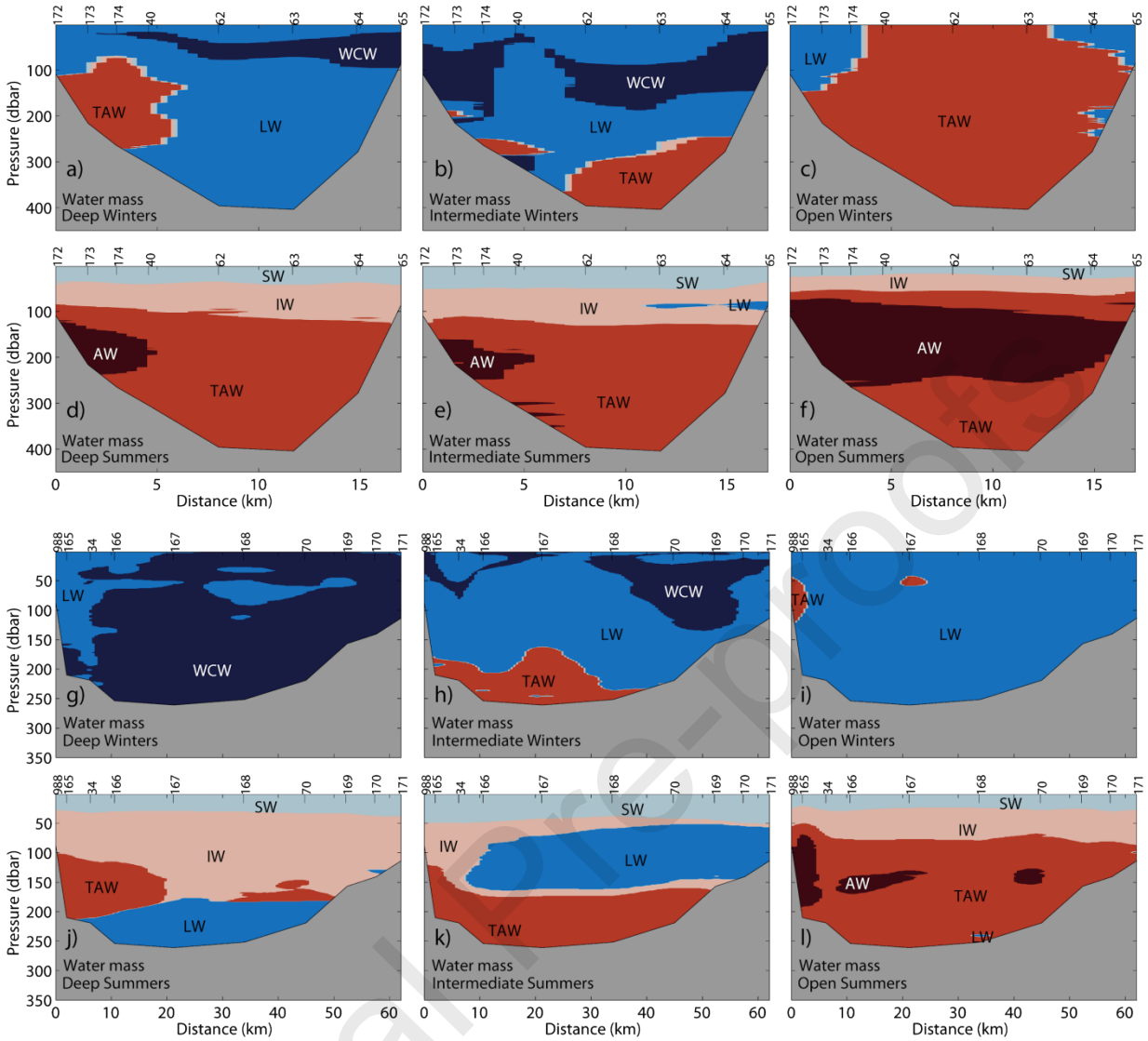

Figure 12: Cross-fjord distribution of mean water masses over a)-c) and g)-i) winters and d)-f) and j)-l) summers after Winter a)-j) Deep, b)-k) Intermediate, and c)-l) Open at a)-f) the mouth from the south (Station 172) to the north (Station 65), and g)-l) in Isfjorden proper from the south (Station 988) to the north (Station 171). The water masses are given in Table 1, and the section locations are shown in Figure 1b.

In Winter Intermediate (Figure 12b), in- and outflow of both LW and WCW are seen in the upper 100 m in the mouth, reflecting colder shelf water in these winters. Only some slight indication of TAW flowing in deep between 200 and 300 m depth is seen on the southern side, which obviously managed to flow into Isfjorden proper along the southern side and circulate

cyclonically at the bottom following the bathymetry (Figure 12 h). WCW was mostly present on the northern side of Isfjorden proper, suggesting more efficient winter convection on this side of the fjord that was less influenced by warmer water from the mouth. A thick layer of LW circulated cyclonically inside Isfjorden proper above the bottom layer of TAW.

Winter Open (Figure 12c) also indicates inflow of water similar to LW from SPC, but only outflow of LW from Isfjorden, reflecting the warmer winter water. Also deeper outflow of denser LW occurred in the north. The section across Isfjorden proper (Figure 12i) indicates a closed cyclonic circulation inside Isfjorden proper also in Winter Open, with limited inflow of TAW high up in the water column despite an extensive presence of TAW at the mouth.

The mean summer cross-section following Winter Deep at the mouth (Figure 12d) indicates a deepening of the IW layer while circulating cyclonically around Isfjorden, being a mixture of SW above and TAW below. Inflow of AW is observable in intermediate depths on the southern side, and the cross-section in Isfjorden proper (Figure 12j) indicates that this inflow mixed with surrounding water masses and transformed to TAW along its cyclonic path in Isfjorden proper, and finally flowed out on the northern side together with IW and some LW. Denser LW seems to circulate cyclonically below.

In summers following Winter Intermediate at the mouth (Figure 12e), the thicker SW layer is seen above a layer of inflowing warm IW on the southern side, and outflowing cold IW and LW on the northern side, indicating admixture of gradually less TAW and more LW along its path. This is also evident across Isfjorden proper (Figure 12k), where the thicker SW layer on the southern and northern side indicates a cyclonically circulating surface layer, above inflowing IW and TAW on the southern side from the mouth, and outflowing LW on the northern side. The

inflowing AW at the mouth entered Isfjorden proper along the bottom most likely circulating cyclonically inside Isfjorden proper following the bathymetry.

Summers following Winter Open show the dominance of AW at the mouth (Figure 12f), with inflow reaching higher up in the water column on the southern side, and slightly thinner outflow on the northern side. AW was gradually transformed through mixing along its cyclonic path resulting in the thicker layer with TAW on the northern side. Across Isfjorden proper (Figure 12l), the thick layer of TAW with cores of AW suggests AW inflow on the southern side along the steepest part of the slope and outflow on the northern side. At the bottom, TAW and some remnants of dense LW were present most likely circulating cyclonically in the deeper parts of Isfjorden proper. Only in summers following Winter Open did (pure) AW present at the mouth manage to reach Isfjorden proper.

5.2.3 Inflow variability and trends in the mouth area

The mean hydrographic sections show a high interannual and seasonal variability in inflow patterns of TAW and AW at the mouth and in Isfjorden proper (for individual sections see Figures S1 to S12 in Supplementary data), and indicate a trend with typically more Winter Intermediate and Deep in the past towards more Winter Open in recent years. In addition to the type of winter convection, these were clearly linked to the presence of TAW and AW at the mouth. In the following, hydrographic time series will be used to quantify the variability and trend of TAW and AW at the mouth, and then to see if these were reflected in Isfjorden proper.

5.2.3.1 Hydrographic time series at I-S and IsA

The seasonal change in temperature and salinity at I-S at the mouth (see Figure 1b for location) is clearly observable (Figure 13a-c). The warmest water column is seen in September, with a well developed surface layer with high temperature and low salinity, in some years reaching 60 m depth. At the bottom, warm and saline TAW and AW were present at varying extent with AW

always at the bottom. In between these two layers, an intermediate layer with warm IW was present, being a mixing product of the warm SW above and TAW or AW below. During fall and early winter, a gradually colder and more saline surface layer developed due to colder atmosphere, shutoff of freshwater supply and stronger winds. Thermal convection and mixing due to wind and tides gradually homogenised the water column and transformed the water towards LW or WCW. This was the case in winter 2011, but for the other winters this typical winter cooling of the water column was interrupted in December or January with full depth occupation of TAW or AW. The penetration of TAW or AW normally started at the bottom and rapidly reached the surface. Then cooling of this water continued and gradually transformed it to colder LW (2012, 2016, and 2017), or was suddenly replaced with LW or WCW again (2013), or switched between mostly LW or WCW and occasionally TAW the rest of the winter (2015). In 2014, TAW and AW continued to occupy the whole water column the rest of the winter. These events in winter might indicate a competition between the SPC (Figure 1a) transporting water similar to LW or WCW along the West Spitsbergen Shelf (WSS), and the STC transporting TAW or AW along the Isfjorden Trough towards the mouth (Nilsen et al., 2016), where the strength of the SPC relative to the STC controlled how far the STC could circulate into the trough. The strength of the SPC was most likely governed by both wind and horizontal density gradients on the WSS. As summer approaches, the sun radiation and a warmer atmosphere start to heat the surface layer, while gradually added freshwater from sea ice melt and river- and glacial runoff along the path of the SPC decrease the surface layer salinity. This will make the surface layer lighter and hence more detached from the water column below, which will become gradually more influenced by AW flowing towards the mouth during summer by the STC. The WSS seems to be flooded with AW in 2014, hence the SPC also transported TAW and AW this year.

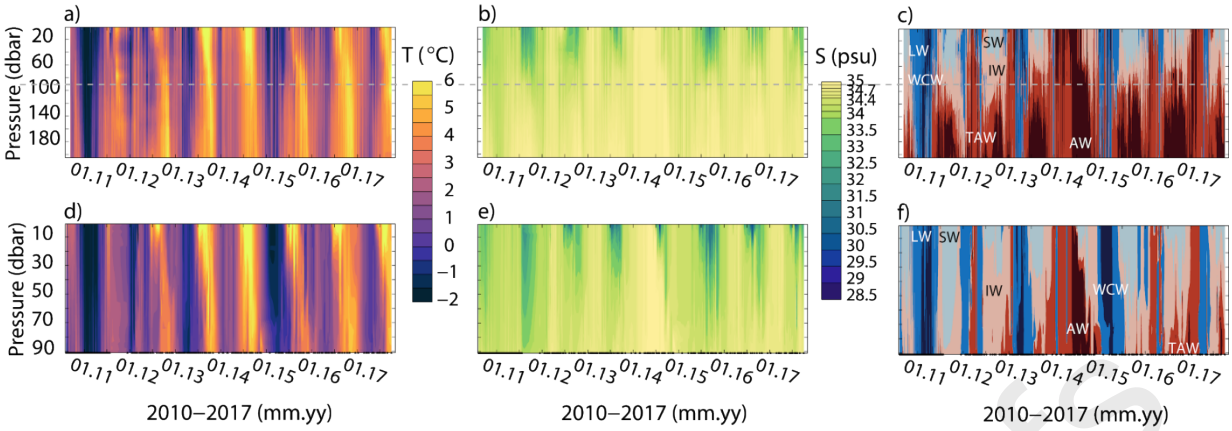

Figure 13: Time series of vertical distribution of a) & d) temperature, b) & e) salinity, and c) & f) water masses based on a) - c) data from mooring I-S and d) - f) combined data from mooring ALKE (Sept. 2010 - Sept. 2011) and CTD profiles at IsA (Dec. 2011 - Oct. 2017). The grey dashed line indicates the 90 m depth at I-S for comparison with IsA. The sampling dates at IsA are indicated with black dots on the time axis. The water masses are listed in Table 1. For locations see Figure 1b.

Similar variability in temperature and salinity is seen at IsA (see Figure 1b for location) as in the upper 90 m at I-S (Figure 13d-f). This shows that Isfjorden proper was influenced by similar seasonal processes as the mouth, and that inflow of TAW and AW from the mouth reached Isfjorden proper, at least in the upper 90 m, both in winter and summer with varying degree. Notably, the shallower Isfjorden proper got colder in winter and the surface layer warmer in summer. Also in some winters like 2012, 2013, and 2017, the presence of TAW and especially AW at IsA were less, or like winter 2015, not observable at IsA. Hence, AW at the mouth did not necessarily reach Isfjorden proper.

5.2.3.2 Atlantic Water index

The monthly AW indexes at I-S and IsA (Section 4.5) from September 2010 to October 2017 (Figure 14) provide a measure of the variability in presence of AW at the mouth and TAW (including AW) in the upper 90 m of Isfjorden proper. Moreover, the AW indexes can be seen

as a measure of the variability in heat content. High AW indexes indicate large heat content in the water column, either due to large occupation of the water column, or because of a high mean AW temperature. Large seasonal and interannual variability are seen in both indexes during the studied time period, but some differences are also observable. At the mouth a positive trend appears in the AW index in summer and early fall, showing stronger presence of AW and therefore larger heat content every summer or fall since 2010. Exceptions from the steady trend are summer 2014, which has the largest AW index of all the studied years and summer 2017, showing a decline compared to the previous summers. No similar trend is seen at IsA, which only represents the upper part of Isfjorden proper, and might depend on the type of winter convection and corresponding inflow pattern. Although the IsA station only represents the upper 90 m, a year to year comparison follows below in order to establish a causal relation between the mouth area and Isfjorden proper.

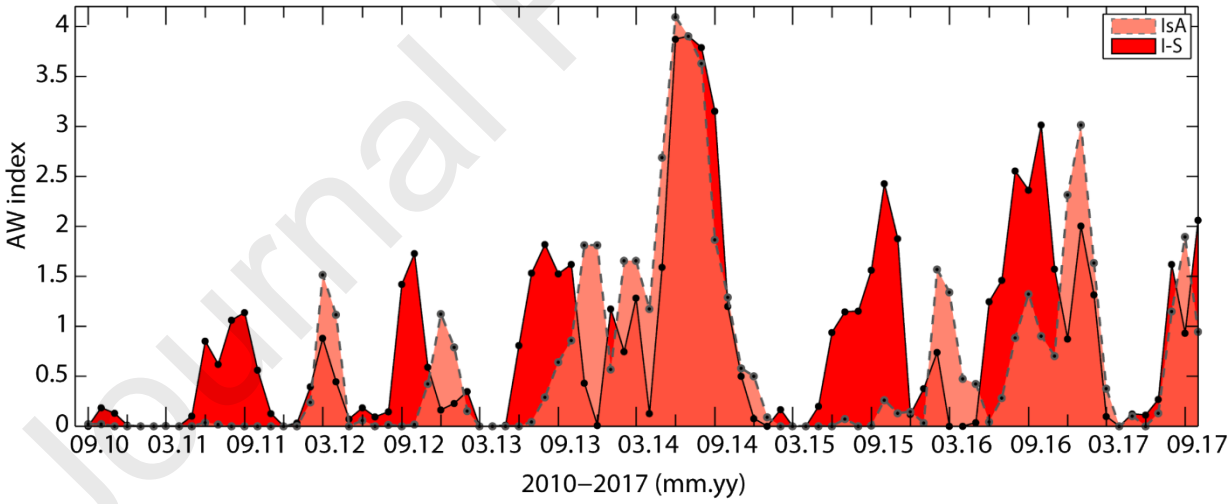

Figure 14: Monthly AW indexes at I-S (red) and IsA (pink transparent) during the time period September 2010 to October 2017. The AW indexes are based on presence of AW at I-S and also TAW at IsA. See Figure 1b for locations.

A weak presence of AW is seen at the mouth in fall 2010 and winter 2011, and TAW did not reach IsA. The following summer when AW was more present at the mouth, still no TAW is seen at IsA. This supports the inflow pattern of Winter Intermediate with deep inflow of TAW and AW (if present at the mouth) to Isfjorden proper, but below the depth of IsA. Both winters 2010 and 2011 are classified as Winter Intermediate (Table S2 in Supplementary data). In winter 2012 (with a maximum in March), AW and TAW were concurrently and strongly present at the mouth and at IsA. AW was guided by the STC towards the mouth, and was further mixed with LW or WCW before ending up as TAW at IsA. Winter 2012 was also Winter Intermediate, but since TAW was seen at IsA, the inflow reached above the IsA depth (90 m). From May to August 2012, the mouth had a weak presence of AW, and no TAW was identified at IsA. The following fall, AW at the mouth was most strongly present (October) about two months before TAW was most strongly present at IsA (December), indicating deep AW inflow that gradually transformed to TAW along the path from the mouth to IsA, and that finally reached the IsA depth two months later.

In winter 2013, AW was present at the mouth and TAW at IsA until March, and then none of them are identified until the following summer when a strong presence of AW at the mouth and also a strong presence of TAW at IsA are seen. This supports an inflow pattern of Winter Open, as winter 2013 is classified. TAW in Isfjorden in late fall and early winter was gradually cooled and transformed to LW during winter, and when dense enough, it stopped the inflow of TAW or AW from the mouth. The strong presence of AW at the mouth and TAW at IsA the following summer resulted in the strong presence in winter 2014, which is also classified as Winter Open. This peak in AW presence at the mouth was most likely a result of atmospheric conditions on the shelf forcing AW to follow shallower isobaths towards the mouth (Nilsen et al., 2016) combined with a lack of sea ice in the northwestern Barents Sea, providing less ArW to the SPC

(Tverberg et al., 2019; see Section 5.2.3.3 for a further discussion). The cooling in Isfjorden during winter 2014 did not manage to transform the TAW to LW, but was strong enough to densify the fjord and limit further inflow later in winter. Summer 2014 had the strongest presence of AW and TAW both at the mouth and at IsA, and they were concurrently present until January 2015.

In winter 2015, no or little AW was present at the mouth and no TAW at IsA, supporting the inflow pattern of Winter Deep with limited or no inflow of AW or TAW. Even with a strong presence of AW at the mouth the following summer, the presence of TAW at IsA was weak and suggested limited intermediate inflow barely reaching the depth of IsA.

In early winter 2016, concomitant increase of AW at the mouth and TAW at IsA is seen, but from March no AW is identified at the mouth, whereas TAW was present at IsA the rest of the winter. Again this supports the inflow pattern of Winter Open with cooling of AW and TAW that appeared in late fall and early winter, and that gradually were transformed towards denser LW limiting more inflow of AW and TAW from the mouth. The following summer also shows a strong presence of first AW at the mouth and then about two months later, TAW at IsA. This presence diminished during the fall, but increased again concurrently at both places in early winter 2017. From March 2017, AW is not identified at the mouth and TAW in Isfjorden was transformed to denser LW limiting further inflow until late in the following summer. The inflow pattern supports the classification of winter 2017 as Winter Open.

The variability of AW at the mouth and TAW at IsA was concurrent (within a month) or lagged by up to a couple of months at IsA. When concurrent, AW was most likely topographically guided along shallower isobaths towards the mouth and further into Isfjorden with no horizontal

density difference between the mouth and Isfjorden proper to limit the inflow. When lagged, the inflow could have been too deep to be registered at IsA until gradual upward mixing transformed water above the IsA depth to TAW up to two months later. Alternatively, a lagged presence could indicate density differences between the mouth and Isfjorden proper that needed to be reduced before inflow could happen. Moreover, inflow could be gradual at intermediate depths with both up- and downward mixing finally transforming water at IsA to TAW up to two months later.

5.2.3.3 Deviation from monthly climatology at I-S

The water masses present at the mouth clearly influenced the inflow pattern to Isfjorden proper. Mooring I-S was positioned on the steepest part of the southern slope in the trough (Isfjordrenna). In this region the water masses depended on the properties of water transported by the SPC, which was either highly influenced by cold and less saline ArW in years with heavy sea ice in northwestern Barents Sea, or more influenced by warm and saline AW in years with lack of sea ice (Tverberg et al., 2019). Moreover, the water masses at the mouth were also influenced by the strength of the SPC relative to the STC, which transports AW and TAW towards the western Spitsbergen fjords along the troughs cutting through the WSS (Nilsen et al., 2016). A comparison between deviation in hydrography and ocean current follows below in order to establish a causal relation between hydrographic properties at the mouth and current properties leading water to the mouth.

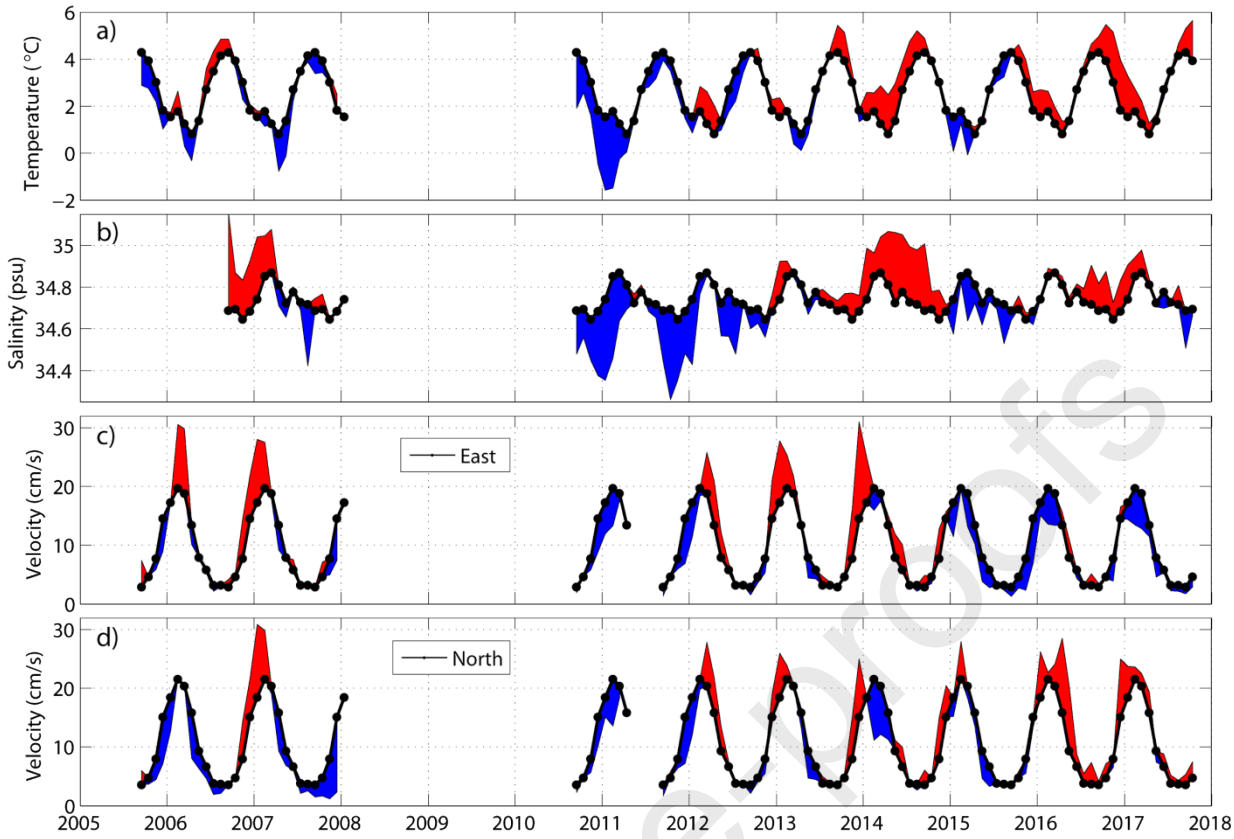

Figure 15: Deviation from the monthly depth-averaged climatology (black dots and line) of a) temperature, b) salinity, c) east- and d) north velocity component from the I-S mooring time series. Red (blue) is a) warmer (colder), b) more (less) saline, c) and d) stronger (weaker) velocity component than the monthly climatology, which is based on the existing time series during the period from 2005 to 2017.

The monthly depth-averaged climatology of temperature, salinity, and velocity components at I-S (Figure 15) show maximum temperature in September (4.3°C) followed by August and October, and minimum temperature in April (0.8°C) followed by March and May. Notably, a local maximum in winter appears in February (1.8°C). Salinity reveals maximum values in March (34.87) followed by February and April, and minimum values in November (34.65). Two local maxima appear; one in June (34.78), and one in October (34.70). Both velocity components show maximum values in February (20 cm s^{-1} eastwards, and 22 cm s^{-1} northwards) followed by

March and January, and minimum values in July to September (3 cm s^{-1} eastwards, and 4 cm s^{-1} northwards).

Hence, the normal situation during the measured time periods reveals strongest currents in winter with water decreasing in temperature and increasing in salinity during winter. The water was too warm and saline to be characterized as ArW (see Table 1), indicating strong influence of AW in winter. This AW influence has been reported for winter 2006 (Cottier et al., 2007), and can be supported herein by the properties of the mean climatology (Figure 15), which is associated with the local maximum in temperature in February combined with the largest increase in salinity at the same time. Our results therefore indicate that AW influence in February has been a common phenomenon in the last decades. The strongest current in February can be explained by strong winds and wind stress curl on the shelf speeding up the WSC, making it follow shallower isobaths along the WSS slope. The strong WSC would subsequently be transferred to a stronger STC also following shallower isobaths in the troughs on the shelf, and hence reaching I-S (Nilsen et al., 2016). Moreover, strong and along shore winds can further bring available AW onto the shelf as a response to Ekman transport (Cottier et al., 2007; Goszczko et al., 2018; Saloranta and Svendsen, 2001; Svendsen et al., 2002), and modified by eddy overturning (Tverberg et al., 2019). With the AW core being higher up in the WSC water column in recent years, such cross shelf exchange mechanisms have become more likely and efficient in transporting AW onto the shelf and towards the Arctic fjords.

Winters like 2012, 2013, 2014, 2016, and 2017, that showed warmer and, for some winters, more saline water than normal during the measured time periods, also showed a stronger current. This indicates more influence of AW most likely transported to the mouth by a stronger STC that managed to pass the SPC. Interestingly, winter 2014, the warmest and most saline winter of all,

experienced a sudden slowdown of the current in February that lasted until May. This is especially seen in the north component that almost halved in strength during this period. Hence the flow was more easterly directed at I-S in winter 2014, indicating more inflow from the mouth to Isfjorden proper than normal. This is confirmed by the hydrographic time series (Figure 13) and the AW index at IsA (Figure 14). Moreover, winters 2016 and 2017 reveal a stronger north component, but a weaker east component. This suggests less inflow from the mouth to Isfjorden proper in these winters, most likely due to very saline and dense water in the fjord hindering inflow, and hence forcing the SPC and the STC to flow more northward at the mouth. In colder and less saline winters like 2011 and 2015, the current was less strong, indicating a weaker STC not able to pass the SPC transporting cold and less saline ArW.

In summer, the current slowed down in response to weaker atmospheric forcing, and was affected by heating from the sun and a warmer atmosphere, and added freshwater along the path of the SPC. A lighter surface layer developed and got increasingly detached from the water column below, and at the same time more easily influenced by wind forcing. In warmer and more saline summers like 2014 and 2016, the current was stronger than normal in summer during the measured time periods, suggesting more inflow of AW with the STC. The opposite seems to happen in cold and less saline summers like 2011 and 2015, with weaker current than normal in summer, indicating weaker inflow from the mouth to Isfjorden proper.

5.3 Currents in Isfjorden

Hydrography clearly suggests a general geostrophic and cyclonic circulation in Isfjorden with inflow on the southern side and outflow on the northern side. The hydrography also indicates a layered circulation dependent on the type of winter convection. Even though a general cyclonic circulation appears from the hydrography, the complex topography of the Isfjorden system with deep basins and shallower areas inside Isfjorden proper would also influence the topographically

steered circulation. Presentations of mean currents from direct measurements in the Isfjorden system follow below in order to support the interpretation of the general circulation pattern deduced from hydrography.

5.3.1 Mean current from moorings

The mean depth-averaged current (residual current with tides removed) from the moorings in the Isfjorden system clearly shows that the mean flow followed the topography with shallower isobaths to the right (Figure 16). The mean depth-averaged current (DAC) was strongest on the southern side of the mouth (I-S) with a speed between 12 cm s^{-1} (2010/2011) and 18 cm s^{-1} (2006/2007), directed northeast towards the fjord mouth. Moreover, the annually varying strength of the east component is apparent through the more northward directed mean DAC in 2015/2016 and 2016/2017 compared to the other years. The direction of the DAC at I-S varied throughout the time series, but less in winter and with higher speed towards the fjord mouth (not shown). Moreover, the speed of the DAC shows high fluctuations throughout the time series with higher values in winter reaching typically 70 cm s^{-1} and a maximum of 80 cm s^{-1} in March 2011 (not shown). The DAC frequently slowed down with nearly no speed in summer, but also occasionally in winter. The variability in the speed of the DAC was most likely due to simultaneous variability in the atmospheric forcing on the shelf driving the SPC and the STC. All the measured periods show a very strong seasonal signal at I-S (Figure 15) with a typical speed of the mean DAC around 5 cm s^{-1} in summer and 30 cm s^{-1} in winter. The mean DAC was significantly lower on the northern side of the mouth (I-N) with a speed of 6 cm s^{-1} in 2015/2016 and 5 cm s^{-1} in 2016/2017, both directed southwest and away from the fjord mouth (Figure 16). The direction of the DAC at I-N varied throughout the time series with higher speeds both away from and towards the fjord mouth, but more often and with the highest speeds away from the mouth (not shown). The two measured periods at I-N also showed a seasonal signal and large

variability in line with the variability at I-S, but the DAC was less strong in winter only reaching speeds of 45 cm s^{-1}.

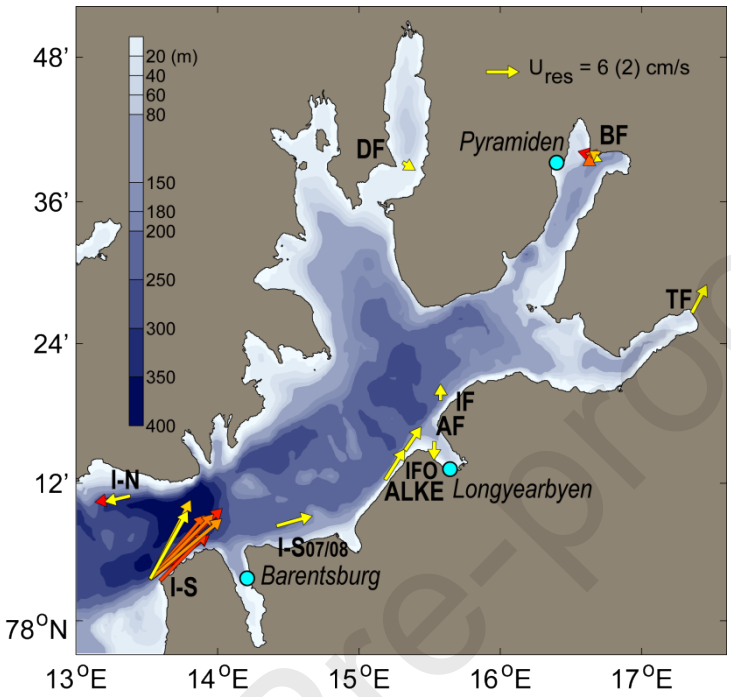

Figure 16: The mean residual current from different mooring locations in Isfjorden estimated over their respective measuring periods. At locations with several yearlong records, red (yellow) arrows are based on the oldest (most recent) depth-averaged current (DAC) time series. The scale of the mean residual current is indicated in the top right corner (the scale for IF, BF, and TF is given in the parentheses).

Behind the fjord entrance towards Isfjorden proper (I-$S_{07/08}$ and ALKE), the mean DAC was reduced to speeds of 7 cm s^{-1} (Figure 16). During the measured periods at I-$S_{07/08}$ and ALKE, the direction and speed of the DAC varied with speeds between zero and 35 cm s^{-1} and the highest speeds along isobaths towards Isfjorden proper (not shown). The time series was too short to reveal any seasonal signal at I-$S_{07/08}$ (Table 3), but at ALKE a stronger DAC is seen in summer and fall (10 cm s^{-1}) and a weaker DAC in late winter (5 cm s^{-1}; not shown). Interestingly, the

main direction of the DAC at ALKE changed towards north in March 2011, hence flowing towards the northern side of Isfjorden instead of Adventfjorden and Sassenfjorden as before. A strong current event with speeds reaching 35 cm s^{-1} appeared in mid-March 2011, and was most likely an advection episode linked to the maximum current speed observed at I-S at the same time. A possible cause could have been the dominating meridional winds on the shelf in March 2011 that first were northerly, then strong southerly, and finally northerly again causing high Ekman transports (Tverberg et al., 2014). Winter 2011 was relatively cold with some sea ice cover in Isfjorden proper (Figure 3; http://polarview.met.no/) that most likely reduced the wind influence, and hence the current speed in Isfjorden proper during the late winter months.

Approaching Adventfjorden (IFO and AF), the mean DAC decreased further to speeds of 5 cm s^{-1} at IFO and 4 cm s^{-1} at AF, and still following the isobaths turning towards Adventfjorden (Figure 16). During the rather short measured period at IFO (Table 3), the direction and speed of the DAC also varied with speeds between zero and 50 cm s^{-1} and the highest speeds directed along the isobaths toward inner Isfjorden proper and Adventfjorden (not shown). Until beginning of December 2016, the speed of the DAC varied around 12 cm s^{-1}. Then suddenly, the values dropped close to zero with occasional episodes reaching 20-30 cm s^{-1} while flowing back and forth along the isobaths for the rest of the measured period. This supports the inflow pattern in winter 2017, which was characterised as Winter Open with limited inflow from the mouth when the cooling of TAW and AW inside Isfjorden started and densified the fjord. When the inflow stopped in December 2016, a new internal circulation in Isfjorden proper most likely started with alternating direction. At AF, the direction and speed of the DAC varied with speeds reaching 20 cm s^{-1} and the highest speeds directed along isobaths towards the southern side of Adventfjorden (not shown). A weak seasonal signal appears with a smaller speed of the mean DAC in winter (2

cm s^{-1}), and a slightly larger in summer and fall (4 cm s^{-1}). This might be a result of increased fresh water content in the surface layer due to maximum river runoff in summer.

Even smaller speeds of the mean current appeared in Tempelfjorden (TF) and Dicksonfjorden (DF) with values of 2 and 3 cm s^{-1}, respectively (Figure 16). The current direction and speed at TF varied throughout the time series with the highest speeds reaching 15 cm s^{-1} into the fjord (not shown). The mean current direction at TF was therefore towards the tidewater glacier Tunabreen in Tempelfjorden that started to surge earlier than expected in 2016 (pers. comm. C. Borstad), and hence, the glacier provided an increased amount of freshwater that flowed out of the fjord and most likely enhanced the estuarine circulation. This may have led to the observed compensation flow into the fjord along the bottom. The current meter at TF was placed 7 meter above the bottom (Table S4 in Supplementary data), and could therefore capture a compensation flow along the bottom. Worth knowing, along-fjord winds rather than glacial freshwater discharge in the surface layer stood out in a model study as important for the water exchange in the inner part of another western Spitsbergen fjord where tidewater glaciers expose calving fronts to the fjord water (Sundfjord et al., 2017). The increased heat content in Isfjorden over the last years have been shown to increase the calving rate at Tunabreeen (Luckman et al., 2015), indicating that a compensating inflow with warmer water can provide a positive feedback to the fjord glacier system in Tempelfjorden. At DF, the mean current followed the isobaths of a shallow topographic feature pointing eastwards behind the sill (Figure 16). The current direction and speed varied throughout the time series but with highest speeds reaching 25 cm s^{-1} in the mean flow direction (not shown). Both TF and DF show slightly weaker currents in late winter than in summer and fall (not shown). The current speeds in late winter were smaller (< 5 cm s^{-1}) due to ice cover and less wind influence. Both of these fjords were ice covered in winters 2016

and 2017 (http://polarview.met.no/); Dicksonfjorden more than Tempelfjorden due to their different locations and sill depths, and thus their connections to Isfjorden proper.

The mean DAC (above sill depth) was weakest in Billefjorden (BF in Figure 16) with a speed of 0.5-1 cm s^{-1} over the measured periods at BF (Table 3), and seem to follow the isobaths with shallower depths to the right. This was due to a highly variable direction of the DAC with slightly higher speeds in the direction of the mean DAC (not shown). No clear seasonal signal appears at BF, except for smaller fluctuations in current strength in winters with heavy sea ice in Billefjorden (i.e. 2009 and 2011; http://polarview.met.no/).

At the entrance to Sassenfjorden (IF) the mean DAC speed was very small (1 cm s^{-1}) compared to the mean DAC speed further out in Isfjorden proper (Figure 16). The direction and speed of the DAC varied a lot throughout the short time series in winter 2013/2014 with slightly higher speeds reaching 10 cm s^{-1}, and 18 cm s^{-1} during a peak event in late December 2013, directed towards Sassenfjorden (not shown). As at IFO, the DAC alternated back and forth along the isobaths. When comparing the mean currents in Isfjorden, it should be taken into consideration that the mean current at IF was based on a short time series. Unfortunately, the measurements stopped just before the large inflow of AW in winter 2014.

All in all, the measured mean currents supported the cyclonic, geostrophically balanced circulation in Isfjorden as deduced from hydrography, but with weaker strength and fluctuations in winter as opposed to the flow at the mouth. The strong current on the southern side of the mouth in winter was perhaps too strong to manage to flow into Isfjorden, and instead passed the fjord mouth and followed the isobath northward and then westward before heading northward again along the shelf. This might be due to a strong front between the fjord and the shelf resulting

in a stronger geostrophic control that limits the inflow (Fraser et al., 2018b; Nilsen et al., 2008a; Tverberg et al., 2019). The strength of the mean current decreased from the mouth towards Isfjorden proper, and further towards the side fjords. From archived sea ice charts for Svalbard (http://polarview.met.no/), the fjord mouth area was less ice covered than Isfjorden in the measured winters, and Isfjorden proper was not fully ice-covered as opposed to its side fjords (Muckenhuber et al., 2016; Nilsen et al., 2008a). But in cold winters with also heavy ice cover in Isfjorden, the local wind influence weakened and the current slowed down, unless some strong advective signal managed to enter from the shelf like in March 2011. Moreover, the strongly wind-influenced surface layer disappeared in winter when the water column was more homogeneous, which also dampened the strong fluctuations in current.

5.3.2 DAC from gliders

The DACs measured by the Isfjorden glider missions of November 2014 and 2016 (Figure 17) generally display large spatial variability in both magnitude and direction. These indicate that changes in flow may be more frequent than shown by hydrography, likely due to wind driven currents in the Ekman layer (see Fraser et al., 2018b). We are therefore cautious when interpreting glider-derived DAC sections as instantaneous snapshots as there may be some temporal evolution of the flow between the individual DAC measurements comprising the section. During the single transect taken in 2014, the fjord mouth displayed a strong and cyclonic circulation pattern, consistent with the moored observations (Figure 16). This type of flow pattern also appears to be prevalent at Section 1, which crosses Isfjorden proper, although some transects did not find inflow near the southern shore. The strength of inflowing current here was therefore spatially and temporally variable, with the current core occasionally too weak, narrow, or close to shore to be captured by the glider. By contrast, the outflow towards the northern shore appears strong and consistent. Both the 2014 and 2016 transects of Section 4, which crosses Sassenfjorden, show similar structure, with a single inflowing DAC vector nearest the southern

boundary and outflow elsewhere. Both glider surveys describe strong, along-isobath flow from northern Sassenfjorden around the headland into southeast Nordfjorden, indicating this may be a consistent feature. In Nordfjorden the structure of the circulation was less clear, with an apparent flow convergence in the Northwest of the fjord (Sections 2 and 3). The picture of isobath following cyclonic flow given by the moored observations was violated at the western side of Section 2, where inflow was consistently observed instead of outflow. Furthermore, we see many instances of cross-isobath flow, particularly in the along Isfjorden sections taken in 2014 (Sections 5 and 7).

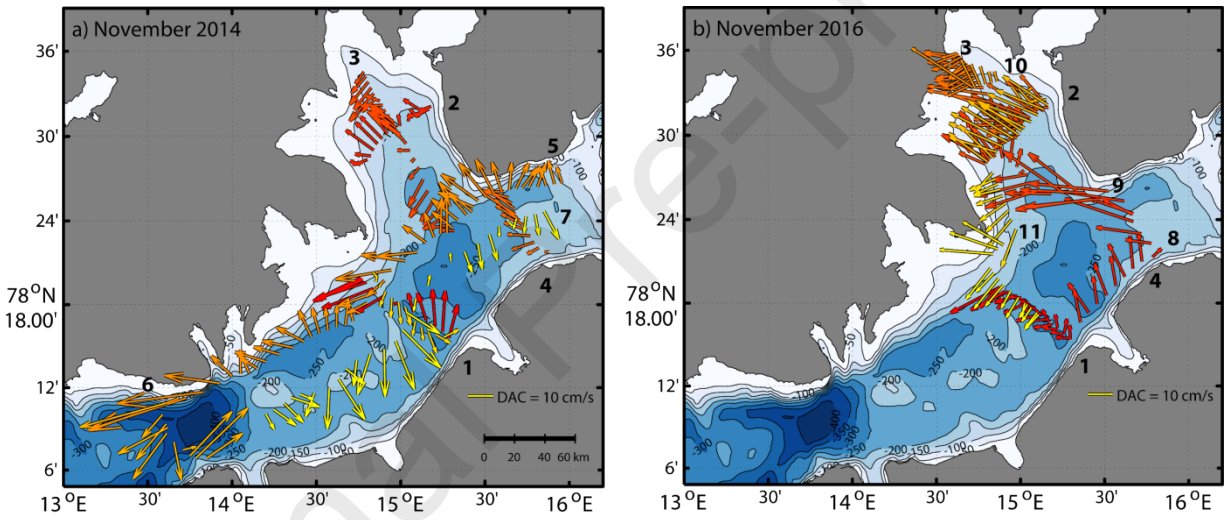

Figure 17: De-tided depth-averaged currents (DACs) estimated during glider sections in Isfjorden in a) November 2014 and b) November 2016. Red (yellow) arrows are based on the earliest (latest) DAC data in each glider campaign. The numbered glider sections are indicated (see Table S5 in Supplementary data). The scale of the DACs is indicated in the lower right corner of the panels.

5.3.3 DAC from VM-ADCP

The DACs measured by the VM-ADCP in July 2007 display a general cyclonic pattern in both layers with inflow on the southern side of the fjord mouth and outflow on the northern side

(Figure 18; Sections A and B), but with some deviation most likely due to topography and wind-induced currents. A southwestward directed outflow is observed in the southwestern part of the diagonal Section A, which was not long enough to reach the southern slope of the mouth, and hence the flow most likely followed the isobaths of the deep topography along the section. Moreover, the DACs appear faster in the upper (30 to 100 m) layer than in the lower (100 m to bottom) layer at the mouth.

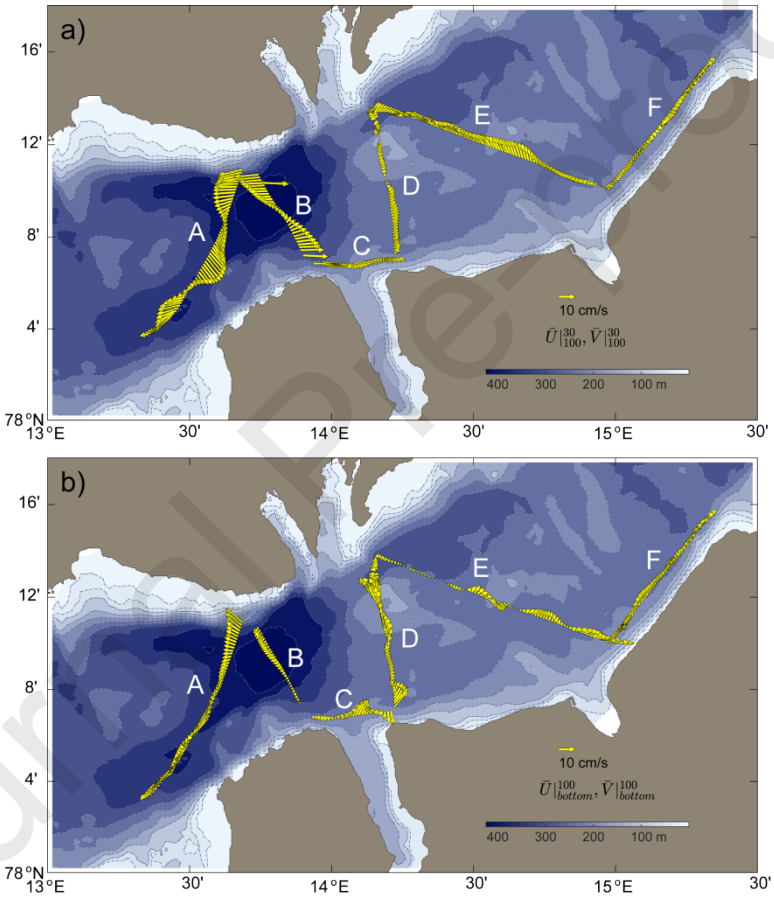

Figure 18: De-tided depth-averaged currents (DACs) over a) 30-100 m depth and b) 100 m depth to bottom, estimated along VM-ADCP sections in the Isfjorden mouth and proper on 29 July 2007. The scale of the DACs is indicated in the lower right corner of the panels.

Inside Isfjorden proper (Sections C to F), the DACs slowed down in the upper layer. A general cyclonic pattern was displayed in both layers, but also with some exceptions that seem to be

related to the changing topography with shallower topographic features in the middle of the sections. The DACs in the lower layer seem to be more influenced by these topographic features than the upper layer. This is evident from Section D, where the DACs in the upper layer flowed slowly towards Isfjorden proper in the southern part and outwards in the northern part, whereas in the lower layer the DACs flowed more northerly and with higher speed in the middle of the section along the topography with shallower isobaths to the right, before turning outwards in the northern part. Along the diagonal Section E in the upper layer, the DACs flowed slowly towards the mouth in the southern part, then faster turning more northwards in the middle of the section, before turning outwards in the northern part. This was most likely due to wind-induced currents in the Ekman layer by an out-fjord wind event while obtaining the section. Wind data from Svalbard Airport reveal a strong and prevailing out-fjord wind event on 27-28 July 2007 (not shown). In the lower layer, a relatively strong inflow is seen in the southern and middle part of the section, though a bit topographically adjusted in the middle part, but an outflow in the northern part was not noticeable. This deviation from a cyclonic circulation supports a circulation induced by across-fjord Ekman transport in the upper layer with upwelling in the southern side and downwelling in the northern side, creating a negative across fjord density gradient towards the northern side. According to the thermal wind relation (Pond and Pickard, 2013), an along-fjord current will then decrease in the positive z direction (i.e. towards the surface). On the southern side, this created a transition from positive inflow in the lower layer towards zero velocity in the upper layer, while on the northern side starting from zero along-fjord current in the lower layer towards a negative outflow in the upper layer. This pattern is also seen in Section F along the southern bank of Isfjorden proper, with weak outflow in the upper layer and stronger inflow in the lower layer. Towards the inner part of Section F, the DACs turned gradually more inwards in the upper layer, either suggesting a stronger barotropic inflow in this area, or that the out-fjord wind event ceased during the collection of the section. Wind data from Svalbard Airport

reveal a gradual cease of the out-fjord wind, and instead turning in-fjord on late 28 until midday on 29 July 2007 (not shown).

Even though the DACs along the VM-ADCP sections are only instantaneous snapshots, where the wind-induced currents have a large impact on the flow, they still support the circulation pattern inferred from hydrography with inflowing water on the southern side and outflowing water on the northern side in both layers. They also revealed a topographically adjusted flow, especially in the lower layer, influenced by the many shallower topographic features in Isfjorden proper, which also is indicated in the hydrographic sections.

5.4 Tides in Isfjorden

Tides may constitute an important mechanism for transport of water masses into the fjord, either by strong tidal currents enhanced by topography or due to mixing by internal waves along pycnoclines (Inall et al., 2015). The harmonic analysis of pressure and DAC time series from the moored instruments in the Isfjorden system (Table 4) reveals a consistent tidal amplitude in surface elevation with the principal lunar semidiurnal tidal constituent (M2) as the most important tidal component with an amplitude of 0.5 m at all locations. The second most important was the principal solar semidiurnal constituent (S2) with an amplitude of 0.2 m, followed by the larger lunar elliptic semidiurnal (N2) and the lunar diurnal (K1) constituents with amplitudes around 0.1 m. Combined, all the significant tidal constituents resulted in a tidal amplitude in elevation of around 1 m. The total variance in the elevation at the fjord mouth was larger than in Isfjorden proper, and especially the side fjords. Hence the percent of total variance in elevation explained by tides increased from about 50% at the mouth to almost 100 % in the side fjords.

Table 4: Harmonic tidal analysis of the deepest pressure (left side) and the DAC time series (right side) from moorings in the Isfjorden system (Figure 1b and Table 3). Parameters of the four most

significant constituents are; tidal elevation, and major (e_{ma}) and minor (e_{mi}) axes of the tidal ellipse. Total (T) and predicted (P; tides) variance and percentage of total variance explained by tides are also listed. Constituents are; Semidiurnal: M2 the principal lunar, S2 the principal solar, N2 the larger lunar elliptic, K2 the lunisolar; Diurnal: K1 and O1 the lunar, P1 the solar, 2Q1 the larger elliptic. M6 and M8 are the shallow water overtides of principal lunar and 2MN6 is a sixth diurnal.

Location	Const.	Elev. (m)	Variance	Const.	e_{ma} (cm s^{-1})	e_{mi} (cm s^{-1})	Variance
I-$S_{14/15}$	**M2**	**0.53**	T: 0.25	**M2**	**4.14**	0.03	T: 214.7
	S2	0.20	P: 0.17	S2	1.55	-0.02	P: 10.4
	N2	0.11	(67.3%)	N2	0.87	0.02	(4.8%)
	K1	0.07		M6	0.51	-0.01	
I-$N_{16/17}$	**M2**	**0.54**	T: 0.29	**M2**	**4.58**	0.13	T: 108.1
	S2	0.18	P: 0.17	S2	1.73	0.08	P: 21.9
	N2	0.09	(57.4%)	N2	0.79	0.01	(20.2%)
	K1	0.06		K1	0.64	0.01	
I-$S_{07/08}$	**M2**	0.51	T: 0.34	**M2**	**3.52**	0.07	T:45.4
	S2	0.21	P: 0.16	S2	1.12	0.11	P: 7.3
	N2	0.12	(48.2%)	N2	0.66	0.07	(16.2%)
	K1	0.09		M6	0.43	0.00	
ALKE	**M2**	**0.52**	T: 0.18	**M2**	**1.88**	0.08	T:95.4
	S2	0.20	P: 0.17	S2	0.83	-0.04	P: 2.6
	N2	0.10	(93.8%)	P1	0.52	0.08	(2.7%)
	K1	0.07		N2	0.40	-0.06	
IFO	**M2**	**0.54**	T: 0.18	**M2**	**2.79**	0.09	T: 83.7
	S2	0.18	P: 0.17	S2	0.93	0.02	P: 4.8
	N2	0.11	(92.4%)	N2	0.71	0.00	(5.7%)
	K1	0.09		M6	0.60	-0.01	
AF	**M2**	**0.51**	T: 0.17	**M2**	**0.71**	-0.06	T: 16.9
	S2	0.19	P: 0.16	S2	0.29	-0.05	P: 1.1
	N2	0.10	(96.4%)	K2	0.13	-0.04	(6.5%)
	K1	0.06		N2	0.11	0.04	
IF	**M2**	**0.54**	T: 0.20	**M2**	**1.73**	-0.04	T: 14.6
	S2	0.19	P: 0.17	S2	0.67	0.22	P: 2.0
	N2	0.11	(88.5%)	2Q1	0.40	-0.17	(13.8%)
	K1	0.08		O1	0.31	0.02	
TF	**M2**	**0.55**	T: 0.19	**M2**	**0.22**	0.04	T: 8.4
	S2	0.20	P: 0.19	S2	0.15	-0.01	P: 1.0
	N2	0.11	(98.3%)	-	-	-	(11.7%)
	K1	0.06		-	-	-	
$BF_{12/13}$	**M2**	**0.55**	T: 0.19	**M2**	**0.36**	-0.06	T: 4.6
	S2	0.21	P: 0.18	S2	0.13	-0.02	P: 0.4
	N2	0.11	(96.5%)	M6	0.06	0.01	(8.5%)
	K1	0.07		2MN6	0.05	-0.01	
DF	**M2**	**0.57**	T: 0.21	**M2**	**2.59**	-0.27	T: 42.2
	S2	0.21	P: 0.20	S2	1.05	-0.15	P: 5.0
	N2	0.11	(94.9%)	M6	0.60	-0.12	(11.8%)
	K1	0.06		K2	0.46	0.09	

The tidal currents were also dominated by M2 followed by S2, but the two next changed from location to location depending on the local topography (Table 4). This was supported by the increased importance of the shallow water constituents M6, M8, and 2MN6. The tidal current at the fjord mouth (I-S and I-N) reached amplitudes around 8 cm s^{-1}, where M2 contributed with nearly half of it. In Isfjorden proper the tidal currents were weaker (~5 cm s^{-1}) and decreased further towards the side fjords. Interestingly, the tidal current was stronger at DF, most likely due to its proximity to the very shallow sill, where tidal currents with amplitudes of 2-3 m s^{-1} have been modelled (Kowalik et al., 2015). The total variance in the current was largest at the mouth and decreased in Isfjorden proper, and further towards the side fjords. The percentage explained by tides was generally low and varied from 3 to 20%.

The tidal ellipses of the most dominant constituent (M2; Figure 19) display a rectilinear tidal flow along the isobaths with the highest amplitudes at the mouth and gradually smaller towards the inner side fjords. The exception was Dicksonfjorden, where a relatively strong tidal current appears, directed along the fjord axis and not along the isobaths as the mean current. Moreover, the tidal currents were less rectilinear in the inner side fjords most likely due to less steep topography at the mooring locations.

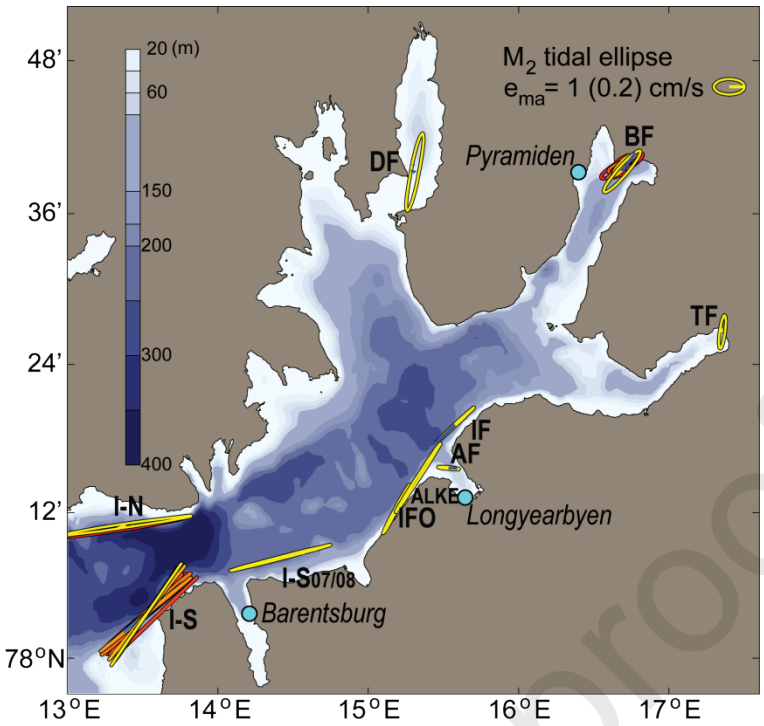

Figure 19: The M2 tidal ellipse from the different mooring locations in Isfjorden estimated over their respective measuring periods. At locations with several yearlong records, red (yellow) ellipses are based on the oldest (most recent) depth-averaged current time series. The scale of the tidal ellipses is indicated in the top right corner (the scale for BF and TF is given in the parentheses).

5.5 Tracing inflow events in winter

Episodes with strong southerly wind stress on the shelf in winter have been demonstrated to speed up the WSC and hence the STC, bringing AW onto the shelf in extreme cases (Nilsen et al., 2016). Moreover, if changes in atmospheric conditions on the shelf then reduce the geostrophic control in front of the fjord mouth by slowing down the SPC, AW might be transported to the mouth area in winter (Fraser et al., 2018b). Intrusion of AW on the shelf in winter has also been linked to Ekman transport (Cottier et al., 2007; Goszczko et al., 2018), and with the lately observed AW core higher up in the WSC water column, Ekman transport might more easily lead to AW exchange across the shelf edge front. According to residual mean theory (sum of Ekman and eddy overturning), the depth level of the exchange and resulting flow of AW

onto the shelf, will very much depend on density differences between the WSC and the shelf water columns (Tverberg et al., 2019, Tverberg & Nøst, 2009). Ekman overturning may then be overruled by eddy overturning; moving less dense water on top of denser water. With lack of sea ice and more saline AW on the shelf in winter, the density of the shelf water column will increase as the water loose heat to the atmosphere. Eddy overturning will then move warmer and lighter AW from the WSC water column over colder and denser shelf water (cooled AW). As seen from the AW index at I-S (Figure 14) and also from the distribution of mean winter water masses along the Isfjorden Transect (Figure 8), presence of AW has been common at the mouth in winter, but with varying degree. Depending on the density difference between the shelf and the fjord (or on the type of winter convection), inflow to Isfjorden proper might then happen in winter, as demonstrated by hydrography.

To trace inflow events to Isfjorden proper in winter, concurrent temperature and salinity time series from different mooring locations in the Isfjorden system are displayed together for respective winters in Figure 20. Generally in winter, the temperature decreased while the salinity increased due to atmospheric cooling and shutdown of freshwater supply, and when freezing started, brine release increased the salinity further. The increased mixing in winter due to stronger winds (see Figure 3) combined with the vertical convection due to cooling and brine release, resulted in a more homogenised water column in winter. This appears to be the typical time evolution in winter 2011 (Figure 20a-b), and in all winters in the side fjords protected by a shallow sill (BF, TF and DF in Figure 20). Due to its proximity to the mouth area and the lack of a protective sill, Isfjorden proper was more influenced by the presence of AW at the mouth. The other winters (Figure 20c-l) show stronger presence of AW at the mouth. During peak AW events at the mouth, AW managed to flow into Isfjorden proper while mixing with surrounding water, interrupting the cooling process and keeping the water column well above the freezing

point. This increased the heat content in Isfjorden proper and most likely affected the water column above the sill depths in the side fjords. Clearly, exchange of water masses across their sills happened in winter, as indicated by their synchronised increase in temperature and salinity. As a result, the side fjords reached the freezing point later in these winters. Moreover, the different cooling rates seen at the mouth, in Isfjorden proper and in the side fjords during the winters can be explained by the air temperature (see Figure 3); the coldest winters (2011, 2013, and 2017) resulted in a steeper cooling rate than the warmest winters (2012, 2014, and 2016). In line with the studies by Cottier et al. (2007), there seems to be two processes governing the transformation of water masses in Isfjorden in winter; the rate of heat loss to the atmosphere, and heat gain from advected AW from the mouth.

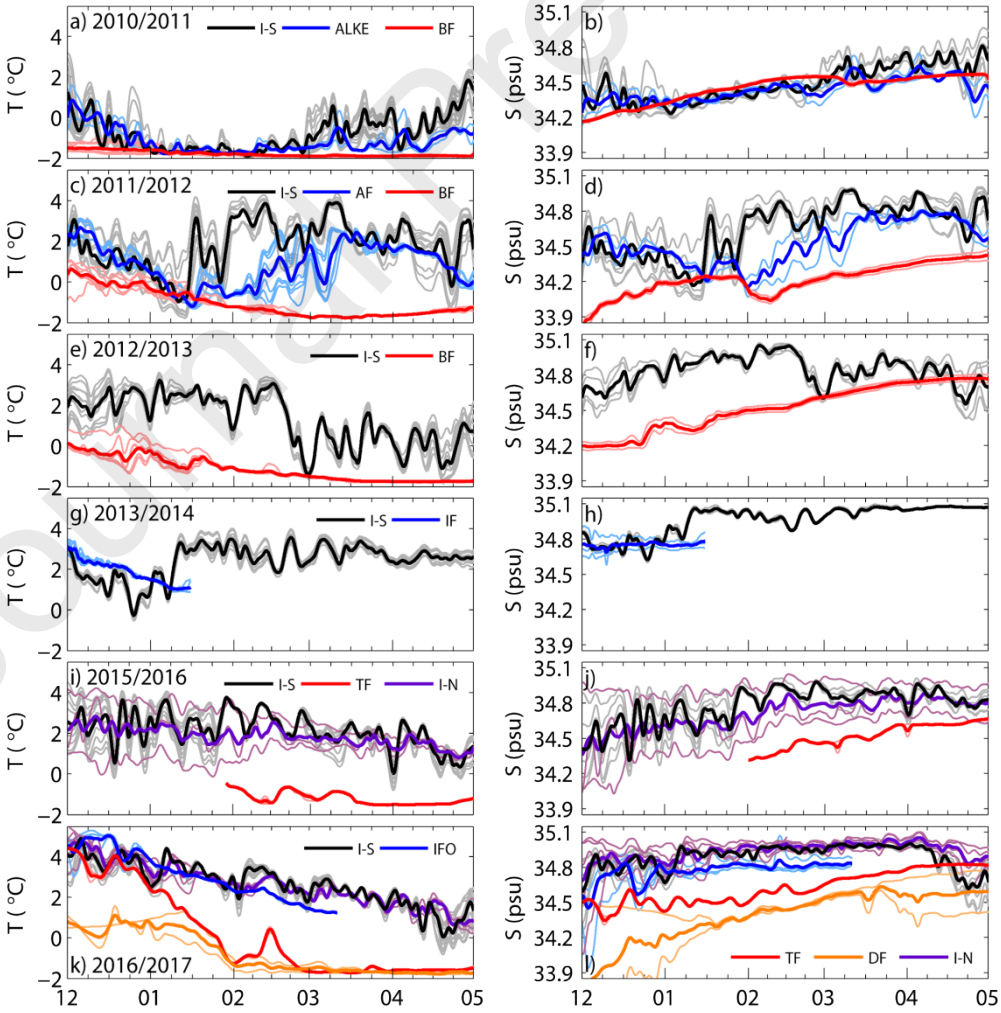

Figure 20: 72-hrs smoothed temperature (left) and salinity (right) time series from the moorings in the Isfjorden system (see Figure 1b and Table 3), showing only the time period from December to May in a)-b) 2010/2011, c)-d) 2011/2012, e)-f) 2012/2013, g)-h) 2013/2014, i)-j) 2015/2016, and k)-l) 2016/2017. The thick lines show the depth-averaged time series, and the thin lines with corresponding lighter colour tones show the time series from each measured depth (see Tables S3 and S4 in Supplementary data).

Looking more closely on winter 2011 (Figure 20a-b), synchronised peaks in temperature and salinity indicating TAW at the mouth in December 2010 and in March and April 2011, propagated to Isfjorden proper (ALKE) within 2-3 days, though with a lower amplitude. The signals did not propagate to inner Billefjorden, indicating deep inflow (deeper than the sill depth), or a heavily transformed inflow by the time it reached BF. Traversing a distance of about 50 km from I-S to ALKE, the propagation speed of these inflows was typically 20-30 cm s^{-1}, which is in line with the DAC time series (Section 5.3.1).

In winter 2012 (Figure 20c-d), a strong cooling was suddenly interrupted in the second week of January by a strong and persistent presence of AW at the mouth that gradually flowed into Isfjorden proper and eventually towards Adventfjorden (AF); first along the bottom, and then also close to surface by mid-March, before cooling started again. During the two months transition period at AF, from a cold homogenised water column in January to a warm and saline homogenised water column in March, several synchronised peaks in temperature and salinity at the mouth seem to have propagated to AF, but with less amplitude, within 3-4 days. This also fits with the DAC time series, given the longer distance from I-S. The high temperature in the whole water column at AF late in winter 2012 increased the heat content above sill level in inner Billefjorden at the same time, clearly suggesting cross-sill exchange of water masses between

Isfjorden proper and Billefjorden. Such cross-sill exchange has been observed in another West Spitsbergen fjord and was linked to internal tidal waves in addition to out-fjord wind stress (Arntsen et al., 2019). A similar situation seemed to happen in winter 2014 (Figure 20 g-h), only more extreme; first less cooling in early winter, and then, in the first week of January, a strong presence of AW in the whole water column at the mouth that lasted with very high salinities the rest of the winter. The AW was not as warm as the warmest AW in winter 2012 though. Unfortunately, mooring IF stopped measuring just when the deepest sensors started to register increased temperatures and salinities, about 3 days after the first AW peak at I-S in the second week of January 2014.

An opposite course of action seems to have happened in winter 2013 (Figure 20e-f), with TAW and AW persistently present at the mouth until end of February when suddenly colder and less saline water arrived at I-S. Unfortunately, no moorings were operative in Isfjorden proper this winter, but the synchronised peaks in temperature and salinity at BF during this time period suggest that TAW and AW must have flowed in high enough in the water column in Isfjorden proper in order to influence the water in inner Billefjorden. Here, the freezing point was reached in mid-March 2013, which was the latest of the measured winters at BF.

Winter 2016 reveals TAW and AW both at the southern and northern side of the mouth (I-S and I-N). No moorings were deployed in Isfjorden proper in winter 2016, but most likely inflow of TAW and AW happened in early winter, before the cooling densified the fjord water and gradually transformed the water inside Isfjorden to very saline and dense LW. Winter 2016 was classified as Winter Open from hydrography, and most likely the water did not reach the freezing point in Isfjorden proper as indicated by the SST (Figure 3c). This is also indicated by the synchronised increases in temperature and salinity at TF, about 10 days after the AW peaks at

I-S. Assuming a distance of about 115 km from I-S to TF, the AW, while being gradually transformed along its path, flowed into Isfjorden proper and further into Tempelfjorden with a mean speed of 13 cm s^{-1}, which is consistent with the current time series at TF (Section 5.3.1). Even though the inflow from the mouth to Isfjorden proper most likely ceased at some point this winter, the water in Tempelfjorden did not reach the freezing point in winter 2016, most likely due to the low cooling rate resulting from the warmer atmosphere this winter (Figure 3). A similar situation appears in winter 2017, which also was classified as Winter Open from hydrography. During fall 2016, the atmosphere stayed warmer than 0 °C and the freshwater supply did not cease until the second week of December, which was quite un-normal for Svalbard (https://www.yr.no/place/Norway/Svalbard/Longyearbyen/climate.html). Underneath this fresh surface layer, warm and saline AW was present and gradually filled the whole water column at the mouth after the freshwater supply stopped. Winter 2017 was colder (Figure 3), so the cooling rate was therefore stronger, but not strong enough for Isfjorden proper to reach the freezing point. Hence, an event with warmer and more saline water entered Tempelfjorden in mid-February about 10 days after the AW peak event at I-S, which also is seen in Isfjorden proper (IFO) some days earlier. Dicksonfjorden was clearly more protected from water exchange with Isfjorden proper. The cooling rate in winter 2017 was strong enough for Tempelfjorden and Dicksonfjorden to reach the freezing point, but some small deviations indicate exchange of water with Isfjorden proper throughout the whole winter.

6 Summary and conclusion

In this review of the Isfjorden hydrography, and in order to make a robust analysis of variability and trends during the time period 1987 to 2017, all non-published hydrographic profiles obtained by UNIS and collaborating partners have been combined with hydrographic profiles available in public databases. Here we have shown that Isfjorden has experienced changes in hydrography and AW inflow pattern the last decades, which only recently have been documented in the Arctic

Ocean north of Svalbard. Hence, we postulate that Isfjorden is a representative system to follow ocean climate change in the Arctic Ocean and in that way, be used as an indicator for climate change in the Eurasian part of Arctic Ocean.

During the time period 1987 to 2017, Isfjorden showed a mean summer structure with annually varying vertical placement of water of Atlantic origin. Before 2006, this warm and saline layer was normally present at the bottom below an intermediate layer of cold and less saline water, and a warm and low salinity surface layer. A regime shift happened from 2006 when this warm and saline layer increased in thickness and appeared higher up in the water column, above cold and less saline water at the bottom, and below warmer and low salinity surface water. A similar shift to fewer days of fast ice cover in Isfjorden was linked to positive trends in mean SST and VT (heat content) in Isfjorden over the same time period, both in winter and summer. In addition to the general atmospheric warming, most likely the positive trend in mean local air temperature in winter and summer was also a partial response to this shift and corresponding trends in the Isfjorden ocean climate. A positive trend in VS in winter and summer strongly suggests that increased advection of water of Atlantic origin, especially in winter, was the main reason for the change in Isfjorden's ocean climate during the studied period. The interannual variability in local mean air temperature in winter was related to the local mean wind direction and sea ice cover in winter, where the local mean wind direction most likely was connected to the path of the regional low-pressure systems passing either east (Barents Sea) or west (Fram Strait) of Svalbard in winter, bringing colder or warmer air masses over Svalbard, respectively (Rogers et al., 2005). Even though increasing numbers of deeper low-pressure systems have been observed to pass Svalbard in the recent decades, no clear trend in their paths has been detected (Zahn et al., 2018), and therefore no trend could be seen in the local mean wind direction in winter. Moreover, the interannual variability in local mean air temperature correlated significantly with the variability

in sea ice cover, mean SST, and VT both in winter and summer, which clearly signalises the impact of Isfjorden's ocean climate on the local terrestrial climate.

The summer layering of Isfjorden and the vertical placement of the warm and saline layer are found to be a combined result of the winter convection inside Isfjorden proper and the presence of AW at the fjord mouth. A conceptual drawing (Figure 21) provides an overview of the different forcing processes involved in the winter types defined as Winter Deep, Winter Intermediate, and Winter Open, combined with their different responses in water mass transformation, layering, and circulation (in- and outflow). A general cyclonic circulation is deduced from the mean hydrography in winter and summer. The inflow along the southern side is found to be narrower than the broad outflow on the northern side, and water mass transformations occur along the circulation path due to mixing with ambient water.

In Winter Deep (upper panels), favourable winds for out-fjord transport of sea ice combined with large heat flux to a cold atmosphere result in highly efficient sea ice formation and corresponding brine release to the water column below. A deep thermal and haline winter convection transforms the water column to cold and dense WCW. Only limited inflow of warmer TAW brought to the mouth by the STC can occur in intermediate layers. This affects the water mass in the inflow layer inside the fjord, leading to a presence of warmer LW instead of colder WCW. In the surface layer, the SPC provides water from the shelf and mouth in the south, while colder WCW from Isfjorden proper feeds the mouth, shelf, and the SPC in the north. In following summers with a reversed heat flux from sun radiation and a warmer atmosphere and freshwater added to the system, a well-defined surface layer with warm and low salinity SW develops. Inflow of AW happens in intermediate layers and transforms to TAW while circulating in Isfjorden proper

above a layer with remnants of colder and denser LW produced in winter. The IW layer becomes warm as a result of mixing between SW and TAW.

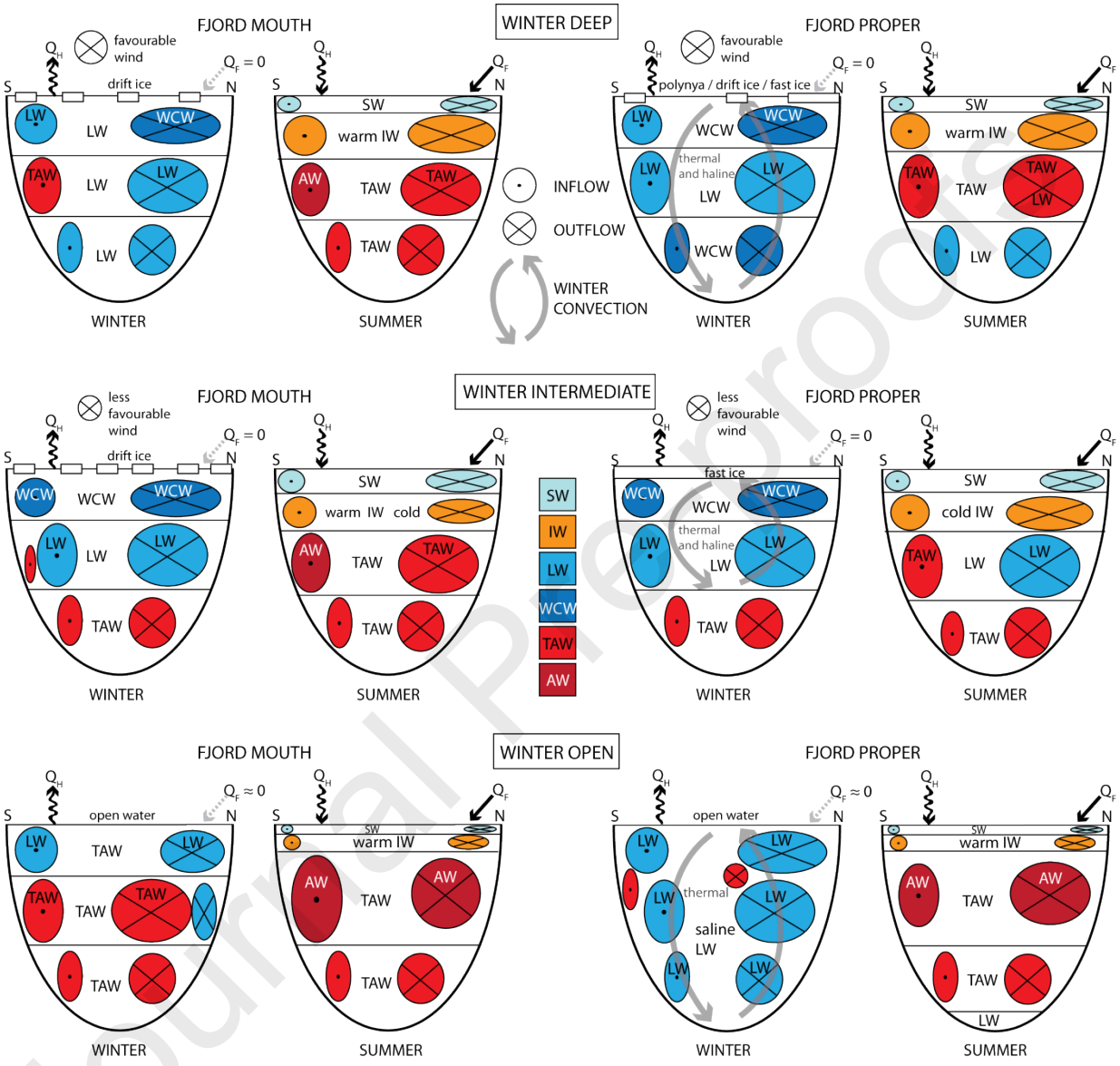

Figure 21: A conceptual drawing of the fjord's response in winter and summer hydrography (layering and water masses) and circulation (in- and outflow) to the three different winter convection types; Winter Deep (deep thermal and haline convection), Winter Intermediate (intermediate thermal and haline convection), and Winter Open (open water with only thermal convection) valid for broad Arctic fjords facing potential inflow of warm water of Atlantic origin

(TAW and AW). Cross sections at the fjord mouth are shown to the left and those in the fjord proper to the right, where S is the southern (inflow) side and N is the northern (outflow) side. Colours indicate the water masses defined for the Isfjorden system (see Table 1). Q_H is heat flux, Q_F is freshwater flux, and the white blocks on the surface in winter indicate drift ice and fast ice cover. Favourable wind means strong wind with direction favouring out-fjord transport of sea ice (Nilsen et al., 2008a).

Winter Intermediate (middle panels) with less favourable wind for out-fjord sea ice transport combined with a strong heat flux to the atmosphere result in more fast ice in Isfjorden. This results in less effective total ice production and corresponding brine release. The thermal and haline convection therefore reaches intermediate depths and transforms the water to the coldest, but less dense LW and WCW. Deep inflow of denser TAW from the mouth enters Isfjorden below cold LW in intermediate layers and cold WCW in the surface layer. Limited and narrow inflow of TAW can also occur in intermediate depths affecting both the mouth and Isfjorden proper. In the surface layer, cold WCW enters Isfjorden with the SPC, and cold WCW from Isfjorden leaves in the north. In summers following Winter Intermediate, the surface layer gets thicker, colder, and less saline. Inflow of TAW happens along the bottom below an intermediate layer with remnants of LW produced in winter. Moreover, narrow inflow of AW at intermediate depths might occur and transforms to TAW on the southern side in Isfjorden proper. This gradual transformation of the intermediate layer from inflowing AW at the mouth towards TAW in Isfjorden proper, and finally to cold LW flowing out on the northern side, mirrors the general cyclonic circulation in Isfjorden. Due to the mixing between SW and underlying water along the circulation path, a layer with warm IW evolves on the southern side close to the mouth and then cold IW in Isfjorden proper and on the northern side of the mouth.

Winter Open (lower panels) is the result of large volume inflow of AW to Isfjorden proper during the preceding fall and early winter. The heat flux from the ocean to the atmosphere is not strong enough to cool the water column down to freezing point. Instead a deep thermal convection combined with wind and tidal mixing transform the warm and saline water column to colder, saline, and the densest LW of all the winter types. Even though TAW is strongly present at the mouth, the very dense water produced by cooling in Isfjorden proper hinders inflow. Hence, an internal cyclonic circulation with LW seems to happen inside Isfjorden proper, and only limited narrow inflow of TAW might occur in shallower depths. In the surface layer, inflow of LW by the SPC happens in the south, and outflow of LW down to intermediate depths from Isfjorden feeds into the SPC in the north. In following summers, very thin and warm layers of SW and IW develop above TAW both at the mouth and in Isfjorden proper. Inflow of AW happens in a thick intermediate layer reaching high up in the water column, and circulates cyclonically in Isfjorden proper above colder and denser TAW, and remnants of very dense LW produced in winter.

In line with the positive trends in VT and VS, Isfjorden has during the last decades changed from being an Arctic type fjord with sea ice and limited or deep inflow of TAW in winter (dominated by Winter Deep and Intermediate) to a more Atlantic type fjord with heavy presence of AW in fall and early winter followed by little or no sea ice and limited inflow of TAW high up in the water column the rest of the winter (dominated by Winter Open). The freshwater content in summer has changed accordingly from typically more freshwater content in summers after Winter Intermediate (up to 4 m) and Deep (less freshwater content on the southern side), to nearly half the freshwater content in summers after Winter Open as a combined effect of advection of saltier water to Isfjorden and melting of less sea ice.

A monthly Atlantic Water index is introduced for the mouth area and for IsA. The indexes showed large seasonal (maximum in summer/early fall) and interannual variability with a maximum peak in 2014, and a positive trend in summer/early fall at the mouth. No similar trend was seen at IsA, reflecting the dependency on the inflow pattern (depth of inflow), and hence the winter type. Simultaneous (within a month) occurrence of AW and TAW at the mouth and IsA indicates topographically guided AW by the STC (Nilsen et al., 2016) towards the mouth and further to IsA. This is explained by a weak or absent density gradient between the shelf and fjord water, and hence no geostrophic control hindering inflow (Nilsen et al., 2008a). A delayed occurrence (within 2 months) of TAW at IsA indicates a gradual breakdown of the geostrophic control, or a deep inflow that gradually mixed towards IsA. Occurrence of AW at the mouth and no TAW at IsA indicate full geostrophic control that prevented inflow of TAW.

Varying presence of water masses at the mouth mirrors the water masses in the SPC competing in strength with the STC. The typical seasonal pattern with winter cooling was frequently interrupted due to advection of AW. In some winters, the water column at the mouth showed a transition back and forth between Arctic type water brought by the SPC along the shelf and Atlantic type water carried by the STC towards the mouth along the Isfjorden Through. Strong alongshore wind stress and wind stress curl on the shelf has been shown to accelerate the WSC and hence the STC, forcing AW to follow shallower isobaths towards the mouth and in extreme cases to flood the shelf (Nilsen et al., 2016). The monthly climatological mean of the fjord mouth hydrography reveals that AW influence has been common in winter the last decades, with February showing a local maximum in mean temperature and the largest increase in mean salinity. A concomitant maximum in mean current speed directed towards the mouth along the isobaths, supports a speedup of the STC to bring Atlantic type water to the mouth area. Moreover, a stronger east component in the mean current at the mouth shows more inflow of TAW to

Isfjorden proper, like in 2014, with no density difference between the shelf and fjord water. A stronger north component indicates less inflow, like in 2016 and 2017 due to denser fjord water. The climatology at the mouth also shows that warm and saline (cold and less saline) water was accompanied with stronger (slower) currents. This leads to the conclusion that AW will manage to enter the mouth when the STC is strong enough to pass the SPC. On the shelf, the lack of sea ice in the northwestern Barents Sea in recent winters will lead to less input of ArW to the SPC (Tverberg et al., 2019). The SPC is therefore likely to carry water in winter more influenced by AW intrusion on the shelf, resulting in denser shelf water accompanied with the heat flux to the atmosphere. Eddy overturning will further lead warmer AW from the WSC water column above more cooled and denser shelf water influenced by AW.

The cyclonic circulation pattern deduced from the hydrography is supported by all the different current data in this study. A seasonal signal is apparent with stronger currents in winter at the mouth due to stronger alongshore winds, whereas weaker currents are seen in Isfjorden and its side fjords, especially in winters with solid sea ice cover. Current speeds reached 80 and 45 cm s^{-1} at the southern and northern side of the mouth, respectively, 50 cm s^{-1} in Isfjorden proper, and typically less than 20 cm s^{-1} in the inner part of the side fjords. The strongest currents were typically oriented along the isobaths following the path of the mean cyclonic circulation, but also show instances of equally strong but reversed flow. DACs from gliders and VM-ADCP also demonstrate some deviations from the general pattern most likely due to wind-induced transport in the surface Ekman layer. As also suggested from hydrography, the DACs from gliders indicate an inflow close to the southern bank with varying strength and width; sometimes too weak, narrow, or close to shore to be captured. Moreover, the outflow on the northern side was broader, strong, and consistent during both glider campaigns supporting the findings from hydrography. The DACs from VM-ADCP showed a faster upper layer at the mouth, but slowed down in

Isfjorden proper. The lower layer was more guided by topography and demonstrated a topographically adjustment due to the shallow topographic features in Isfjorden proper, and hence confirming the bottom layer circulation deduced from hydrography.

Tides were found to play a minor role in the current variance (3% at the mouth and up to 20% in the side fjords), but a major role in the variance of sea surface elevation (50% at the mouth and up to 100% in the side fjords). The dominant components in the tidal elevation were M2 (0.5 m), S2 (0.2 m), N2 (0.1 m), and K1 (0.1 m), and the total tidal amplitude was about 1 m at all mooring locations. The tidal currents were dominated by the same constituents, but also by shallow water constituents depending on the location. The M2 tidal ellipses reveal a rectilinear tidal flow along isobaths. The tidal current was 8 cm s^{-1} at the mouth, typically 5 cm s^{-1} in Isfjorden proper, and < 2 cm s^{-1} in the inner side fjords. Despite small tidal currents, the tidal elevation can play a major role in cross-sill exchange flow between Isfjorden proper and its sill-protected side fjords.

Concomitant hydrographic time series in winter at different locations in the Isfjorden system show that peak signals of AW at the mouth propagated into Isfjorden proper. Assuming mixing with surrounding water masses lowered the temperature and salinity signals, the propagation speeds were in line with the mean current. The local cooling process was therefore interrupted and the temperature stayed above freezing. Even the sill fjords were affected with increased temperature and salinity, especially in winters when signals propagated along shallower depths due to extreme presence of AW at the mouth. This suggests exchange of water between the warmer Isfjorden proper and its side fjords throughout the winter. This can severely impact the sea ice cover, by delaying or even preventing its formation during extreme winters. Moreover, the melting of an established sea ice cover through these exchange processes is becoming a problem for both local wildlife and human settlements in winter.

7 Acknowledgement

This study was financially supported by the projects REOCIRC (#222696/F50) and GrønnBille (#227067, RIS-ID 6700) funded by the Research Council of Norway (RCN). We would like to thank all the students and colleagues at UNIS for their valuable effort in collecting data during the UNIS student and research cruises over the years. IFO was funded by the Svalbard Environmental Protection Fund through the project «Blir det is på Isfjorden i år?» (RIS-ID 10586). Arild Sundfjord at the Norwegian Polar Institute is acknowledged for the ALKE data, which were obtained through the ALKEKONGE project funded by the Polish-Norwegian Research grant PNRF-234-AI-1/07. Abdirahman Omar at the Uni Research in Bergen is acknowledged for the DF data obtained through the SKD-project BASIC at the Bjerknes Centre for Climate Research. Denis Moiseev at the Murmansk Marine Biological Institute is acknowledged for CTD data in December 2015. SAMS moorings (BF, AF and IF) were supported by the RCN projects: Circa (#214271) and Cleopatra I and II (#178766, #216537). We acknowledge the contributions of Colin Griffiths, Estelle Dumont and Lewis Drysdale in the preparation of the SAMS data. FCs contribution to this work is supported by SAGES (www.sages.ac.uk) and RCN project Arctic ABC (#244319). We thank the two anonymous reviewers for their constructive comments that greatly improved the manuscript.

UNIS HD is available in the NPI dataset catalogue (Skogseth et al., 2019; https://doi.org/10.21334/unis-hydrography) in addition to the I-S (Skogseth and Ellingsen, 2019; 2005-2006: https://doi.org/10.21334/npolar.2019.176eea39; 2006-2007: https://doi.org/10.21334/npolar.2019.a1239ca3; 2007-2008: https://doi.org/10.21334/npolar.2019.064a09b7; 2010-2011: https://doi.org/10.21334/npolar.2019.b0e473c4; 2011-2012: https://doi.org/10.21334/npolar.2019.2be7bdee; 2012-2013: https://doi.org/10.21334/npolar.2019.a247e9a9; 2013-2014: https://doi.org/10.21334/npolar.2019.6813ce6d; 2014-2015: https://doi.org/10.21334/npolar.2019.11b7e849; 2015-2016: https://doi.org/10.21334/npolar.2019.21838303; 2016-2017: https://doi.org/10.21334/npolar.2019.cd7a2f7c), the I-N (Skogseth and Ellingsen, 2019; 2015-2016: https://doi.org/10.21334/npolar.2019.111aca43; 2016-2017: https://doi.org/10.21334/npolar.2019.3078f619), the IFO (Skogseth and Ellingsen, 2019; https://doi.org/10.21334/npolar.2019.7718a106), and the TF (Skogseth and Ellingsen, 2019; https://doi.org/10.21334/npolar.2019.5add522e) mooring data.

8 References

Arntsen, M., Sundfjord, A., Skogseth, R., Błaszczyk, M., Promińska, A., 2019. Inflow of Warm Water to the Inner Hornsund Fjord, Svalbard: Exchange Mechanisms and Influence on Local Sea Ice Cover and Glacier Front Melting. Journal of Geophysical Research: Oceans. https://doi.org/10.1029/2018jc014315

Barnes, E.A., Dunn-Sigouin, E., Masato, G., Woollings, T., 2014. Exploring recent trends in Northern Hemisphere blocking. Geophys. Res. Lett. 41, 638–644.

Berge, J., Heggland, K., Lønne, O.J., Cottier, F., Hop, H., Gabrielsen, G.W., Nøttestad, L., Misund, O.A., 2015. First Records of Atlantic Mackerel (Scomber scombrus) from the Svalbard Archipelago, Norway, with Possible Explanations for the Extension of Its Distribution. ARCTIC. https://doi.org/10.14430/arctic4455

Berge, J., Johnsen, G., Nilsen, F., Gulliksen, B., Slagstad, D., 2005. Ocean temperature oscillations enable reappearance of blue mussels Mytilus edulis in Svalbard after a 1000 year absence. Mar. Ecol. Prog. Ser. 303, 167–175.

Berge, J., Renaud, P.E., Eiane, K., Gulliksen, B., Cottier, F.R., Varpe, Ø., Brattegard, T., 2009. Changes in the decapod fauna of an Arctic fjord during the last 100 years (1908–2007). Polar Biology. https://doi.org/10.1007/s00300-009-0594-5

Bergstad, O.A., Johannesen, E., Høines, Å., Ellingsen, K.E., Lien, V.S., Byrkjedal, I., Yoccoz, N.G., Tveraa, T., Wienerroither, R., Langhelle, G., de Lange Wenneck, T., 2018. Demersal fish assemblages in the boreo-Arctic shelf waters around Svalbard during the warm period 2007–2014. Polar Biology. https://doi.org/10.1007/s00300-017-2176-2

Beszczynska-Moller, A., Fahrbach, E., Schauer, U., Hansen, E., 2012. Variability in Atlantic water temperature and transport at the entrance to the Arctic Ocean, 1997-2010. ICES J. Mar. Sci. 69, 852–863.

Carmack, E., Polyakov, I., Padman, L., Fer, I., Hunke, E., Hutchings, J., Jackson, J., Kelley, D., Kwok, R., Layton, C., Melling, H., Perovich, D., Persson, O., Ruddick, B., -L. Timmermans, M., Toole, J., Ross, T., Vavrus, S., Winsor, P., 2015. Toward Quantifying the Increasing Role of Oceanic Heat in Sea Ice Loss in the New Arctic. Bull. Am. Meteorol. Soc. 96, 2079–2105.

Cottier, F.R., Nilsen, F., Inall, M.E., Gerland, S., Tverberg, V., Svendsen, H., 2007. Wintertime warming of an Arctic shelf in response to large-scale atmospheric circulation. Geophys. Res. Lett. 34. https://doi.org/10.1029/2007gl029948

Dalpadado, P., Hop, H., Rønning, J., Pavlov, V., Sperfeld, E., Buchholz, F., Rey, A., Wold, A., 2016. Distribution and abundance of euphausiids and pelagic amphipods in Kongsfjorden, Isfjorden and Rijpfjorden (Svalbard) and changes in their relative importance as key prey in a warming marine ecosystem. Polar Biology. https://doi.org/10.1007/s00300-015-1874-x

Darnis, G., Hobbs, L., Geoffroy, M., Grenvald, J.C., Renaud, P.E., Berge, J., Cottier, F., Kristiansen, S., Daase, M., Søreide, J.E., Wold, A., Morata, N., Gabrielsen, T., 2017. From polar night to midnight sun: Diel vertical migration, metabolism and biogeochemical role of zooplankton in a high Arctic fjord (Kongsfjorden, Svalbard). Limnology and Oceanography. https://doi.org/10.1002/lno.10519

Donlon, C.J., Martin, M., Stark, J., Roberts-Jones, J., Fiedler, E., Wimmer, W., 2012. The Operational Sea Surface Temperature and Sea Ice Analysis (OSTIA) system. Remote Sens. Environ. 116, 140–158.

Ericson, Y., Falck, E., Chierici, M., Fransson, A., Kristiansen, S., Platt, S.M., Hermansen, O., Myhre, C.L., 2018. Temporal Variability in Surface Water p CO2 in Adventfjorden (West Spitsbergen) With Emphasis on Physical and Biogeochemical Drivers. J. Geophys. Res. C: Oceans 123, 4888–4905.

Falk-Petersen, S., Pavlov, V., Berge, J., Cottier, F., Kovacs, K.M., Lydersen, C., 2015. At the rainbow's end: high productivity fueled by winter upwelling along an Arctic shelf. Pol. Biology 38, 5–11.

Francis, J.A., Vavrus, S.J., 2012. Evidence linking Arctic amplification to extreme weather in mid-latitudes. Geophys. Res. Lett. 39. https://doi.org/10.1029/2012gl051000

Fraser, N.J., Inall, M.E., 2018. Influence of Barrier Wind Forcing on Heat Delivery Toward the Greenland Ice Sheet. J. Geophys. Res. C: Oceans 123, 2513–2538.

Fraser, N.J., Inall, M.E., Magaldi, M.G., Haine, T.W.N., Jones, S.C., 2018a. Wintertime Fjord-Shelf Interaction and Ice Sheet Melting in Southeast Greenland. J. Geophys. Res. C: Oceans. https://doi.org/10.1029/2018jc014435

Fraser, N.J., Skogseth, R., Nilsen, F., Inall, M.E., 2018b. Circulation and exchange in a broad Arctic fjord using glider-based observations. Polar Res. 37, 1485417.

Geoffroy, M., Berge, J., Majaneva, S., Johnsen, G., Langbehn, T.J., Cottier, F., Mogstad, A.A., Zolich, A., Last, K., 2018. Increased occurrence of the jellyfish Periphylla periphylla in the European high Arctic. Polar Biology. https://doi.org/10.1007/s00300-018-2368-4

Gluchowska, M., Kwasniewski, S., Prominska, A., Olszewska, A., Goszczko, I., Falk-Petersen, S., Hop, H., Weslawski, J.M., 2016. Zooplankton in Svalbard fjords on the Atlantic–Arctic boundary. Polar Biology. https://doi.org/10.1007/s00300-016-1991-1

Goszczko, I., Ingvaldsen, R.B., Onarheim, I.H., 2018. Wind-Driven Cross-Shelf Exchange-West Spitsbergen Current as a Source of Heat and Salt for the Adjacent Shelf in Arctic Winters. J. Geophys. Res. C: Oceans 123, 2668–2696.

Hagen, J.O., Kohler, J., Melvold, K., Winther, J.-G., 2003. Glaciers in Svalbard: mass balance, runoff and freshwater flux. Polar Res. 22, 145–159.

Hanssen-Bauer, I., Førland, E.J., Hisdal, H., Mayer, S., Sandø, A.B., Sorteberg, A., 2019. Climate in Svalbard 2100 – a knowledge base for climate adaptation (No. 1). The Norwegian Centre for Climate Services.

Hegseth, E.N., Tverberg, V., 2013. Effect of Atlantic water inflow on timing of the phytoplankton spring bloom in a high Arctic fjord (Kongsfjorden, Svalbard). J. Mar. Syst. 113-114, 94–105.

Helland-Hansen, B., Nansen, F., 1909. The Norwegian Sea: Its Physical Oceanography Based Upon the Norwegian Researches 1900-1904.

Hop, H., Wold, A., Vihtakari, M., Daase, M., Kwasniewski, S., Gluchowska, M., Lischka, S., Buchholz, F., Falk-Petersen, S., 2019. Zooplankton in Kongsfjorden (1996-2016) in relation to climate change, in: Hop, H., Wiencke, C. (Eds.), The Ecosystem of Kongsfjorden, Svalbard, Advances in Polar Ecology. Springer Verlag.

Hünerlage, L.K., 2015. Krill in the Arctic and the Atlantic: Climatic Variability and Adaptive Capacity (PhD). University of Hamburg .

Inall, M.E., Murray, T., Cottier, F.R., Scharrer, K., Boyd, T.J., Heywood, K.J., Bevan, S.L., 2014. Oceanic heat delivery via Kangerdlugssuaq Fjord to the south-east Greenland ice sheet. J. Geophys. Res. C: Oceans 119, 631–645.

Inall, M.E., Nilsen, F., Cottier, F.R., Daae, R., 2015. Shelf/fjord exchange driven by coastal-trapped waves in the Arctic. J. Geophys. Res. C: Oceans 120, 8283–8303.

Jackson, R.H., Lentz, S.J., Straneo, F., 2018. The Dynamics of Shelf Forcing in Greenlandic Fjords. J. Phys. Oceanogr. 48, 2799–2827.

Jakobsson, M., Mayer, L. A., Coakley, B., Dowdeswell, J. A., Forbes, S., Fridman, B., Hodnesdal, H., Noormets, R., Pedersen, R., Rebesco, M., Schenke, H.-W., Zarayskaya, Y., Accettella, A, D., Armstrong, A., Anderson, R. M., Bienhoff, P., Camerlenghi, A., Church, I., Edwards, M., Gardner, J. V., Hall, J. K., Hell, B., Hestvik, O. B., Kristoffersen, Y., Marcussen, C., Mohammad, R., Mosher, D., Nghiem, S. V., Pedrosa, M. T., Travaglini, P. G., Weatherall, P., 2012. The International Bathymetric Chart of the Arctic Ocean (IBCAO) Version 3.0, Geophysical Research Letters, Vol.39, L12609, doi:10.1029/2012GL052219.

Killingtveit, Å., Pettersson, L.-E., Sand, K., 2003. Water balance investigations in Svalbard. Polar Res. 22, 161–174.

Kortsch, S., Primicerio, R., Beuchel, F., Renaud, P.E., Rodrigues, J., Lønne, O.J., Gulliksen, B., 2012. Climate-driven regime shifts in Arctic marine benthos. Proc. Natl. Acad. Sci. U. S. A. 109, 14052–14057.

Kowalik, Z., Marchenko, A., Brazhnikov, D., Marchenko, N., 2015. Tidal currents in the western Svalbard Fjords. Oceanologia 57, 318–327.

Kubiszyn, A.M., Piwosz, K., Wiktor, J.M., Wiktor, J.M., 2014. The effect of inter-annual Atlantic water inflow variability on the planktonic protist community structure in the

West Spitsbergen waters during the summer. Journal of Plankton Research. https://doi.org/10.1093/plankt/fbu044

Kubiszyn, A.M., Wiktor, J.M., Wiktor, J.M., Griffiths, C., Kristiansen, S., Gabrielsen, T.M., 2017. The annual planktonic protist community structure in an ice-free high Arctic fjord (Adventfjorden, West Spitsbergen). J. Mar. Syst. 169, 61–72.

Leopold, P., Renaud, P.E., Ambrose, W.G., Berge, J., 2019. High Arctic Mytilus spp.: occurrence, distribution and history of dispersal. Polar Biology. https://doi.org/10.1007/s00300-018-2415-1

Lind, S., Ingvaldsen, R.B., Furevik, T., 2018. Arctic warming hotspot in the northern Barents Sea linked to declining sea-ice import. Nat. Clim. Chang. 8, 634–639.

Loeng, H., 1991. Features of the physical oceanographic conditions of the Barents Sea. Polar Res. 10, 5–18.

Lowther, A.D., Fisk, A., Kovacs, K.M., Lydersen, C., 2017. Interdecadal changes in the marine food web along the west Spitsbergen coast detected in the stable isotope composition of ringed seal (Pusa hispida) whiskers. Polar Biology. https://doi.org/10.1007/s00300-017-2122-3

Luckman, A., Benn, D.I., Cottier, F., Bevan, S., Nilsen, F., Inall, M., 2015. Calving rates at tidewater glaciers vary strongly with ocean temperature. Nat. Commun. 6. https://doi.org/10.1038/ncomms9566

Marquardt, M., Vader, A., Stübner, E.I., Reigstad, M., Gabrielsen, T.M., 2016. Strong Seasonality of Marine Microbial Eukaryotes in a High-Arctic Fjord (Isfjorden, in West Spitsbergen, Norway). Appl. Environ. Microbiol. 82, 1868–1880.

Marquardt, M., Skogseth, R., Wiedmann, I., Vader, A., Reigstad, M., Cottier, F., Gabrielsen, T.M., 2019. Vertical export of marine pelagic protists in an ice-free high-Arctic fjord throughout 2011-2012 (Adventfjorden, West Spitsbergen). Accepted in Aquatic Microbial Ecology.

Merckelbach, L.M., Briggs, R.D., Smeed, D.A., Griffiths, G., 2008. Current measurements from autonomous underwater gliders, in: 2008 IEEE/OES 9th Working Conference on Current Measurement Technology. https://doi.org/10.1109/ccm.2008.4480845

Muckenhuber, S., Nilsen, F., Korosov, A., Sandven, S., 2016. Sea ice cover in Isfjorden and Hornsund, Svalbard (2000–2014) from remote sensing data. The Cryosphere 10, 149–158.

Nilsen, F., Cottier, F., Skogseth, R., Mattsson, S., 2008a. Fjord–shelf exchanges controlled by ice and brine production: The inter-annual variation of Atlantic Water in Isfjorden, Svalbard. Cont. Shelf Res. 28, 1838–1853.

Nilsen, F., Skogseth, R., Vaardal-Lunde, J., Inall, M., 2016. A Simple Shelf Circulation Model: Intrusion of Atlantic Water on the West Spitsbergen Shelf. J. Phys. Oceanogr. 46, 1209–1230.

Nilsen, J.E., Hátún, H., Mork, K.A., Valdimarsson, H., 2008b. The NISE Dataset (No. 08-01). Faroese Fisheries Laboratory. https://doi.org/10.13140/RG.2.1.3097.944

Nordli, Ø., Przybylak, R., Ogilvie, A.E.J., Isaksen, K., 2014. Long-term temperature trends and variability on Spitsbergen: the extended Svalbard Airport temperature series, 1898–2012. Polar Res. 33, 21349.

Onarheim, I.H., Eldevik, T., Smedsrud, L.H., Stroeve, J.C., 2018. Seasonal and Regional Manifestation of Arctic Sea Ice Loss. J. Clim. 31, 4917–4932.

Onarheim, I.H., Smedsrud, L.H., Ingvaldsen, R.B., Nilsen, F., 2014. Loss of sea ice during winter north of Svalbard. Tellus Ser. A Dyn. Meteorol. Oceanogr. 66, 23933.

Padman, L., Erofeeva, S., 2004. A barotropic inverse tidal model for the Arctic Ocean. Geophys. Res. Lett. 31. https://doi.org/10.1029/2003gl019003

Paulsen, M.L., Doré, H., Garczarek, L., Seuthe, L., Müller, O., Sandaa, R.-A., Bratbak, G., Larsen, A., 2016. Synechococcus in the Atlantic Gateway to the Arctic Ocean. Frontiers in Marine Science. https://doi.org/10.3389/fmars.2016.00191

Pavlov, A.K., Tverberg, V., Ivanov, B.V., Nilsen, F., Falk-Petersen, S., Granskog, M.A., 2013. Warming of Atlantic Water in two west Spitsbergen fjords over the last century (1912–2009). Polar Research. https://doi.org/10.3402/polar.v32i0.11206

Pawlowicz, R., Beardsley, B., Lentz, S., 2002. Classical tidal harmonic analysis including error estimates in MATLAB using T_TIDE. Comput. Geosci. 28, 929–937.

Pedlosky, J., 1987. Geophysical Fluid Dynamics. Springer, www.springer-ny.com.

Polyakov, I.V., Pnyushkov, A.V., Alkire, M.B., Ashik, I.M., Baumann, T.M., Carmack, E.C., Goszczko, I., Guthrie, J., Ivanov, V.V., Kanzow, T., Krishfield, R., Kwok, R., Sundfjord, A., Morison, J., Rember, R., Yulin, A., 2017. Greater role for Atlantic inflows on sea-ice loss in the Eurasian Basin of the Arctic Ocean. Science 356, 285–291.

Pond, S., Pickard, G.L., 2013. Introductory Dynamical Oceanography. Elsevier.

Promińska, A., Falck, E., Walczowski, W., 2018. Inter-annual variability in hydrography and water mass distribution in Hornsund, an Arctic fjord in Svalbard. Polar Res. 37, 1495546.

Rasmussen, T.L., Forwick, M., Mackensen, A., 2013. Reprint of: Reconstruction of inflow of Atlantic Water to Isfjorden, Svalbard during the Holocene: Correlation to climate and seasonality. Mar. Micropaleontol. 99, 18–28.

Reistad, M., Breivik, Ø., Haakenstad, H., Aarnes, O.J., Furevik, B.R., Bidlot, J.-R., 2011. A high-resolution hindcast of wind and waves for the North Sea, the Norwegian Sea, and the Barents Sea. J. Geophys. Res. 116. https://doi.org/10.1029/2010jc006402

Renaud, P.E., Berge, J., Varpe, Ø., Lønne, O.J., Nahrgang, J., Ottesen, C., Hallanger, I., 2012. Is the poleward expansion by Atlantic cod and haddock threatening native polar cod, Boreogadus saida? Polar Biology. https://doi.org/10.1007/s00300-011-1085-z

Rogers, J.C., Yang, L., Li, L., 2005. The role of Fram Strait winter cyclones on sea ice flux and on Spitsbergen air temperatures. Geophys. Res. Letters 32. https://doi.org/10.1029/2004gl022262

Saloranta, T.M., Svendsen, H., 2001. Across the Arctic front west of Spitsbergen: high-resolution CTD sections from 1998-2000. Polar Res. 20, 177–184.

Serreze, M.C., Barry, R.G., 2011. Processes and impacts of Arctic amplification: A research synthesis. Glob. Planet. Change 77, 85–96.

Skarðhamar, J., Svendsen, H., 2010. Short-term hydrographic variability in a stratified Arctic fjord. Geological Society, London, Special Publications 344, 51–60.

Skeie, P., Grønås, S., 2000. Strongly stratified easterly flows across Spitsbergen. Tellus Ser. A Dyn. Meteorol. Oceanogr. 52, 473–486.

Skogseth, R., Ellingsen, P., Berge, J., Cottier, F., Falk-Petersen, S., Ivanov, B., Nilsen, F., Søreide, J., Vader, A. (2019). UNIS hydrographic database [Data set]. Norwegian Polar Institute. https://doi.org/10.21334/unis-hydrography

Straneo, F., Hamilton, G.S., Sutherland, D.A., Stearns, L.A., Davidson, F., Hammill, M.O., Stenson, G.B., Rosing-Asvid, A., 2010. Rapid circulation of warm subtropical waters in a major glacial fjord in East Greenland. Nat. Geosci. 3, 182–186.

Stroeve, J., Notz, D., 2018. Changing state of Arctic sea ice across all seasons. Environ. Res. Lett. 13, 103001.

Stübner, E.I., Søreide, J.E., Reigstad, M., Marquardt, M., Blachowiak-Samolyk, K., 2016. Year-round meroplankton dynamics in high-Arctic Svalbard. J. Plankton Res. 38, 522–536.

Sundfjord, A., Albretsen, J., Kasajima, Y., Skogseth, R., Kohler, J., Nuth, C., Skarðhamar, J., Cottier, F., Nilsen, F., Asplin, L., Gerland, S., Torsvik, T., 2017. Effects of glacier runoff and wind on surface layer dynamics and Atlantic Water exchange in

Kongsfjorden, Svalbard; a model study. Estuarine, Coastal and Shelf Science. https://doi.org/10.1016/j.ecss.2017.01.015

Svendsen, H., Beszczynska-Møller, A., Hagen, J.O., Lefauconnier, B., Tverberg, V., Gerland, S., Ørbæk, J.B., Bischof, K., Papucci, C., Zajaczkowski, M., Azzolini, R., Bruland, O., Wiencke, C., 2002. The physical environment of Kongsfjorden–Krossfjorden, an Arctic fjord system in Svalbard. Polar Res. 21, 133–166.

Tartu, S., Bourgeon, S., Aars, J., Andersen, M., Polder, A., Thiemann, G.W., Welker, J.M., Routti, H., 2017. Sea ice-associated decline in body condition leads to increased concentrations of lipophilic pollutants in polar bears (Ursus maritimus) from Svalbard, Norway. Sci. Total Environ. 576, 409–419.

Teigen, S.H., Nilsen, F., Gjevik, B., 2010. Barotropic instability in the West Spitsbergen Current. J. Geophys. Res. 115. https://doi.org/10.1029/2009jc005996

Teigen, S.H., Nilsen, F., Skogseth, R., Gjevik, B., Beszczynska-Möller, A., 2011. Baroclinic instability in the West Spitsbergen Current. J. Geophys. Res. 116. https://doi.org/10.1029/2011jc006974

Tverberg, V., Nøst, O.A., 2009. Eddy overturning across a shelf edge front: Kongsfjorden, west Spitsbergen. J. Geophys. Res. 114. https://doi.org/10.1029/2008jc005106

Tverberg, V., Nøst, O.A., Lydersen, C., Kovacs, K.M., 2014. Winter sea ice melting in the Atlantic Water subduction area, Svalbard Norway. Journal of Geophysical Research: Oceans. https://doi.org/10.1002/2014jc010013

Tverberg, V., Skogseth, R., Cottier, F., Sundfjord, A., Walczowski, W., Inall, M., Falck, E., Pavlova, O., Nilsen, F., 2019. The Kongsfjorden Transect: seasonal and inter-annual variability in hydrography, in: Hop, H., Weincke, C. (Eds.), The Ecosystem of Kongsfjorden, Svalbard, Advances in Polar Ecology. Springer Verlag.

Uppala, S.M., Kållberg, P.W., Simmons, A.J., Andreae, U., Da Costa Bechtold, V., Fiorino, M., Gibson, J.K., Haseler, J., Hernandez, A., Kelly, G.A., Li, X., Onogi, K., Saarinen, S., Sokka, N., Allan, R.P., Andersson, E., Arpe, K., Balmaseda, M.A., Van Der Berg, L., Beljaars, A.C.M., Bidlot, J., Bormann, N., Caires, S., Chevallier, F., Dethof, A., Dragosavac, M., Fisher, M., Fuentes, M., Hagemann, Hoskins, B.J., Isaksen, L., Janssen, P.A.E.M., Jenne, R., McNally, A.P., Mahfouf, J.-F., Morcrette, J.-J., Rayner, N.A., Saunders, R.W., Simon, P., Sterl, A., Trenberth, K.E., Untch, A., Vasiljevic, D., Viterbo, P., Woolen, J., 2005. The ERA-40 re-analysis. Q. J. Royal Meteorol. Soc. 131, 2961–3012.

Vihtakari, M., Welcker, J., Moe, B., Chastel, O., Tartu, S., Hop, H., Bech, C., Descamps, S., Gabrielsen, G.W., 2018. Black-legged kittiwakes as messengers of Atlantification in the Arctic. Sci. Rep. 8, 1178.

Vogedes, D., Eiane, K., Båtnes, A.S., Berge, J., 2014. Variability inCalanusspp. abundance on fine- to mesoscales in an Arctic fjord: implications for little auk feeding. Marine Biology Research. https://doi.org/10.1080/17451000.2013.815781

Walczowski, W., Beszczynska-Möller, A., Wieczorek, P., Merchel, M., Grynczel, A., 2017. Oceanographic observations in the Nordic Sea and Fram Strait in 2016 under the IO PAN long-term monitoring program AREX. Oceanologia 59, 187–194.

Wiedmann, I., Reigstad, M., Marquardt, M., Vader, A., Gabrielsen, T.M., 2016. Seasonality of vertical flux and sinking particle characteristics in an ice-free high arctic fjord—Different from subarctic fjords? J. Mar. Syst. 154, 192–205.

Zahn, M., Akperov, M., Rinke, A., Feser, F., Mokhov, I.I., 2018. Trends of Cyclone Characteristics in the Arctic and Their Patterns From Different Reanalysis Data. J. Geophys. Res. D: Atmos. 123, 2737–2751.

S. Supplementary data

In the following, tables with complementary details of instrumentation and data collection are provided for the manuscript "Variability and decadal trends in the Isfjorden (Svalbard) ocean climate and circulation – an indicator for climate change in the Arctic Ocean" by Skogseth et al. A description of each mooring accompanies the tables listing their deployment details. Also, an overview of the classified winters is provided in a table. Distribution of temperature, salinity, potential density anomaly, and water masses for each summer and winter with enough data to obtain interpolated sections along the Isfjorden Transect are shown and sorted by their classified winter type, i.e. Winter Deep, Winter Intermediate, and Winter Open.

S.1 Tables

S.1.1 Instrument accuracy and resolution

Table S1: Initial accuracy and resolution of the sensors providing temperature (T), conductivity (C), pressure (p), current speed (u_{sp}) and direction (u_{dir}), and vertical speed (w_{sp}) on the most common CTDs used to collect data in UNIS HD (Skogseth et al., 2019), and on the recording instruments mounted on the different moorings in the Isfjorden system listed in Tables S4 and S5.

Instrument	Initial accuracy	Resolution
Sea-Bird Scientific:		
SBE 911+	T: ±0.001°C; C: ±0.0003 S m^{-1} p: ± 0.015% *fso**	T: 0.0002°C; C: 0.00004 S m^{-1} p: 0.001% *fso*
SBE 19 plus V2	T: ±0.005°C; C: ±0.0005 S m^{-1} p: ±0.1% *fso*	T: 0.0001°C; C: 0.00005 S m^{-1} p: 0.002% *fso*
SBE 37 MicroCAT	T: ±0.002°C; C: ±0.0003 S m^{-1} p: ±0.1% *fso*	T: 0.0001°C; C: 0.00001 S m^{-1} p: 0.001% *fso*
SBE 16 SeaCAT	T: ±0.005°C, C: ±0.0005 S m^{-1} p: ±0.1% *fso*	T: 0.0001°C; C: 0.00005 S m^{-1} p: 0.002% *fso*
Neil Brown Mark III	T: ±0.005°C, C: ±0.001 S m^{-1}	T: 0.0001°C; C: 0.00001 S m^{-1}
SAIV SD204	T: ±0.01°C, C: ±0.002 S m^{-1} p: ±0.01% *fso*	T: 0.001°C; C: 0.001 S m^{-1} p: 0.01 db
SAIV SD208	T: ±0.003°C, C: ±0.0003 S m^{-1}	T: 0.0002°C; C: 0.000008 S m^{-1}

	p: ± 0.01% *fso*	p: 0.01 db
Aanderaa Data Inst.:		
RCM7	T: ±0.05°C; C: ±0.0074 S m^{-1} p: ±0.5% *fso*; u_{sp}: ±1 cm s^{-1} or 4% of speed; u_{dir}: ±5°	T: 0.02°C; C: 0.0074 S m^{-1} p: 0.1% *fso*; u_{sp}: ≥2 cm s^{-1} u_{dir}: 0.35°
RCM9	T: ±0.05°C; C: ±0.005 S m^{-1} p: ±0.25% *fso* u_{sp}: ±0.15 cm s^{-1}; u_{dir}: ±5°	T: 0.02°C; C: 0.0002 S m^{-1} p: 0.1% *fso*; u_{sp}: 0.3 cm s^{-1} u_{dir}: 0.35°
SeaGuard	T: ±0.03°C; C: ±0.0018 S m^{-1} p: ±0.02% *fso* u_{sp}: ±0.15 cm s^{-1}; u_{dir}: ±2°	T: 0.001°C; C: 0.0002 S m^{-1} p: 0.0001% fso; u_{sp}: 0.01 cm s^{-1} u_{dir}: 0.01°
RDCP-600	T: ±0.03°C; C: ±0.0018 S m^{-1} p: ±0.04% *fso*; u_{sp}: ±0.5 cm s^{-1} or 1.5% of reading; u_{dir}: ±4° w_{sp}: 1.0 cm s^{-1}	T: 0.001°C; C: 0.0002 S m^{-1} p: 0.0001% *fso*
SeaGuard II w/SeaGuard string	T: ±0.03°C; C: ±0.0018 S m^{-1} p: ±0.02% *fso*; u_{sp}: 0.3 cm s^{-1} or ±1,5% of reading; u_{dir}: ± 3.5°	T: 0.001°C; C: 0.0002 S m^{-1} p: <0.0001% fso u_{sp}: 0.1 cm s^{-1}; u_{dir}: 0.1°
RDI 300 kHz ADCP	T: ±0.4°C; u_{sp}: 0.5% of the water velocity relative to the ADCP ±0.5 cm s^{-1}; u_{dir}: ±2°	T: 0.01°C; u_{sp}: 0.1 cm s^{-1} u_{dir}: 0.01°
Temperature loggers:		
VEMCO	±0.1°C	0.01°C
HOBO	±0.2°C	0.01°C

**fso = full scale output*

S.1.2 Winter classification and number of profiles in the Isfjorden Transect

Table S2: List of numbers of profiles within a distance of ±0.05°N from the Isfjorden Transect for the winters and summers with good enough data coverage to create interpolated sections along the Isfjorden Transect. For locations of the profiles see the corresponding maps inserted in Figures S7-S12.

Year	Winter	Summer	Winter type
1987	x	14	Deep
1994	x	14	Intermediate
1995	x	5	Intermediate
1996	x	17	Intermediate
1998	x	7	Intermediate
1999	9	13	Intermediate
2000	x	16	Deep
2001	7	x	Deep
2002	x	82	Deep
2003	20	90	Deep
2004	6	71	Intermediate

2005	33	110	Intermediate
2006	41	98	Deep
2007	26	119	Deep
2008	32	58	Deep
2009	x	71	Deep
2010	26	52	Intermediate
2011	45	95	Intermediate
2012	16	95	Intermediate
2013	18	62	Open
2014	4	56	Open
2015	53	60	Deep
2016	17	62	Open
2017	53	48	Open

S.1.3 Moorings

S.1.3.1 Isfjorden mouth south (I-S)

Mooring I-S has been deployed yearly by UNIS since 2005 from typically September to September outside the southern side of the Isfjorden Mouth (see Figure 1b), except in 2007/2008, 2008/2009 and 2009/2010, to monitor the amount of inflow of Atlantic Water to Isfjorden. The I-S mooring data are available in the NPI dataset catalogue for 2005/2006 (Skogseth and Ellingsen, 2019; https://doi.org/10.21334/npolar.2019.176eea39), 2006/2007 (Skogseth and Ellingsen, 2019; https://doi.org/10.21334/npolar.2019.a1239ca3), 2007/2008 (Skogseth and Ellingsen, 2019; https://doi.org/10.21334/npolar.2019.064a09b7), 2010/2011 (Skogseth and Ellingsen, 2019; https://doi.org/10.21334/npolar.2019.b0e473c4), 2011/2012 (Skogseth and Ellingsen, 2019; https://doi.org/10.21334/npolar.2019.2be7bdee), 2012/2013 (Skogseth and Ellingsen, 2019; https://doi.org/10.21334/npolar.2019.a247e9a9), 2013/2014 (Skogseth and Ellingsen, 2019; https://doi.org/10.21334/npolar.2019.6813ce6d), 2014/2015 (Skogseth and Ellingsen, 2019; https://doi.org/10.21334/npolar.2019.11b7e849), 2015/2016 (Skogseth and Ellingsen, 2019; https://doi.org/10.21334/npolar.2019.21838303), and 2016/2017 (Skogseth and Ellingsen, 2019; https://doi.org/10.21334/npolar.2019.cd7a2f7c). From September 2007 to the end of January 2008, I-S was located inside Isfjorden on the southern side east of the Isfjorden Mouth (Figure 1b). The location of I-S is on the steepest part of the southern slope of Isfjordrenna and small changes in the position each year have accordingly led to different bottom depths each

year ranging between 199 m and 220 m. As seen in Table S3, I-S was the first two years only equipped with three Aanderaa Instruments recording current meters (RCMs) with auxiliary CTD sensors typically covering the upper layer (~50 m depth), the intermediate layer (~100 m depth) and the bottom layer (~200 m depth). From 2010, the water column was better resolved by adding three SBE 37 MicroCAT CTDs and typically five VEMCO mini temperature loggers that were evenly distributed over the water column. In 2010/2011, 2015/2016, and 2016/2017, the upper RCM was replaced by an Aanderaa Instrument recording Doppler current profiler (RDCP) measuring the current every 2 m over the surface layer. Unfortunately, the RDCP current data in 2010/2011 were not reliable since the compass didn't work properly. In some years, different instruments stopped logging before mooring recovery, and these are indicated in Table S3.

Table S3: Setup of mooring I-S for the existing measuring periods with position, bottom (echo) depth (D_E), measuring instruments, and their measured period, mean depth (D_M), and parameter, and their sampling frequency (F_S). *u* and *v* are the horizontal velocity components, *w* the vertical velocity component, *T* the temperature, *C* the conductivity, and *p* the pressure. For location of the I-S mooring position see Figure 1.

Position	D_E (m)	Measuring instrument	Measured period	D_M (m)	Measured parameter	F_S (min)
78°03.650' N; 013°31.369' E	210	RCM7 sn.777 RCM7 sn.780 WLR7 sn.1912	16.09.2005 - 15.09.2006	47 189 205	*u*, *v*, *T*, *p* *u*, *v*, *T*, *C*, *p* *T*, *p*	60 60 60
78°03.674' N; 013°31.464' E	203	RCM9 sn.784 RCM9 sn.783 RCM9 sn.782	23.09.2006 - 07.09.2007 **19.03.2007*	44 96 183	*u*, *v*, *T*, *C*, *p* *u*, *v*, *T*, *C*, *p* *u*, *v*, *T*, *C*, *p*	60 60 60
78°08.300' N; 014°25.030' E	220	RCM7 sn.12349 RCM7 sn.10801	06.09.2007 - 28.01.2008	131 211	*u*, *v*, *T*, *C*, *p* *u*, *v*, *T*	60 60
78°03.502' N; 013°35.609' E	205	VEMCO sn.1088 SBE37 sn.5206 RDCP sn.408 VEMCO sn.1089	09.09.2010 - 03.09.2011	34 46 55 77	*T* *T*, *C*, *p* *T*, *C*, *p* *T*	20 20 60 20

		SBE37 sn.5207		89	*T*, *C*, *p*	20
		VEMCO sn.1090		102	*T*	20
		RCM9 sn.784		112	*u*, *v*, *T*, *C*, *p*	60
		VEMCO sn.1091		139	*T*	20
		SBE37 sn.5453		159	*T*, *C*, *p*	20
		VEMCO sn.1092		179	*T*	20
		SeaGuard sn.464	**03.04.2011*	200	*u*, *v*, *T*, *C*, *p*	60
78°03.637’ N;	205	VEMCO sn.1088	08.09.2011 -	14	*T*	20
013°31.271’ E		SBE37 sn.5206	03.09.2012	26	*T*, *C*, *p*	20
		RCM9 sn.783	**03.08.2012*	36	*u, v, T, C, p*	60
		VEMCO sn.1089		52	*T*	20
		SBE37 sn.5207		64	*T*, *C*, *p*	20
		VEMCO sn.1090		77	*T*	20
		RCM9 sn.784		90	*u*, *v*, *T*, *C*, *p*	60
		VEMCO sn.1091		113	*T*	20
		SBE37 sn.5453		133	*T*, *C*, *p*	20
		VEMCO sn.1092		153	*T*	20
		SeaGuard sn.464		179	*u*, *v*, *T*, *C*, *p*	60
78°03.643’ N;	202	VEMCO sn.1088	06.09.2012 -	17	*T*	20
013°31.327’ E		SBE37 sn.7497	28.08.2013	29	*T*, *C*, *p*	20
		RCM9 sn.783		42	*u, v, T, C, p*	60
		VEMCO sn.1089		58	*T*	20
		SBE37 sn.7498		70	*T*, *C*, *p*	20
		VEMCO sn.1090		83	*T*	20
		RCM9 sn.784		97	*u*, *v*, *T*, *p*	60
		VEMCO sn.1091		121	*T*	20
		SBE37 sn.5453		141	*T*, *C*, *p*	20
		VEMCO sn.1092		161	*T*	20
		SeaGuard sn.464		185	*u*, *v*, *T*, *C*, *p*	60
78°03.625’ N;	199	VEMCO sn.1088	**13.01.2014*	20	*T*	20
013°31.267’ E		SBE37 sn.7497	02.09.2013 -	32	*T*, *C*, *p*	20
		RCM9 sn.783	26.08.2014	45	*u, v, T, C, p*	60
		SBE37 sn.7498		73	*T*, *C*, *p*	20
		VEMCO sn.1090	**02.02.2014*	86	*T*	20
		RCM9 sn.1121		94	*u*, *v*, *T*, *p*	60
		VEMCO sn.1091	**06.05.2014*	118	*T*	20
		VEMCO sn.1092	**28.04.2014*	158	*T*	20
		SeaGuard sn.464	**30.12.2013*	188	*u*, *v*, *T*, *C*, *p*	60
78°03.764’ N;	211	AQUAlog. sn.454	31.08.2014 -	25	*T*, *p*	5
013°31.701’ E		SBE37 sn.7497	24.08.2015	37	*T*, *C*, *p*	20
		RCM9 sn.1121		50	*u, v, T, p*	60
		AQUAlog. sn.455		66	*T*, *p*	5
		SBE37 sn.7498		78	*T*, *C*, *p*	20
		AQUAlog. sn.465		91	*T*, *p*	5
		SeaG. sn.1060		105	*u*, *v*, *T*, *C*, *p*	60
		AQUAlog. sn.466		128	*T*, *p*	5
		SBE37 sn.5453		149	*T*, *C*, *p*	20

		SeaGuard sn.464		193	*u*, *v*, *T*, *C*, *p*	60
78°03.667' N; 013°31.492' E	205	VEMCO sn.556	31.08.2015 - 12.08.2016	20	*T*	20
		SBE37 sn.7497		32	*T*, *C*, *p*	20
		RDCP sn.408		44	*u, v, w, T*, *C*, *p*	60
		VEMCO sn.557		61	*T*	20
		SBE37 sn.7498		73	*T*, *C*, *p*	20
		VEMCO sn.558		86	*T*	20
		SeaG. sn.1060		100	*u*, *v*, *T*, *C*, *p*	60
		VEMCO sn.559		124	*T*	20
		SBE37 sn.5453		144	*T*, *C*, *p*	20
		VEMCO sn.560		164	*T*	20
		SeaGuard sn.464		188	*u*, *v*, *T*, *C*, *p*	60
78°03.644' N; 013°31.442' E	205	VEMCO sn.556	19.08.2016 - 02.10.2017	20	*T*	20
		SBE37 sn.7497		32	*T*, *C*, *p*	20
		RDCP sn.408		44	*u, v, w, T*, *C*, *p*	60
		VEMCO sn.557		61	*T*	20
		SBE37 sn.7498		73	*T*, *C*, *p*	20
		VEMCO sn.558		86	*T*	20
		SeaG. sn.1060		100	*u*, *v*, *T*, *C*, *p*	60
		VEMCO sn.559		124	*T*	20
		SBE37 sn.5453		144	*T*, *C*, *p*	20
		VEMCO sn.560		164	*T*	20
		SeaGuard sn.464	**08.08.2017*	195	*u*, *v*, *T*, *C*, *p*	60

**Stopped*

S.1.3.2 Isfjorden mouth north (I-N)

On the northern slope of Isfjordrenna outside the Isfjorden Mouth, mooring I-N has been deployed by UNIS each year since 2015 at 224-228 m depth (see Figure 1b) to monitor the outflow from Isfjorden and the hydrographic differences between the northern and southern part of the mouth. The I-N mooring data are available in the NPI dataset catalogue for 2015/2016 (Skogseth and Ellingsen, 2019; https://doi.org/10.21334/npolar.2019.111aca43), and 2016/2017 (Skogseth and Ellingsen, 2019; https://doi.org/10.21334/npolar.2019.3078f619). As seen in Table S4 in Supplementary data, I-N was first equipped with three Aanderaa Instruments acoustic Doppler RCMs (SeaGuards) with auxiliary CTD sensors covering the upper,

intermediate, and bottom layers. In 2016/2017, two SBE 37 MicroCAT CTDs were added in between the current meters to better resolve the water column.

S.1.3.3 Isfjorden proper (ALKE)

As part of the project ALKEKONGE studying the impact of climate warming on Arctic zooplankton communities, little auks and their physical environment, mooring ALKE was deployed by the Norwegian Polar Institute in collaboration with UNIS in Isfjorden proper from August 2010 to September 2011 at 96 m depth (see Figure 1b) to monitor the interactions between water masses, and marine and terrestrial ecosystems. ALKE was equipped with an RDCP with auxiliary CTD sensors at 88 m depth measuring the current with 1.5-m bins, and a SBE 37 MicroCAT CTD at 39 m depth. The RDCP stopped logging on 24 July 2011.

S.1.3.4 Isfjorden online (IFO)

The Isfjorden online mooring (IFO), constituting an Aanderaa Instruments recording Doppler current profiler (SeaGuard II) configured with 2-m bins and with auxiliary CTD sensors, was deployed on 30 September 2016 in Isfjorden proper in a bottom frame at 60 m depth (see Figure 1b). IFO was part of the UNIS-led project “Blir det is på Isfjorden i år?” funded by the Svalbard Environmental Protection Fund to monitor inflow of Atlantic Water to Isfjorden and possible presence of sea ice on the surface. The IFO mooring data are available in the NPI dataset catalogue (Skogseth and Ellingsen, 2019; https://doi.org/10.21334/npolar.2019.7718a106). On 3 November 2016, a 40 m SeaGuard string with temperature and conductivity sensors at 46 m and 33 m depths was connected to the SeaGuard II and ended in an in-line SeaGuard with auxiliary CTD sensors at 20 m depth. Unfortunately, the sea cable providing power to the instruments and transferring data to land, was cut off on 11 March 2017 due to strong currents and waves in the tidal zone.

S.1.3.5 Isfjorden-Adventfjorden (AF)

Mooring AF was deployed at the entrance to Adventfjorden (see Figure 1b) from September 2011 to September 2012 at 85 m depth by UNIS in collaboration with the Scottish Association for Marine Science (SAMS) and was part of the sampling program at IsA. As shown in Table S4, AF was equipped with a SBE 37 MicroCAT CTD followed by an upward-looking RDI 300 kHz acoustic Doppler current profiler (ADCP) close to the bottom measuring the current with 4-m bins, a SBE16 SeaCAT CTD in the surface layer and four HOBO temperature loggers evenly distributed over the water column. The SBE 37 stopped logging on 31 July 2012, and the ADCP stopped logging on 7 August 2012.

S.1.3.6 Isfjorden proper (IF)

From October 2013 to mid-January 2014 mooring IF was deployed further into Isfjorden proper closer to Sassenfjorden (see Figure 1b) at 182 m depth by UNIS in collaboration with SAMS. IF was equipped with three SBE 37 MicroCAT CTDs, two SBE 56 temperature loggers, and three VEMCO mini temperature loggers evenly distributed over the water column. Additionally, IF was equipped with two RDI 300 kHz ADCP; one downward-looking at 78 m depth and one upward-looking at 72 m depth that both were started on 1 December 2013 configured with 4-m bins and high-frequent sampling.

S.1.3.7 Tempelfjorden (TF)

At the head of Tempelfjorden, UNIS deployed in collaboration with SAMS, mooring TF (see Figure 1b) from January 2016 to June 2017 at 52 meter depth, to monitor any influence of water temperature on the tidewater glacier Tunabreen. The TF mooring data are available in the NPI dataset catalogue (Skogseth and Ellingsen, 2019; https://doi.org/10.21334/npolar.2019.5add522e). As listed in Table S4 in Supplementary data, TF was equipped with one SeaGuard with auxiliary CTD sensors close to the bottom and three SBE 37 MicroCAT CTDs distributed within 10 m above the SeaGuard. The conductivity sensors

were highly affected by the sediment-rich water from the glacier and hence only the salinity data from 35 m and 44 m depths were used in this study.

S.1.3.8 Billefjorden (BF)

To monitor the interaction between fjord circulation, hydrography, sea ice, and marine ecology close to the tidewater glacier Nordenskiöldbreen, UNIS in collaboration with SAMS, deployed mooring BF at the head of Billefjorden at 188-193 m depth from typically September to September in 2008/2009 and from 2010/2011 to 2012/2013 (for location see Figure 1b). As seen in Table S4 in Supplementary data, BF was first equipped with an upward-looking Aanderaa Instruments RDCP with auxiliary CTD sensors at 43 m depth configured with 1-m bins, two upward-looking RDI 300 kHz ADCPs at 83 m and 177 m depths configured with 4-m bins, one SBE 16 SeaCAT CTD, three SBE 37 MicroCAT CTDs, and five VEMCO mini temperature loggers distributed evenly over the water column. In 2010/2011, there were only two ADCPs mounted at 80 m and 83 m depths; one upward-looking and one downward-looking with 4-m bins. Three SBE 16 SeaCAT CTDs were placed in the surface layer, one SBE 37 MicroCAT CTD was put in the bottom layer, and eight VEMCO mini temperature loggers were distributed over the water column. During both these years, the ADCPs covering the bottom layer, provided poor data due to few particles and little movement in the water. BF only had one upward-looking ADCP at 77 m depth in 2011/2012, and at 90 m depth in 2012/2013, covering both the intermediate layer from around sill depth (~70 m depth) and the surface layer with 4-m bins. Further, BF had only two CTDs (SBE 16 SeaCAT or SBE 37 MicroCAT) placed in the surface layer instead of three, but was still equipped with one SBE 37 MicroCAT CTD at the bottom and eight evenly distributed VEMCO mini temperature loggers.

S.1.3.9 Dicksonfjorden (DF)

Just behind the sill in Dicksonfjorden, mooring DF was deployed from October 2016 to the end of September 2017 at 109 m depth, initiated by the Bjerknes Centre for Climate Research and deployed in collaboration with UNIS (for location see Figure 1b). DF was designed in the project BASIC to monitor the vertical carbon flux associated with sea ice formation and brine release in a sill-fjord where brine-enriched winter water gets trapped behind the sill. In this study, only data from the SeaGuard with auxiliary CTD sensors in the surface layer, and the SBE 37 MicroCAT CTD in the bottom layer have been used (see Table S4 in Supplementary data).

Table S4: List of moorings in Isfjorden with position, echo depth (D_E), measuring instruments, and their measured period, mean depth (D_M), parameter, and sampling frequency (F_S). *u* and *v* are the horizontal velocity components, *w* the vertical velocity component, *T* temperature, *C* conductivity, and *p* pressure. The mooring positions are shown in Figure 1b.

Position	D_E (m)	Measuring instrument	Measured period	D_M (m)	Measured parameter	F_S (min)
Mooring: I-N; Owner: UNIS						
78°10.829' N; 013°22.737' E	228	SeaG. sn.1318 SeaGuard sn.645 SeaGuard sn.646	31.08.2015 - 12.08.2016	21 95 201	*u*, *v*, *T*, *C*, *p* *u*, *v*, *T*, *C*, *p* *u*, *v*, *T*, *C*, *p*	60 60 60
78°10.927' N; 013°23.000' E	224	SeaG. sn.1318 SBE37 sn.5206 SeaGuard sn.646 SBE37 sn.10963 SeaGuard sn.645	15.08.2016 - 02.10.2017 ***15.02.2017*	42 92 115 164 221	*u*, *v*, *T*, *C*, *p* *T*, *C*, *p* *u*, *v*, *T*, *C*, *p* *T*, *C*, *p* *u*, *v*, *T*, *C*, *p*	60 20 60 20 60
Mooring: ALKE; Owner: NPI/UNIS						
78°12.300' N; 015°11.202' E	96	SBE37 sn.7683 RDCP sn.406	08.08.2010 - 13.09.2011 ***24.07.2011*	39 88	*T*, *C*, *p* *u*, *v*, *w*, *T*, *C*, *p*	15 15
Mooring: IFO; Owner: UNIS						
78°14.845' N; 015°19.870' E	60	In-line DCS sn.42 40m SeaG. string	03.11.2016 - 11.03.2017	20 33	*u*, *v*, *T*, *C*, *p* *T*, *C*	10 10

		SeaG. II Plf. sn.1797	**30.09.2016*	46 60	*T*, *C* *u*, *v*, *w*, *T*, *C*, *p*	10 10
Mooring: AF; Owner: SAMS/UNIS						
78°15.636' N; 015°10.698' E	85	HOBO sn.363 SBE16 sn.5181 HOBO sn.364 HOBO sn.366 HOBO sn.367 ADCP sn.11047 SBE37 sn.5456	28.09.2011 - 06.09.2012 ***07.08.2012* ***31.07.2012*	20 25 30 37 65 76 77	*T* *T*, *C*, *p* *T* *T* *T* *u*, *v*, *w*, *T*, *p* *T*, *C*, *p*	15 60 15 15 15 20 20
Mooring: IF; Owner: SAMS/UNIS						
78°19.129' N; 015°34.643' E	182	SBE37 sn.8478 SBE56 sn.2668 SBE37 sn.8479 VEMCO sn.1602 ADCP sn.11047 SBE56 sn.2669 ADCP sn.9579 VEMCO sn.1622 VEMCO sn.1623 SBE37 sn.5511	06.10.2013 - 15.01.2014 **01.12.2013* **01.12.2013* 	27 40 41 57 72 74 78 103 131 161	*T*, *C*, *p* *T* *T*, *C*, *p* *T* *u*, *v*, *w*, *T*, *p* *T* *u*, *v*, *w*, *T*, *p* *T* *T* *T*, *C*, *p*	5 5 5 5 3 5 3 5 5 5
Mooring: TF; Owner: UNIS						
78°26.606' N; 017°21.269' E	52	SBE37 sn.7768 SBE37 sn.8479 SBE37 sn.7769 SeaG. sn.1705	29.01.2016 - 23.06.2017	35 40 44 45	*T*, *C*, *p* *T*, *p* *T*, *C*, *p* *u*, *v*, *T*	20 20 20 60
Mooring: BF; Owner: SAMS/UNIS						
78°39.760' N; 016°41.247' E	191	SBE37 sn.5509 SBE16 sn.6066 RDCP sn.213 VEMCO sn.1106 VEMCO sn.7326 ADCP sn.11192 SBE37 sn.5510 VEMCO sn.1066 VEMCO sn.1068 VEMCO sn.1443 ADCP sn.11047 SBE37 sn.5511	08.09.2008 - 24.08..2009 ***17.06.2009*	20 29 43 43 53 83 88 96 126 152 177 186	*T*, *C*, *p* *T*, *C*, *p* *u*, *v*, *w*, *T*, *C*, *p* *T* *T* *u*, *v*, *w*, *T*, *p* *T*, *C*, *p* *T* *T* *T* *T*, *p* *T*, *C*, *p*	12 60 20 15 15 20 12 15 15 15 20 12
78°39.800' N; 016°41.500' E	191	VEMCO sn.1613 SBE16 sn.6472 SBE16 sn.6066 VEMCO sn.1621	07.10.2010 - 26.08.2011	12 12 19 29	*T* *T*, *C*, *p* *T*, *C*, *p* *T*	15 60 60 15

		SBE16 sn.6101		29	*T*, *C*, *p*	60
		VEMCO sn.1626		39	*T*	15
		VEMCO sn.1627		59	*T*	15
		VEMCO sn.1630		79	*T*	15
		ADCP sn.11192		80	*u*, *v*, *w, T*, *p*	20
		ADCP sn.13616		83	*u*, *v*, *w, T*, *p*	20
		VEMCO sn.1684		95	*T*	15
		VEMCO sn.1685		127	*T*	15
		VEMCO sn.1690		149	*T*	15
		SBE37 sn.5511		179	*T*, *C*, *p*	12
78°39.799’ N;	188	SBE37 sn.5509	16.09.2011 -	16	*T*, *C*, *p*	12
016°41.283’ E		SBE16 sn.6472	07.09.2012	26	*T*, *C*, *p*	60
		VEMCO sn.1592		26	*T*	15
		VEMCO sn.1593		37	*T*	15
		VEMCO sn.1598		47	*T*	15
		VEMCO sn.1602		57	*T*	15
		VEMCO sn.1620		77	*T*	15
		ADCP sn.8031	***05.09.2012*	77	*u*, *v*, *w, T*	20
		VEMCO sn.1622		90	*T*	15
		VEMCO sn.1623		112	*T*	15
		VEMCO sn.1624		143	*T*	15
		SBE37 sn.5510		176	*T*, *C*, *p*	12
78°39.340’ N;	193	SBE16 sn.6472	07.10.2012 -	20	*T*, *C*, *p*	60
016°41.329’ E		VEMCO sn.1613	07.09.2013	21	*T*	15
		VEMCO sn.1621		26	*T*	15
		VEMCO sn.1626		39	*T*	15
		SBE16 sn.6067		39	*T*, *C*, *p*	60
		VEMCO sn.1627		49	*T*	15
		VEMCO sn.1630		70	*T*	15
		VEMCO sn.1684		90	*T*	15
		ADCP sn.11047		90	*u*, *v*, *w, T*, *p*	20
		VEMCO sn.1685		111	*T*	15
		VEMCO sn.1690		131	*T*	15
		SBE37 sn.5511		181	*T*, *C*, *p*	12
Mooring: DF; Owner: BCCR UoB						
78°39.294’ N;	109	SeaG. sn.1751	12.10.2016 -	13	*u*, *v*, *T*, *C*, *p*	60
015°18.606’ E		SBE37 sn.14618	30.09.2017	103	*T*, *C*, *p*	60

**Started; **Stopped*

S.1.4 Glider sections

Table S5: List of each glider section taken during the 2014 and 2016 campaigns. Orientations X, A, and D indicated cross-fjord, along-fjord, and diagonal sections. The section number is indicated by *n* while *m* is the number of dives on a section.

n	Location	Orient.	Start time	End time	*m*
1a	Isfjorden	X	2014-11-07 19:30	2014-11-08 17:05	12
2a	Nordfjorden	X	2014-11-11 08:25	2014-11-12 05:41	16
3a	Nordfjorden	A	2014-11-12 21:45	2014-11-14 14:38	27
4a	Sassenfjorden	X	2014-11-15 09:05	2014-11-16 08:02	13
5	Isfjorden	A	2014-11-18 19:50	2014-11-22 07:05	46
6	Isfjorden Mouth	X	2014-11-22 07:55	2014-11-23 00:50	10
7	Isfjorden	A	2014-11-18 12:25	2014-11-21 17:35	27
1b	Isfjorden	X	2014-11-26 13:30	2014-11-27 14:30	13
1c	Isfjorden	X	2016-11-09 13:43	2016-11-10 05:46	11
1d	Isfjorden	X	2016-11-10 09:34	2016-11-11 01:26	11
8	Sassenfjorden	A	2016-11-11 06:16	2016-11-11 18:08	9
4b	Sassenfjorden	X	2016-11-11 22:01	2016-11-12 05:25	6
9	Nordfjorden	D	2016-11-12 09:50	2016-11-13 09:49	18
2b	Nordfjorden	X	2016-11-13 12:18	2016-11-14 02:56	13
2c	Nordfjorden	X	2016-11-14 05:45	2016-11-14 13:27	8
3b	Nordfjorden	A	2016-11-14 17:57	2016-11-15 07:52	16
3c	Nordfjorden	A	2016-11-15 09:49	2016-11-15 16:54	11
10	Nordfjorden	X	2016-11-15 22:23	2016-11-16 02:00	5
2d	Nordfjorden	X	2016-11-16 13:06	2016-11-17 03:23	13
11	Nordfjorden	A	2016-11-17 08:17	2016-11-17 18:10	9
1e	Isfjorden	X	2016-11-18 03:55	2016-11-18 15:30	11

S.1.5 Vessel-mounted acoustic Doppler current profiler (VM-ADCP) sections

Table S6: List of the VM-ADCP sections taken during 29 July 2007 with R/V Jan Mayen. Orientations X, A, and D indicated cross-fjord, along-fjord, and diagonal sections. The section identification is indicated by *n*.

n	Location	Orient.	Start time	End time
A	Isfjorden Mouth	D	2007-07-29 00:54	2007-07-29 01:47
B	Isfjorden Mouth	X	2007-07-29 06:47	2007-07-29 07:17
C	Grønfjorden Mouth	A	2007-07-29 07:22	2007-07-29 07:48
D	Isfjorden	X	2007-07-29 07:50	2007-07-29 08:41
E	Isfjorden	D	2007-07-29 08:43	2007-07-29 10:04
F	Isfjorden	A	2007-07-29 10:04	2007-07-29 10:50

S.2 Figures

S.2.1 Distribution of annual mean temperature, salinity, and density: deep winters and following summers

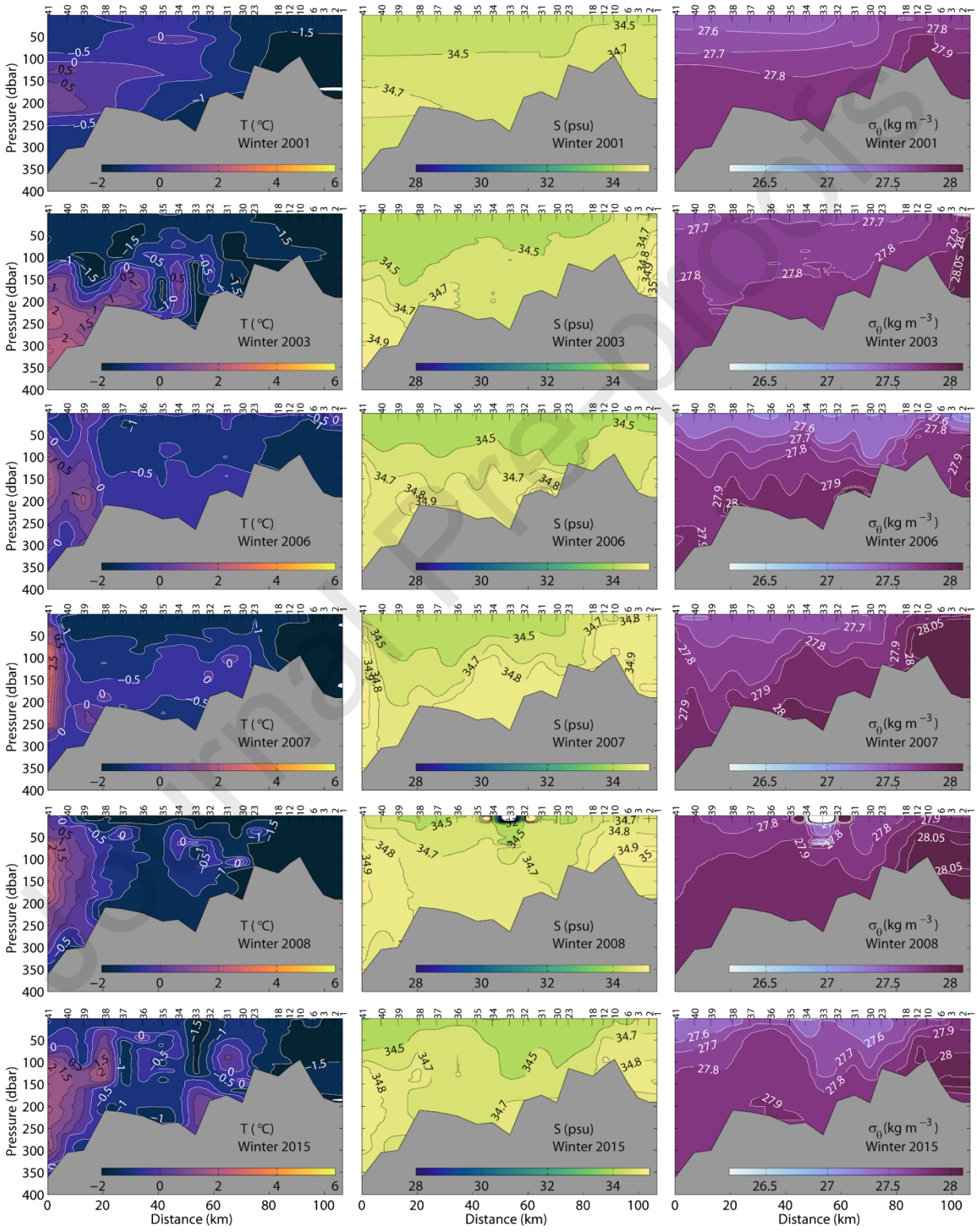

Figure S1: Distribution of mean winter temperature (left), salinity (middle), and density (right) along the Isfjorden Transect from the mouth area (Station 41) to the head of Billefjorden (Station 1) over the winter months (JFMAM) for covered winters of type deep in the time period 1987-2017 (from top to bottom: 2003, 2006, 2007, 2008, and 2015).

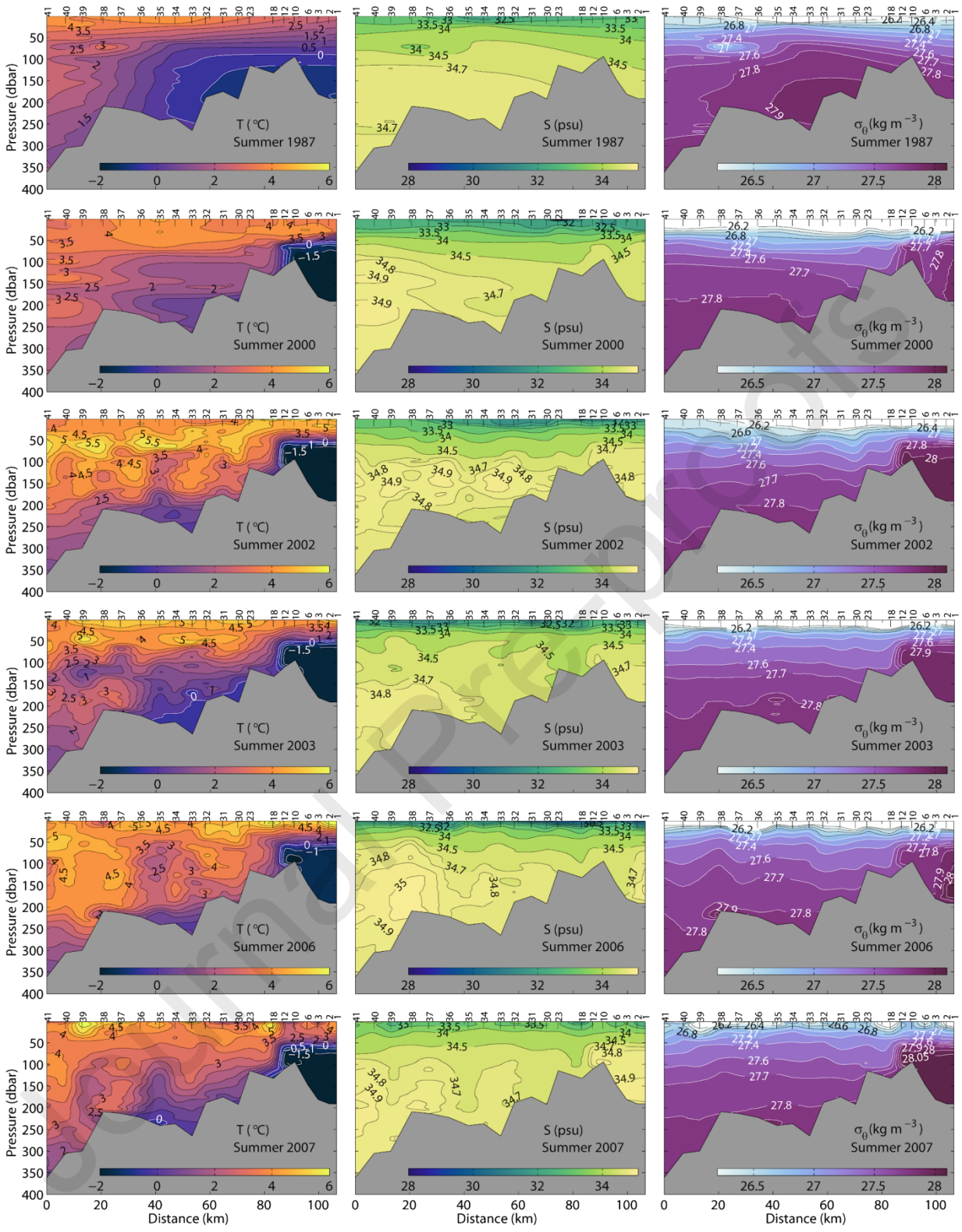

Figure S2: Distribution of mean summer temperature (left), salinity (middle), and density (right) along the Isfjorden Transect from the mouth area (Station 41) to the head of Billefjorden (Station 1) over the summers months (JAS) for covered summers following winters of type deep in the

time period 1987-2017 (from top to bottom: 1987, 2000, 2002, 2003, 2006, 2007, 2008, 2009, and 2015).

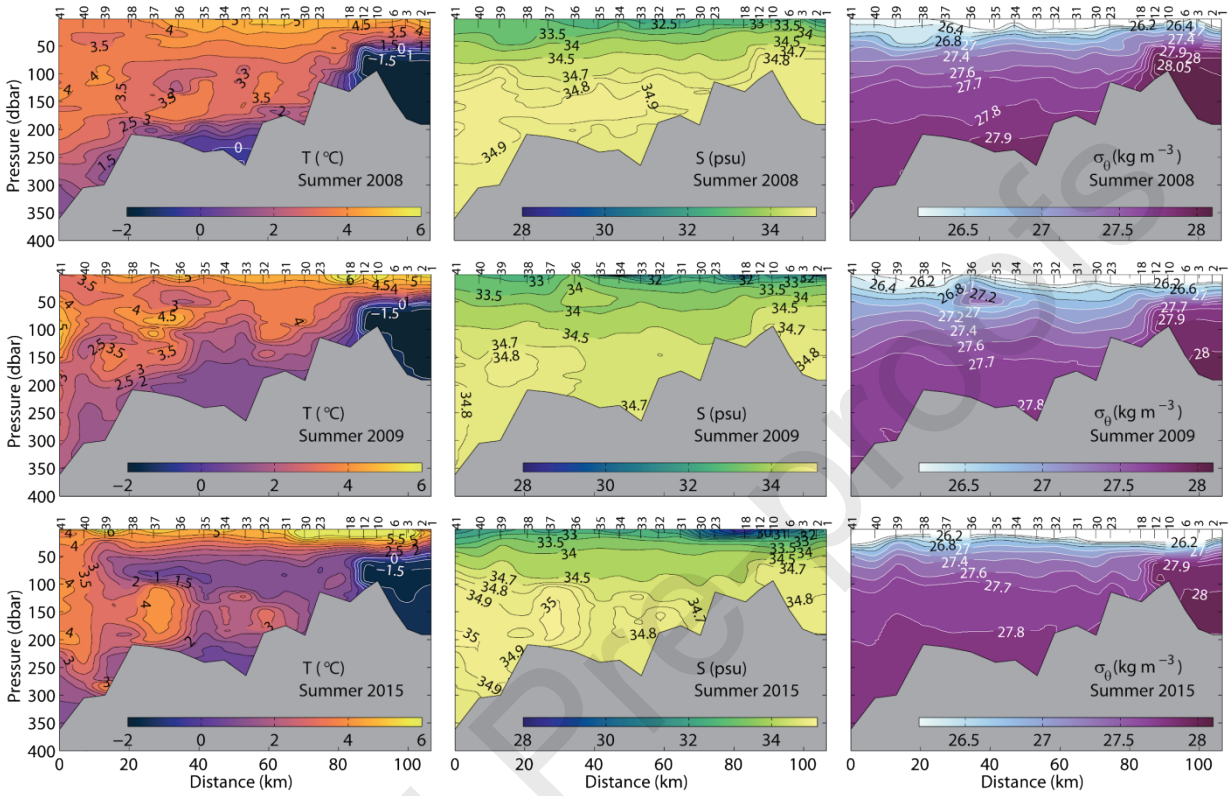

Figure S2: cont.

S.2.2 Distribution of mean temperature, salinity, and density: intermediate winters and following summers

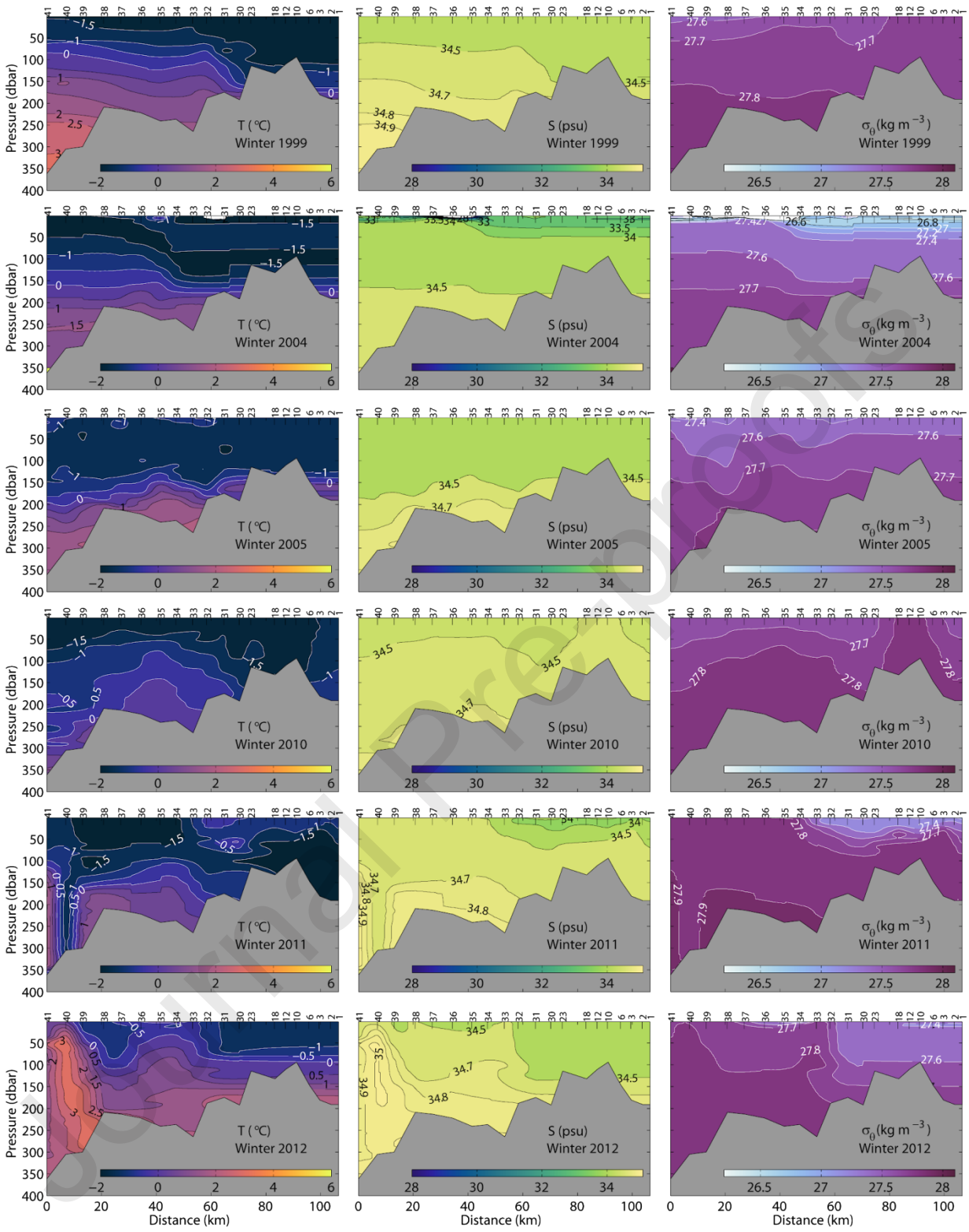

Figure S3: Distribution of mean winter temperature (left), salinity (middle), and density (right) along the Isfjorden Transect from the mouth area (Station 41) to the head of Billefjorden (Station 1) over the winter months (JFMAM) for covered winters of type intermediate in the time period 1987-2017 (from top to bottom: 1999, 2004, 2005, 2010, 2011, and 2012).

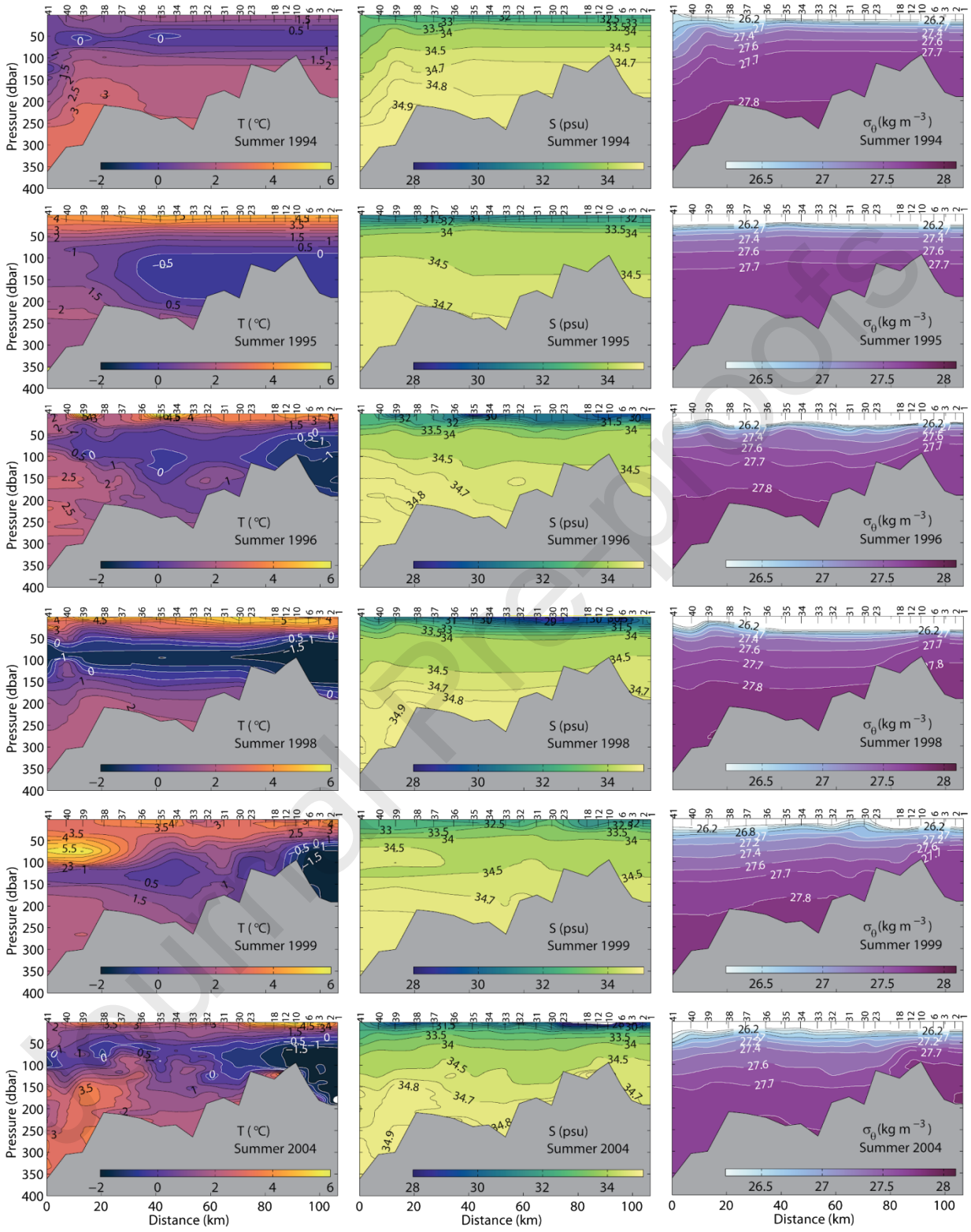

Figure S4: Distribution of mean summer temperature (left), salinity (middle), and density (right) along the Isfjorden Transect from the mouth area (Station 41) to the head of Billefjorden (Station 1) over the summers months (JAS) for covered summers following winters of type intermediate

in the time period 1987-2017 (from top to bottom: 1994, 1995, 1996, 1998, 1999, 2004, 2005, 2010, 2011, and 2012).

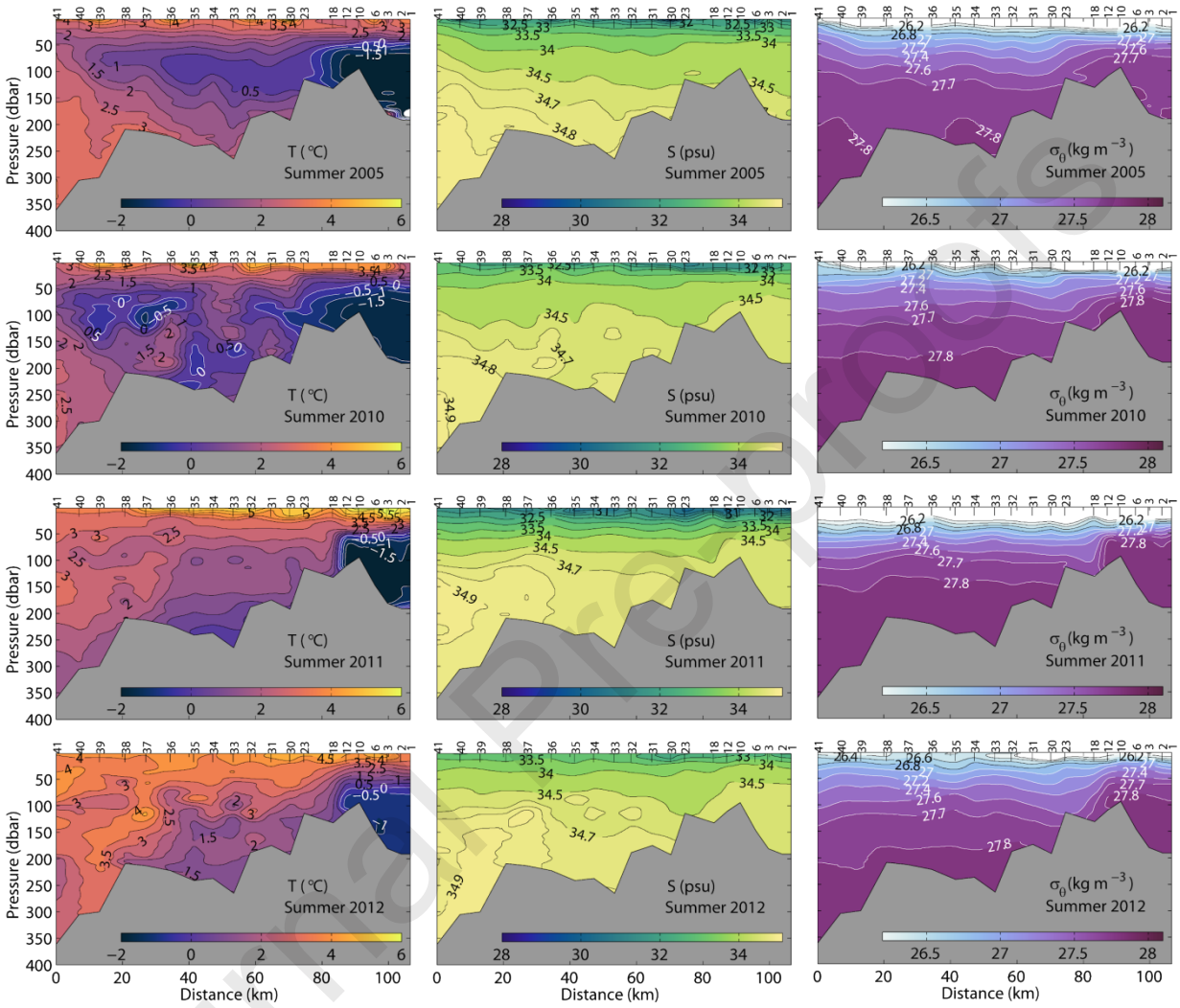

Figure S4: cont.

S.2.3 Distribution of mean temperature, salinity, and density: open winters and following summers

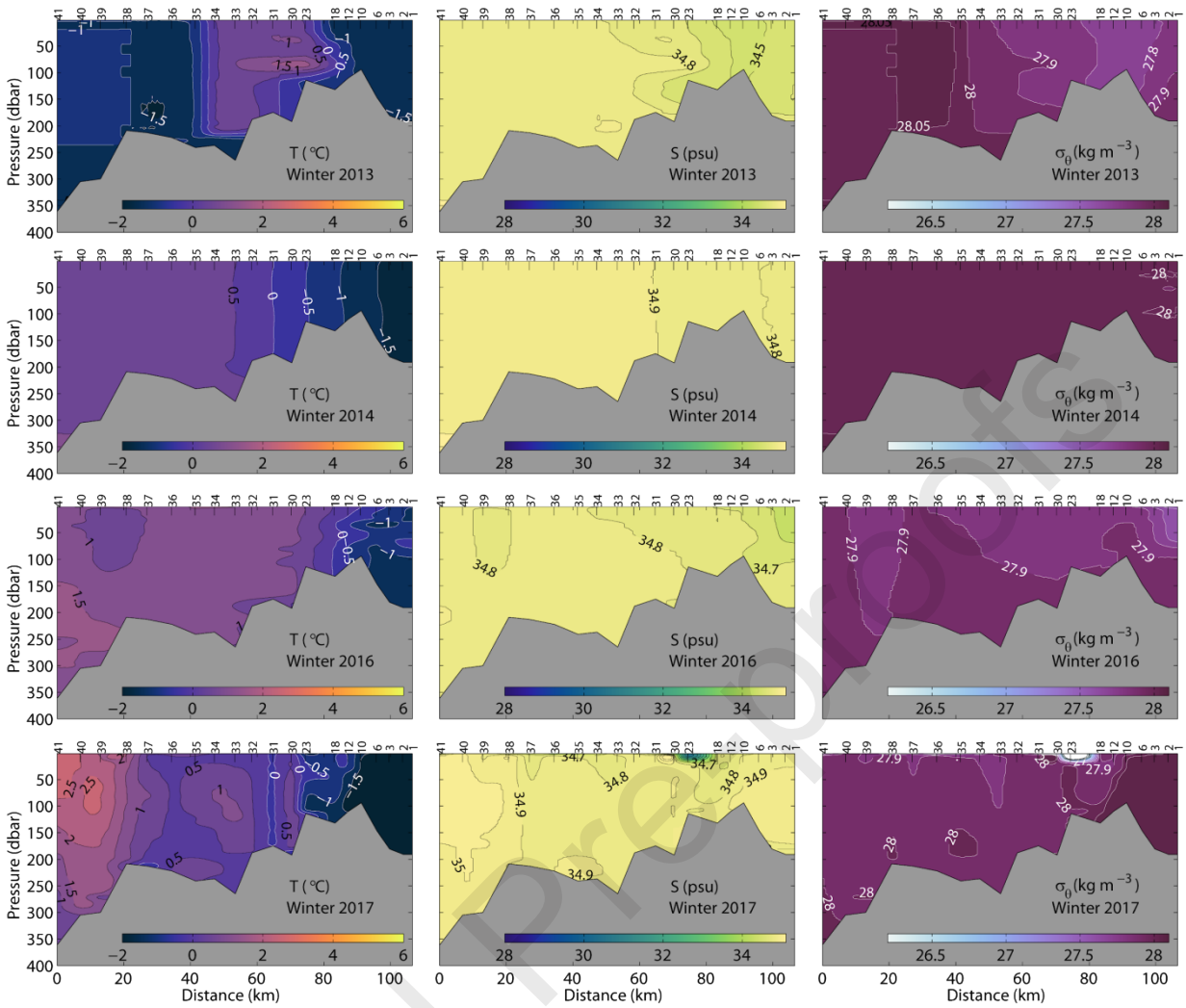

Figure S5: Distribution of mean winter temperature (left), salinity (middle), and density (right) along the Isfjorden Transect from the mouth area (Station 41) to the head of Billefjorden (Station 1) over the winter months (JFMAM) for covered winters of type open in the time period 1987-2017 (from top to bottom: 2013, 2014, 2016, and 2017).

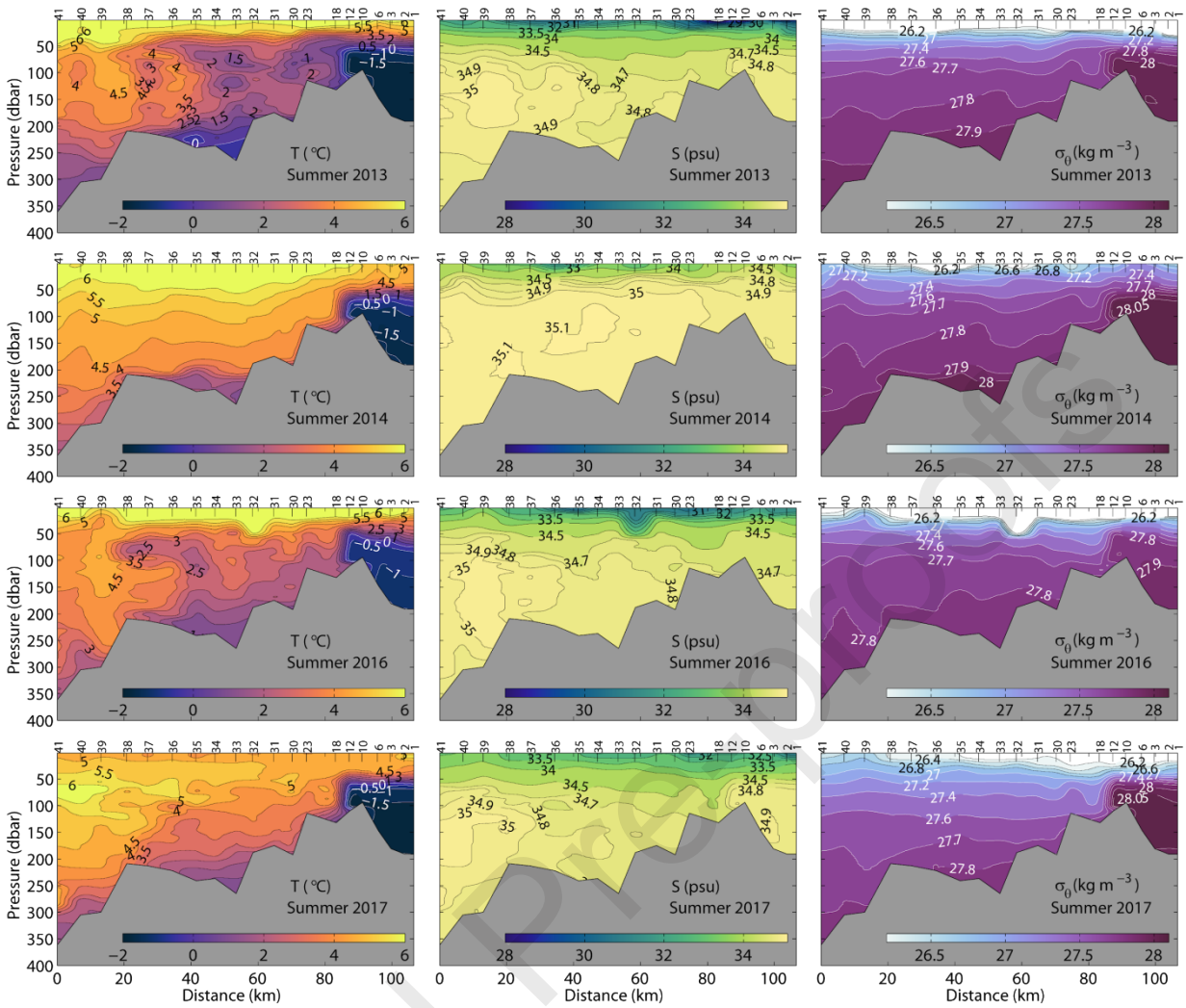

Figure S6: Distribution of mean summer temperature (left), salinity (middle), and density (right) along the Isfjorden Transect from the mouth area (Station 41) to the head of Billefjorden (Station 1) over the summers months (JAS) for covered summers following winters of type open in the time period 1987-2017 (from top to bottom: 2013, 2014, 2016, and 2017).

S.2.4 Distribution of mean water masses: deep winters and following summers

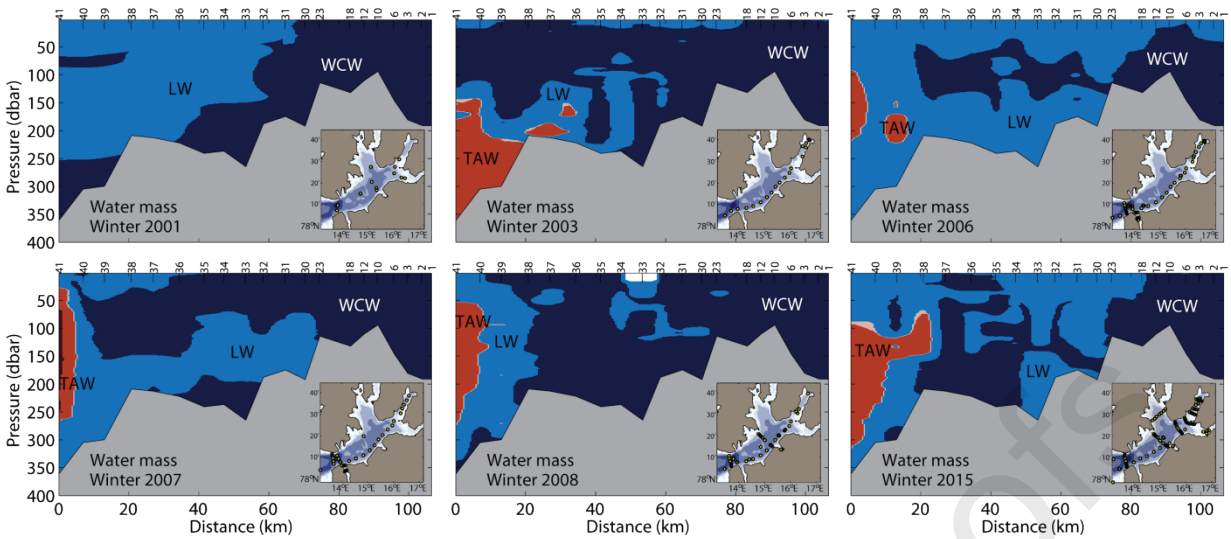

Figure S7: Distribution of winter mean water masses along the Isfjorden Transect from the mouth area (Station 41) to the head of Billefjorden (Station 1) over the winter months (JFMAM) for covered winters of type deep in the time period 1987-2017 (from top left to bottom right: 2001, 2003, 2006, 2007, 2008, and 2015). The yellow dots on the inserted maps indicate the positions of available profiles each winter. The water masses indicated are LW = Local Water, WCW = Winter-Cooled Water, and TAW = Transformed Atlantic Water.

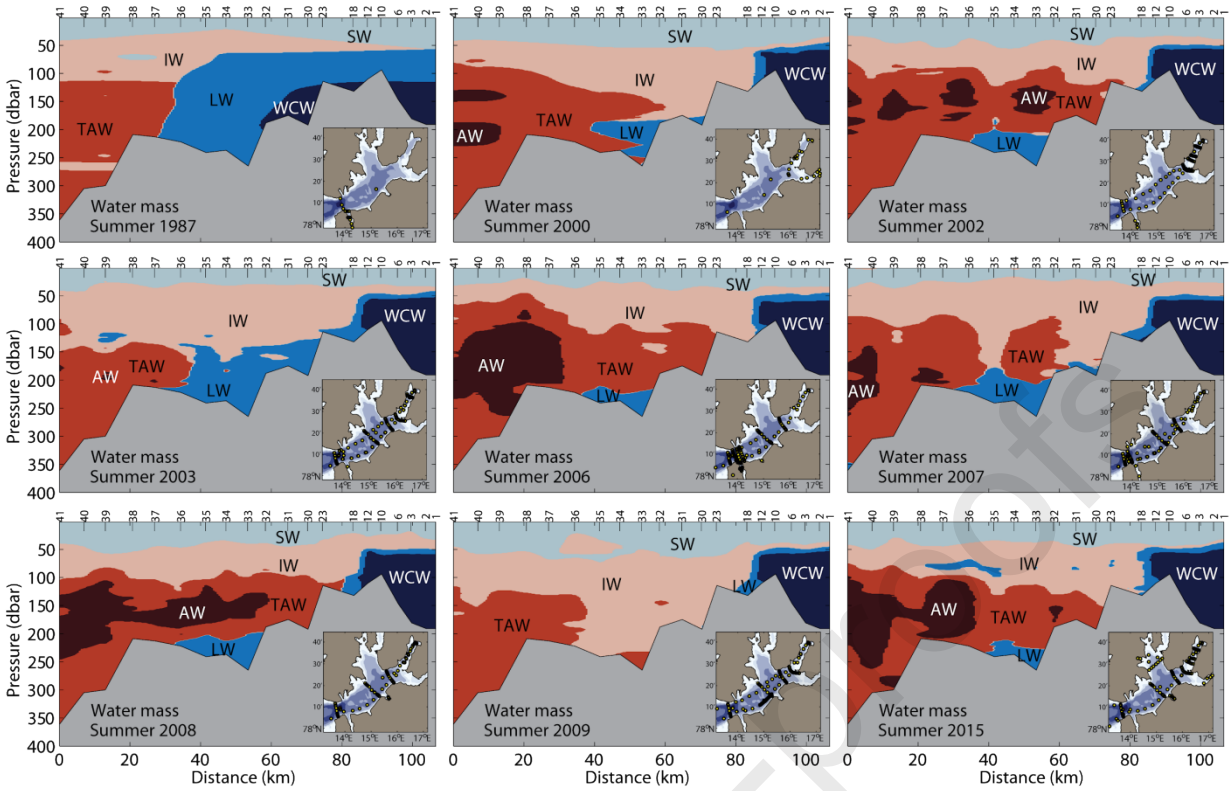

Figure S8: Distribution of summer mean water masses along the Isfjorden Transect from the mouth area (Station 41) to the head of Billefjorden (Station 1) over the summer months (JAS) for covered summers after winter of type deep in the time period 1987-2017 (from top left to bottom right: 1987, 2000, 2002, 2003, 2006, 2007, 2008, 2009, and 2015). The yellow dots on the inserted maps indicate the positions of available profiles each winter. The water masses indicated are SW = Surface Water, IW = Intermediate Water, LW = Local Water, WCW = Winter-Cooled Water, TAW = Transformed Atlantic Water, and AW = Atlantic Water.

S.2.5 Distribution of mean water masses: intermediate winters and following summers

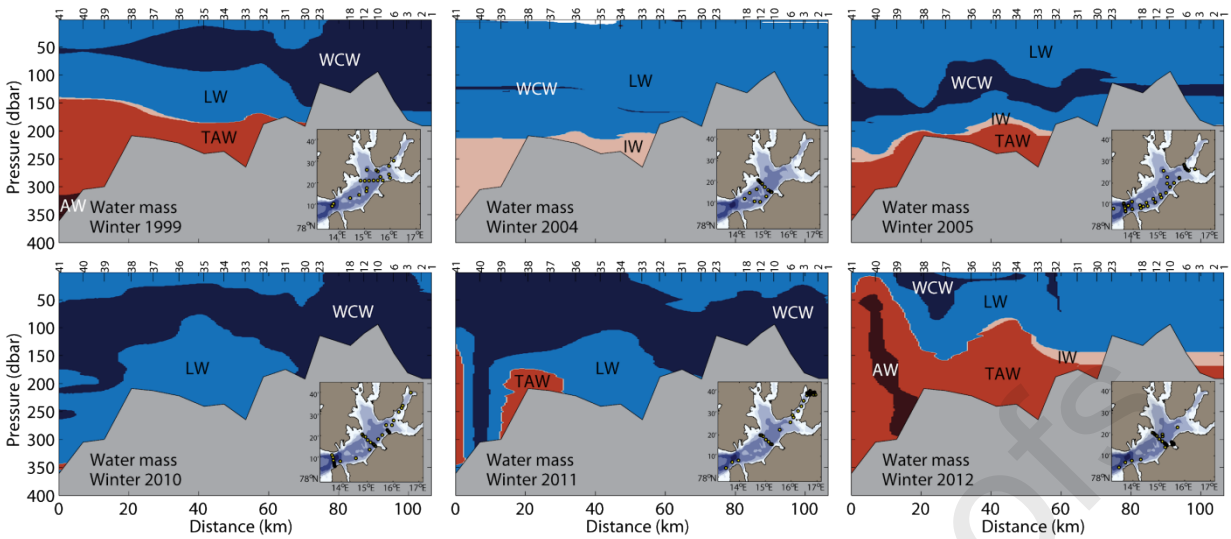

Figure S9: Distribution of winter mean water masses along the Isfjorden Transect from the mouth area (Station 41) to the head of Billefjorden (Station 1) over the winter months (JFMAM) for covered winters of type intermediate in the time period 1987-2017 (from top left to bottom right: 2004, 2005, 2010, 2011, and 2012). The yellow dots on the inserted maps indicate the positions of available profiles each winter. The water masses indicated are IW = Intermediate Water, LW = Local Water, WCW = Winter-Cooled Water, TAW = Transformed Atlantic Water, and AW = Atlantic Water.

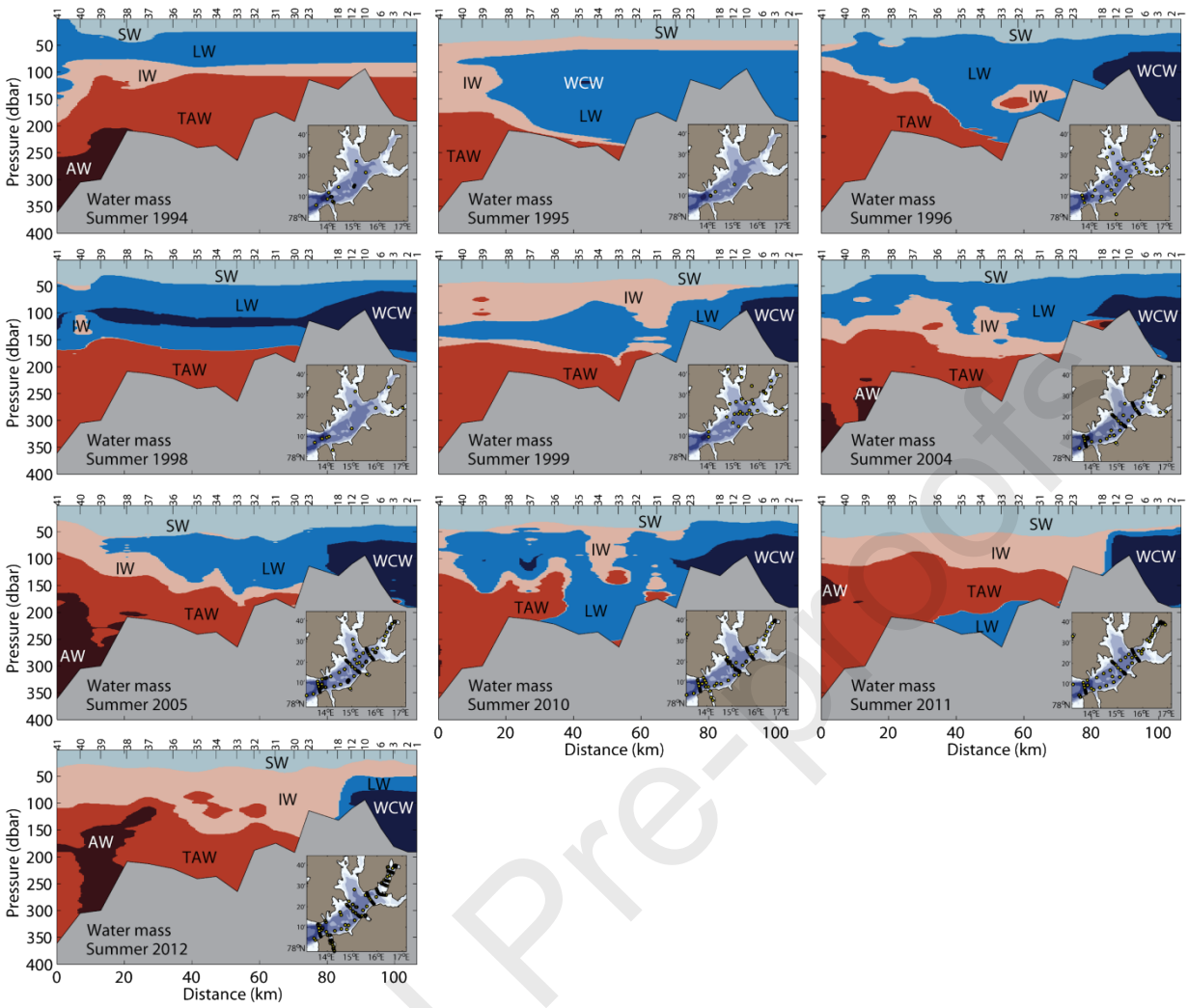

Figure S10: Distribution of summer mean water masses along the Isfjorden Transect from the mouth area (Station 41) to the head of Billefjorden (Station 1) over the summer months (JAS) for covered summers after winter of type intermediate in the time period 1987-2017 (from top left to bottom right: 1994, 1995, 1996, 1998, 1999, 2004, 2005, 2010, 2011, and 2012). The yellow dots on the inserted maps indicate the positions of available profiles each winter. The water masses indicated are SW = Surface Water, IW = Intermediate Water, LW = Local Water, WCW = Winter-Cooled Water, TAW = Transformed Atlantic Water, and AW = Atlantic Water.

S.2.6 Distribution of mean water masses: open winters and following summers

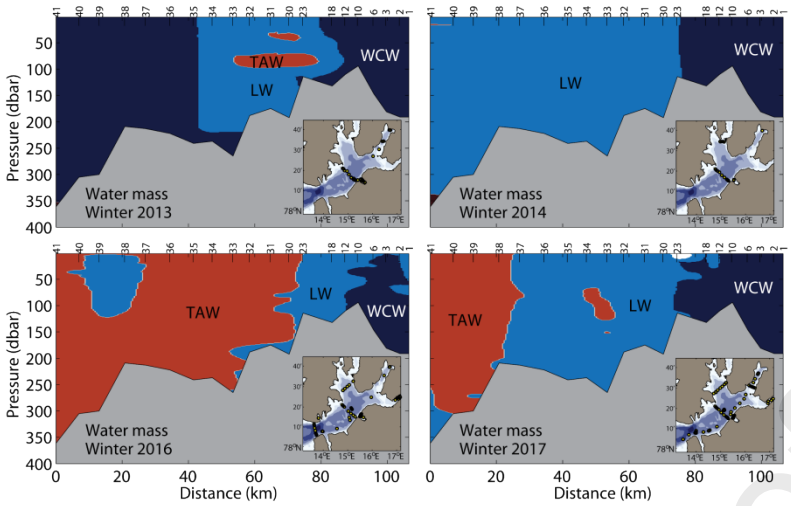

Figure S11: Distribution of winter mean water masses along the Isfjorden Transect from the mouth area (Station 41) to the head of Billefjorden (Station 1) over the winter months (JFMAM) for covered winters of type open in the time period 1987-2017 (from top left to bottom right: 2013, 2014, 2016, and 2017). The yellow dots on the inserted maps indicate the positions of available profiles each winter. The water masses indicated are LW = Local Water, WCW = Winter-Cooled Water, and TAW = Transformed Atlantic Water.

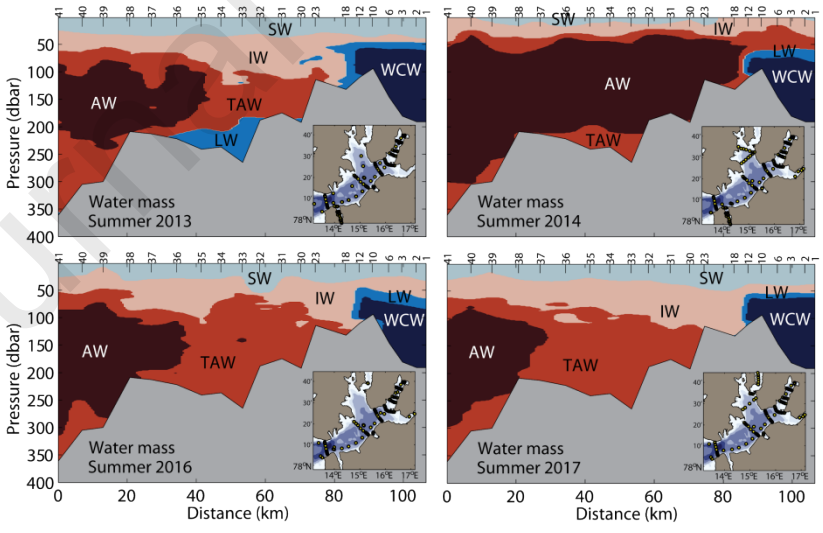

Figure S12: Distribution of summer mean water masses along the Isfjorden Transect from the mouth area (Station 41) to the head of Billefjorden (Station 1) over the summer months (JAS) for covered summers after winter of type open in the time period 1987-2017 (from top left to bottom right: 2013, 2014, 2016, and 2017). The yellow dots on the inserted maps indicate the

positions of available profiles each winter. The water masses indicated are SW = Surface Water, IW = Intermediate Water, LW = Local Water, WCW = Winter-Cooled Water, TAW = Transformed Atlantic Water, and AW = Atlantic Water.

Highlights

- Isfjorden experienced a shift in sea ice cover and summer ocean structure in 2006 associated with positive decadal trends in heat and salt content, changing the fjord from an Arctic to Atlantic type.
- The fjord has a crucial impact on the local terrestrial climate.
- The "Atlantification" of the West Spitsbergen Shelf and a change in winter convection in the fjord lead to warm Atlantic Water penetrating the fjord in the surface layer in contrast to normal inflow along deep or intermediate layers.